HAIDONG LI

THE ANALYTICAL SINGULARITY LOCUS EQUATION AND THE DETERMINATION OF SINGULARITY-FREE ZONES IN THE WORKSPACE OF THE GENERAL GOUGH-STEWART PLATFORM

Thèse présentée
à la Faculté des études supérieures de l'Université Laval
dans le cadre du programme de doctorat en génie mécanique
pour l'obtention du grade de Philosophiæ Doctor (Ph.D.)

FACULTÉ DES SCIENCES ET DE GÉNIE
UNIVERSITÉ LAVAL
QUÉBEC

JANVIER 2005

Abstract

It is well known that one of the main factors that hinders the application of parallel mechanisms is that singular configurations may exist within their workspace, which is a serious problem. Therefore, it is of primary importance to avoid the singularities in the workspace. From a design point of view, it is desirable to obtain the analytic expression of the singularity locus of a parallel mechanism; then, with a given set of structural parameters, the singularity locus can be illustrated graphically.

According to the classification given in [14], there are three types of singularities for closed-loop mechanisms, based on the properties of the Jacobian matrices of the chain. The second type of singularity is the focus of our study, i.e., the determinant of the instantaneous direct kinematics matrix is equal to zero. In this thesis, first, an expansion algorithm is developed to obtain the analytical expression for the singularity locus in the 6-dimensional Cartesian space of the general Gough-Stewart platform, i.e., a polynomial in six variables (three position variables x, y, z, and three orientation variables, ψ, θ and ϕ), which consists of 2173 terms. Then, with the expression obtained here and a given set of structural parameters, the singularity locus for either constant orientation or constant position can be obtained immediately. Although the expression is rather complicated, it is possible to obtain graphical representations.

The singularity locus expression is applicable to all Gough-Stewart platform regardless of the geometric parameters. The expression developed here is of great interest for the design and analysis of Gough-Stewart platforms. It allows the designer to visualize interactively the singularity locus superimposed on the given workspace for either constant orientation or constant position or combinations of both.

The closed-loop nature of parallel mechanisms limits the motion of the platform and creates complex kinematic singularities inside the workspace. Because of the limited workspace coupled with singularities, the trajectory planning of parallel mechanisms is a difficult problem. Hence, it is highly desirable to develop an algorithm to locate the singularity-free zones in the workspace.

In this thesis, algorithms are developed for the identification of singularity-free zones in the workspace of $3-RPR$ planar parallel mechanisms and the general Gough-Stewart platform. Several procedures adapted to different situations are developed. With the procedures proposed in this thesis, the end-effector can be moved arbitrarily in a zone, which means that it can undergo any trajectory, and the trajectories do not have to be further checked for singularities.

The procedures developed in this thesis are all similar in nature. They are based on the use of Lagrange multipliers to transform the constrained problems into unconstrained problems. In principle, the procedure can be applied to any mechanism with a known singularity equation. The results obtained are not previously available and are easy to understand. For different parallel mechanisms, the procedures allow the determination of singularity-free zones of different shapes, such as cylinders and spheres.

Although the procedures developed in this thesis are formulated mathematically, they also have geometric interpretations. Therefore, graphical illutrations are presented to illustrate the effectiveness of the procedures as well as to verify the results. All the results presented in this thesis will be of great help for the design and trajectory planning of parallel mechanisms.

Résumé

Il est bien connu qu'un des facteurs principaux qui gêne l'application des mécanismes parallèles réside dans le fait que des configurations singulières peuvent exister à l'intérieur de leur zone de travail. Par conséquent, il est très important d'éviter les singularités dans la zone de travail. D'un point de vue de conception, il est souhaitable d'obtenir l'expression analytique du lieu de singularité d'un mécanisme parallèle, puis, avec un ensemble donné de paramètres structuraux, les lieux de singularité peuvent être déterminés.

Selon la classification donnée dans [14], il existe trois types de singularités pour les mécanismes constitués de chaînes cinématiques fermées. En se basant sur les propriétés des matrices jacobiennes de la chaîne, le deuxième type de singularité est le centre de notre étude, c.-à-d., le déterminant de la matrice jacobienne directe est égal à zéro. Dans cette thèse, un algorithme d'expansion est développé pour obtenir l'expression analytique pour le lieu de singularité dans l'espace en dimensions cartésiennes de la plate-forme générale de Gough-Stewart, c.-à-d., un polynôme avec six variables (trois variables de position x, y, z et trois variables d'orientation, ψ, θ, ϕ), qui est constitué de 2173 termes. À partir de l'expression obtenue ici et un ensemble de paramètres structuraux, le lieu de singularité pour l'orientation constante où la position constante peut être obtenu immédiatement. Bien que l'expression soit plutôt compliquée, il est possible d'obtenir certaines représentations graphiques en 3-D.

L'expression du lieu de singularité est applicable à chacune des plate-formes 6-6 de Gough-Stewart indépendamment des paramètres géométriques. L'expression développée ici est d'un grand intérêt pour la conception et l'analyse des plate-formes de Gough-

Stewart. Elle permet au concepteur de visualiser interactivement le lieu des singularités superposé à la zone de travail donnée pour une orientation ou une position constante ou pour une combinaison des deux.

L'architecture en boucles fermées des mécanismes parallèles limite le mouvement de la plate-forme et crée des singularités cinématiques complexes à l'intérieur de la zone de travail. En raison de la zone de travail limitée couplée aux singularités, la planification de trajectoire des mécanismes parallèles est un problème difficile. Par conséquent, il est fortement souhaitable de développer un algorithme pour localiser l'espace libre des singularités dans la zone de travail.

Dans cette thèse, des algorithmes sont développés pour l'identification des zones libres de singularités dans l'espace de travail des mécanismes parallèles plans de type $3-RPR$ et de la plate-forme générale de Gough-Stewart. Plusieurs procédures adaptées à différentes situations sont développées. Les procédures développées dans cette thèse sont toutes semblables en nature. Elles sont basées sur l'utilisation des multiplicateurs de Lagrange afin de transformer les problèmes avec contraintes en problèmes sans contraintes. En principe, la procédure peut être appliquée à n'importe quel mécanisme dont l'équation de singularité est connue. Les résultats obtenus sont originaux et sont faciles à comprendre. Pour différents mécanismes parallèles, les procédures permettent la détermination des zones libres de singularités de différentes formes, comme des cylindres et des sphères.

Bien que les procédures développées dans cette thèse soient formulées mathématiquement elles ont également des interprétations géométriques. Par conséquent, des illutrations graphiques en 3-D sont présentées pour illustrer l'efficacité des procédures aussi bien que pour vérifier les résultats. Tous les résultats présentés dans cette thèse seront utiles pour la conception et la planification de trajectoire des mécanismes parallèles.

Foreword

This thesis describes the most important aspects of my work in the Robotics Laboratory of the Department of Mechanical Engineering of Laval University, Québec, Canada.

Firstly, I would like to express my sincere gratitude to my supervisor, Professor Clément M. Gosselin, for his excellent guidance, continuous encouragement and support during the whole research as well as the critical review of the manuscript. I am also grateful to my supervisor, Professor Marc J. Richard, for his great support and inspiration during these years as well as the precious comments on my thesis. Their broad knowledge played an important role in the fulfillment of this work.

Thanks Professor Illian Bonev of École de technologie de supérieure Montréal, Professor Leila Notash of Queen's unviersity and Professor Oscar Altuzarra of university Bilbao of Spain for the examination of my thesis and their precious comments.

Special thanks go to Boris Mayer St-Onge for his help with programming and using the laboratory facilities, his role is important in the fulfillment of the research work. Thanks all the colleagues of Robotics laboratory for their help in many aspects.

Finally, I would like to thank my husband, Haibo Wang, my daughter, Ziqi Wang and my parents for their love and support.

Contents

List of Tables

List of Figures

Chapter 1

Introduction

The word *robot* entered the English vocabulary as early as 1923 [6]. According to *Webster's New Word College Dictionary*, it is defined as: *any anthropomorphic mechanical being built to do routine manual work for human beings.* For different people, the word *robot* means different things, some people have the impression that robots are humanoids of science fiction. Actually, referring to the definition used by *the Robotics Institute of America: A robot is a re-programmable multi-functional manipulator design to move material, parts, tools, or specialized devices, through variable programmed motions for the performance of a variety of tasks.* According to this definition, robots can be mechanical manipulators, numerically controlled machines, walking machines and the humanoid of science fiction. Today, most industrial robots are mechanical manipulators instead of humanoid in appearance. Figure 1.1 shows two typical industrial robots.

(a) A serial mechanism (Courtesy of Mitsubishi Heavy Industries).

(b) A parallel mechanism (Courtesy of Polytec PI, Inc.).

Figure 1.1: Two typical industrial robots.

Robots can be classified according to different criteria, such as their degrees of freedom, kinematic structure, workspace envelope, drive technology, and motion characteristics. According to the different kinematic structures, robots are generally classified as serial mechanisms and parallel mechanisms. A robot is said to be a *serial robot* or *open-loop mechanism* if its kinematic structure takes the form of an open-loop chain, a *parallel mechanism* if it is made up of a closed-loop chain, or a *hybrid mechanism* if it consists of both open- and closed-loop chains. A kinematic chain is an assemblage of links that are connected by joints. When every link in a kinematic chain is connected to every other link by at least two distinct paths, the kinematic chain forms one or more closed loops and is called a closed-loop chain, otherwise it is an open-loop chain [49].

In this thesis, the term *parallel mechanism* is frequently mentioned. Similar equivalent terms may also be found in the literature such as parallel manipulator, parallel kinematic machine, hexapod, or closed-loop kinematic chain. A kinematic chain is called a mechanism when one of its links is fixed to the ground. The fixed link is called the *base*. In a mechanism, one or more links may be assigned as the input links. As the input link(s) move with respect to the fixed link, all the other links will move according to kinematic constraints imposed by the joints. Thus a mechanism is a device that transforms motion or torque from one or more input links to the others. In this thesis, we exclusively focus on the relative motion between the mobile platform (end-effector)

and the base. Hence, the use of the term parallel mechanism throughout the thesis.

In general, a n-degree-of-freedom (DOF) fully-parallel mechanism is one in which the end-effector or mobile platform is connected to the base with n distinct kinematic chains and in which one joint of each of these chains is actuated. The variables that describe the actuated joints are referred to as the input variables or also as the active joint variables. On the other hand, the variables that describe the pose of the mobile platform are referred to as output variables or Cartesian variables.

In this thesis, we study two types of fully-parallel mechanisms. In Chapter 3, a planar 3-DOF fully-parallel mechanism is studied, which is shown in Figure 1.2(a). In Chapters 2, 4 and 5, a 6-DOF fully-parallel mechanism called *the general Gough-Stewart platform* is studied. Based on the history of parallel mechanisms and on robotics, in general, *the general Gough-Stewart platform* is defined as a 6-DOF fully-parallel mechanism with six identical kinematic chains, which consists of a mobile platform and a base connected by six extensible legs with spherical joints at both ends or a spherical joint at one end and a universal joint at the other. As the above two architectures are equivalent from the viewpoint of kinematic and static input-output relationships and differ only regarding the passive freedoms of the legs, the present work is applicable to both of them. The general Gough-Stewart platform with six UPS legs is shown in Figure 1.2(b), in which U denotes a Hooke joint and S represents a spherical joint, which are passive, while P denotes an actuated prismatic joint.

Parallel mechanisms differ from the serial mechanisms by virtue of their kinematic structure. A serial mechanism consists of several links connected in series by various types of joints, typically revolute and prismatic joints. One end of the mechanism is attached to the ground and the other end is free to move in space as shown in Figure 1.1(a). Compared to parallel mechanisms as shown in Figure 1.1(b), serial mechanisms have a simpler structure, wider reachable area and relatively simpler kinematics. These advantages lead to the application of this type of mechanism in the industry, such as, for assembling, welding, painting, etc, where large load or high speed and accuracy are not needed.

As opposed to serial mechanisms, parallel mechnaisms are composed of multiple closed kinematic loops. Typically, these kinematic loops are formed by two or more kinematic chains that connect a moving platform to a base, where one joint in the

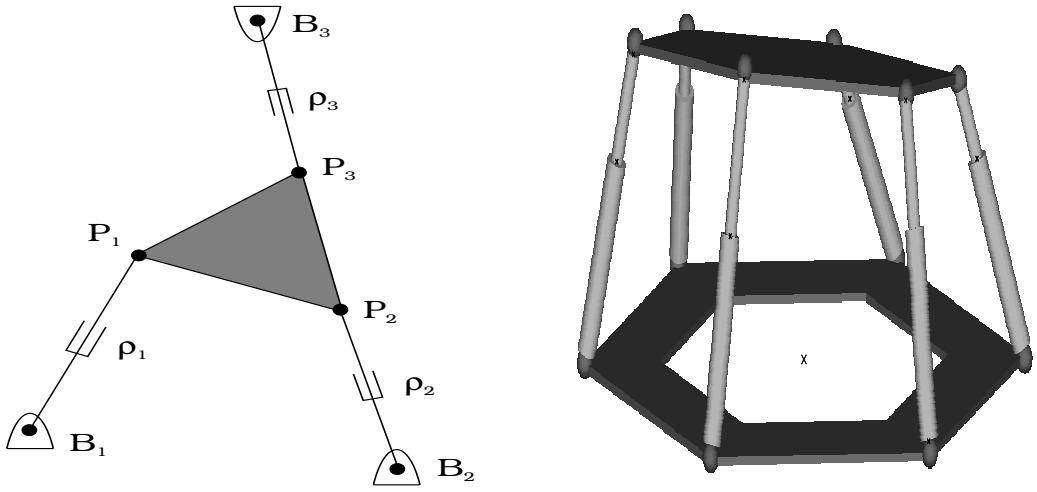

(a) Planar 3-RPR parallel mechanisms.

(b) The general Gough-Stewart platform.

Figure 1.2: Parallel mechanisms studied in this thesis.

chain is actuated and the other joints are passive. This kinematic structure allows parallel mechanisms to be driven by actuators positioned on or near the base of the mechanism. In contrast, serial mechanisms do not have closed kinematic loops and are usually actuated at each joint on the serial linkage. Accordingly, the actuators that are located at each joint on the serial linkage can account for a significant portion of the loading experienced by the mechanism, whereas the links of a parallel mechanism generally need not carry the load of the actuators. This allows the parallel mechanism links to be made lighter than the links of an analogous serial mechanism. Hence, parallel mechanisms can enjoy the potential benefits associated with light weight construction such as high-speed operation and improved load to weight ratios. When a mechanism performs a given task, such as lifting up a workpiece, its end-effector exerts a force and a moment to the external environment at the point(s) of contact. This force and moment are generated by the actuators installed at various points of connection. For brevity, we often use the term *force* to imply both force and moment. For a serial mechanism, actuator forces are transmitted through an open-loop chain to the point of contact, while for a parallel mechanism, actuator forces are transmitted through several parallel paths to the end-effector, which leads to an increased load-carrying capacity and high stiffness.

Parallel mechanisms can be used in many applications where these advantages are of

primary importance while a limited workspace is acceptable. The most famous parallel mechanism is the Gough-Stewart platform, which was described in a publication by Stewart [46] as a flight simulator. It should be noted that although this mechanism is commonly referred to as the *Stewart platform*, it was first proposed by Gough [17] and was used to test tires. Therefore, this mechanism will be referred to here as the *Gough-Stewart platform*, a term that is now generally accepted in the robotics and mechanisms community.

Parallel mechanisms have attracted more and more attention over the last decades (see for instance, [9], [21], [22], [29]). However, their application has been limited to only a few areas so far. It is well known that one of the main factors that hinders the application of parallel mechanisms is that singular configurations may exist within their workspaces, which is a serious problem. When a mechanism is in a singular configuration, the number of degrees of freedom of the mechanism changes instantaneously. In such configurations, the mechanism gains one or more degrees of freedom and becomes uncontrollable. Furthermore, the actuator forces may become very large, which will result in a breakdown of the mechanism. Therefore, it is of primary importance to avoid the singularities in the workspace.

For decades, singularities, an inherent property of parallel mechanisms, has attracted the attention of several researchers: Gosselin and Angeles [14] used the Jacobian matrices of the input-output velocity equation of parallel mechanisms to classify the different types of singularities. Two main types of singularities which can occur in parallel mechanims have been identified: one associated with the direct kinematics and the other with the inverse kinematics. Depending on which matrix is singular, a parallel mechanism may be at a direct kinematic singular configuration, an inverse kinematic singular configuration, or both. That is, there are three types of singularities. According to this singularity classification, the first type of singularity corresponds to the boundaries of the workspace, which leads to simple expressions. Both the first and the third type of singularity can be avoided easily. However, the second type of singularity corresponds to the breakdown of the mechanism, which is the focus of our study. In 1994, the above singularity classification has been further refined in [55], in which six types of singularities reflecting different possibilities for the occurence of degeneracies of the instantaneous forward and inverse kinematics are defined, where the physical interpretations are provided in details. Later on, another type of singularity, which is called constraint singularities, has been identified in [56]. It should be noted that the

mechanisms studied in this thesis cannot have constraint singularity.

From a design point of view, it is desirable to develop a tool that will allow the determination of the singularity locus in the mechanism's workspace. In other words, given a set of design parameters, provide the designers with a graphical representation of singularity locus of the mechanism. With it, it is easier to identify the locations of the singularities within the workspace and whether the singularities can be avoided.

Using the method of classification of Gosselin and Angeles [14], analytical expressions for the singularity loci of mechanisms with 2-DOF and 3-DOF ([44], [45], [50], [51], [15], [5]) were obtained. However, such expressions for mechanisms with more than 3-DOF are more difficult to obtain because of the complexity of the determinant. For instance, Gosselin and Wang [52] used numerical methods to study the singularity loci of 4-DOF parallel mechanisms.

For 6-DOF parallel mechanisms, earlier studies led to the identification of a few special cases of singularities. Hunt [21] first pointed out a singularity that occurs when all the lines associated with the prismatic actuators intersect a common line. Then, Fichter [11] showed that a singular configuration is attained when the platform is rotated around an axis orthogonal to the plane of the base by an angle of $\pm 90^\circ$ using a simplifed Gough-Stewart platform. Later on, Merlet [28] studied the singularities of some simplified Gough-Stewart platforms. This led to a list of geometric conditions under which these special configurations are encountered. Although the geometric approach can give a physical insight, it is difficult to establish a correspondence with the location of the singularities in the Cartesian workspace. Other geometric approaches have also been used by some authors on simplified Gough-Stewart platforms ([23], [37]). Only in 1998, Kim [26] obtained the analytical expression of singularity locus equation of the general Gough-Stewart platform with constant orientation using the concept of local structurization method with extra sensors, which is a three-degree polynomial in three position varaibles. Later on, Mayer St-Onge and Gosselin [33] found the same result by expanding the Jacobian matrix of the mechanism with constant orientation using linear decomposition and cofactor expansion.

In Chapter 2 of this thesis, the general Gough-Stewart platform is studied, the general architecture is as shown in Figure 1.2(b). The derivation of the velocity equation and the corresponding Jacobian matrices is first presented. According to the classi-

fication of the singularities defined by Gosselin and Angeles [14], using the velocity equation, the singularity of type II is analyzed by equating the determinant of the direct instantaneous Jacobian matrix to zero. The expansion of the latter determinant is rather complicated because of the coupling between the structural parameters, the orientation variables and the position variables. Finally, the analytical singularity locus equation in the 6-D space is obtained, i.e., a polynomial in six variables (three position variables x, y, z, and three orientation variables, e.g., three Euler angles ψ, θ, ϕ), which consists of 2173 terms. It is shown that although the expression is very complex, it can be handled both numerically and analytically. Finally, a numerical procedure is then introduced to represent graphically the singularity locus within a given workspace for either constant orientations or constant positions or combinations of both cases, and the results are shown to be coherent with those reported previously in [33].

With the expression developed in Chapter 2, the graphical representation of the singularity locus in the Cartesian space can be obtained interactively. Such graphical representations are of great interest in a context of design since they allow one to obtain a complete picture of the location of the singular configurations in the workspace. For a given architecture, it is therefore possible to verify whether there are singularities in a planned workspace. However, the graphical visualization is limited to three dimensions and this approch is more difficult to apply to six-DOF mechanisms.

The closed-loop nature of parallel mechanisms limits the motion of the platform and creates complex singularities inside the workspace. Because of the limited workspace coupled with singularities, the trajectory planning of parallel mechanisms is a difficult problem. Hence, it is highly desirable to develop an algorithm that can locate singularity-free zones in the workspace. This issue has attracted the attention of several researchers (see for instance, [2], [7], [31], [48]). Most studies addressing the trajectory planning formulate the following problem: given two end-effector poses, namely the initial and the final ones, a singularity-free path is constructed within the workspace connecting the two poses, which means, the trajectory of the end-effector is fixed for a prescribed task.

In a context of design and/or trajectory planning, an important problem is to find singularity-free zones in the workspace of the mechanism. In Chapters 3 to 5, algorithms are developed for the identification of singularity-free zones in the workspace of the planar $3-RPR$ parallel mechanisms and the general Gough-Stewart platform.

Several procedures adapted to different situations are developed. The procedures are mainly based on the use of Lagrange multipliers to transform the constrained problems into unconstrained problems. In principle, the procedure can be applied to any mechanism with a known singularity equation. More importantly, the procedures serve as a demonstration of how advanced mathematical techniques can be applied to trajectory planning problems. Since no assumption is made on the geometry of the mechanisms, the procedures can be extended to use with different parallel mechanisms.

In Chapter 3, planar 3-RPR parallel mechanisms, which have been studied in detail by several researchers (see for instance, [13], [44], [45]) are introduced. The kinematic and singularity analyses of the mechanisms are briefly recalled. The analytical expression of the singularity locus of the mechanism is obtained. Then, a procedure is presented to determine the maximal singularity-free zones for given ranges of rotation. Finally, applying the procedure, numerical examples are presented to illustrate the singularity-free zones with different ranges of the rotation variable.

In addition, the general Gough-Stewart platform is also studied using the same approach. Indeed, by fixing two of the three orientation variables and a position variable, the simplified singularity equation has a form similar to that of the planar 3-RPR parallel mechanisms. Graphical illustrations are presented to illustrate the singularity-free zones.

Inspired by these results, two procedures for locating the maximal singularity-free zones for both constant orientation and constant position of the general Gough-Stewart platform are presented in Chapter 4. For a constant orientation of the general Gough-Stewart platform, the new procedure is introduced to address the following problem: For a given position $(x_o, y_o,\ z_o)$ within the given workspace, find the largest singularity-free zone centred in $(x_o, y_o,\ z_o)$ in the (x, y, z) position space for the prescribed orientation. For a constant position of the general Gough-Stewart platform, another procedure is developed to address the following problem: For a given orientation (T_{1o}, T_{2o}, T_{3o}) within the given workspace, find the largest singularity-free zone centred in (T_{1o}, T_{2o}, T_{3o}) in the (T_1, T_2, T_3) orientation space for the prescribed position. Graphical illustrations are given to demonstrate the effectiveness of the procedures.

It is well known that one of the other main drawbacks of parallel mechanisms is their limited and complex workspace when compared to serial mechanisms. The determi-

nation of the workspace of parallel mechanisms has been studied by many researchers (see for instance, [12], [16], [25], [3], [4]). As the complete workspace of the general Gough-Stewart platform is a six-dimensional entity which is impossible to visualize, algorithms for *constant-orientation workspace* and *orientation workspace*, have been proposed by several researchers ([25], [36], [12], [30], [16], [29], [4], [40]). In Chapter 5, for the purpose of simplicity, first, we assume that the workspace of the general Gough-Stewart platform is known and is given with proper ranges of the six variables in 6-D space. Then, two new procedures are presented to determine the maximal singularity-free zones in given 3-D and 6-D workspaces, respectively. The procedure for locating the singularity-free zones in 3-D space is different from that of Chapters 3 and 4, and can be formulated as follows: For a given rotational/position ranges of motion $((T_{1min} \leq T_1 \leq T_{1max})$, $(T_{2min} \leq T_2 \leq T_{2max})$ and $(T_{3min} \leq T_3 \leq T_{3max}))/((x_{min} \leq x \leq x_{max})$, $(y_{min} \leq y \leq y_{max})$ and $(z_{min} \leq z \leq z_{max}))$ and a given center of position/orientation $(x_o, y_o, z_o)/(T_{1o}, T_{2o}, T_{3o})$ within a given workspace, find the largest singularity-free zone in 3-D position/orientation space, which is free from singularities with any orientation/position variables in the given ranges.

Finally, the procedure for locating the singularity-free zones in 6-D space is formulated as follows: For a given point $(x_o, y_o, z_o, T_{1o}, T_{2o}, T_{3o})$ within the 6-D workspace, find the maximal singularity-free zone in 6-D space centred in $(x_o, y_o, z_o, T_{1o}, T_{2o}, T_{3o})$.

Although the problems addressed in this thesis are formulated analytically, they also have geometric interpretations. Therefore, whenever possible, graphical representations will be used to illustrate the procedures as well as to verify the results. It is to be hoped that the results presented in this thesis will provide new tools for the design and trajectory planning of parallel mechanisms.

Chapter 2

Analytic Form of the Six-dimensional Singularity Locus of the General Gough-Stewart Platform

2.1 Introduction

A general Gough-Stewart platform is illustrated in Figure 1.2(b), in which the mobile platform is connected to the base by six identical legs. The Gough-Stewart platform is undoubtedly the best known parallel mechanism and has attracted considerable attention. It was extensively studied over the last decades. Pertaining to this mechanism, there are numerous research references on several topics, such as, inverse and

forward kinematic analysis (see for instance [11], [53], [20], [24], [22]) dynamics (see for instance, [27], [47]), workspace analysis (see for instance, [12], [54]), practical design/construction considerations (such as, [11]), calibration (such as, [57]), singularities (see for instance, [33], [28]) and a variety of applications (see for instance, [10], [8]).

In a context of design, the determination of the singular configurations of the mechanisms is an important issue. From a design point of view, it is desirable to obtain the analytical expression of the singularity locus of a mechanism. Then with a given set of design parameters, the designers can obtain a graphical representation of the singularity locus of the mechanism. In [44], [45], [50] and [51], the analytical singularity loci of the the 2-DOF and 3-DOF planar and spherical parallel mechanisms in the Cartesian space have been obtained, while the singularity loci equation of a spatial 4-DOF mechanism was presented in [52]. The singularities of Gough-Stewart platforms were addressed by several researchers (see for instance, [21], [11], [28], [18], [20]), However, for the general Gough-Stewart platform, only in [33] and [26] the analytical expression of singularity locus equation with constant orientation was presented. To the best of our knowlege, there is no reference available for the singularity locus equation of the general Gough-Stewart platform with six variables, i.e., three position variables and three orientation variables.

The determination of the expression of the singularity locus of the mechanisms is a powerful design tool since it provides an exact analytic form of the location of the singular configurations in the workspace of the mechanisms. This expression helps the designer to determine the exact locus of the singular configurations of a particular design and hence determine whether or not singularities are encountered within the workspace.

2.2 Kinematic analysis

Kinematics deals with the aspects of motion without regard to the forces and/or torques that cause it. The science of kinematics deals with the position, velocity, acceleration, and higher-order derivatives of the position variables with respect to time or other variables, which is important in the study of mechanisms. A better understanding of the kinematics is the first concern in the design and control of robotic mechanisms.

Usually, the kinematic analysis consists of the *forward kinematics* and the *inverse kinematics*. For a given mechanism, typically a set of desired positions and/or orientations, and perhaps the time derivatives of the positions and/or orientations of the end effector, are specified in space. The problem is to find all possible sets of actuated joint variables and their corresponding time derivatives which will bring the end effector to the set of desired positions and/or orientations with the desired motion characteristics. This is known as *inverse kinematics*. On the other hand, sometimes the actuated joint variables and possibly the time derivatives are obtained from the reading of sensors installed at the joints, from which we wish to find all possible sets of end-effector positions and/or orientations and their corresponding time derivatives. This is called *direct kinematics*. Unlike serial mechanisms, the direct kinematic analysis of parallel mechanisms is more complex than its inverse kinematic analysis. For example, for the general Gough-Stewart platform, the inverse kinematic analysis is very simple while the direct kinematic analysis is extremely difficult and only numerical solutions can be obtained. Fortunately, the solution of the direct kinematics of a parallel mechanism is not necessary for its kinematic design, and is not discussed here. Therefore, the kinematic analysis presented here consists of the inverse kinematics, the velocity equations and the singularity analysis of the general Gough-Stewart platform.

2.2.1 Inverse kinematics and the velocity equations

As shown in Figure 2.1, the general Gough-Stewart platform consists of a mobile platform $P_1P_2P_3P_4P_5P_6$ and a base $B_1B_2B_3B_4B_5B_6$ connected via six identical UPS legs (B_iP_i). Here U denotes a Hooke joint and S represents a spherical joint, which are passive, while P denotes an actuated prismatic joint. For the general Gough-Stewart platform, the attachment points of $B_i, i = 1, .., 6$, on the base do not need to necessarily lie on the same plane, likewise for the attachment points of $P_i, i = 1, .., 6$, on the platform. The distance between B_i and P_i, noted ρ_i, is the leg length. Hence, the mechanism has six degrees of freedom and can be controlled by adjusting the length of the six legs. Since no specific assumptions are made on the geometry, the procedures developed in this thesis can be used for any Gough-Stewart platform.

In Figure. 2.1, a reference frame $\mathcal{R}(Oxyz)$ is attached to the base and a mobile frame $\mathcal{R}'(O'x'y'z')$ is attached to the moving platform. The position of point B_i on the

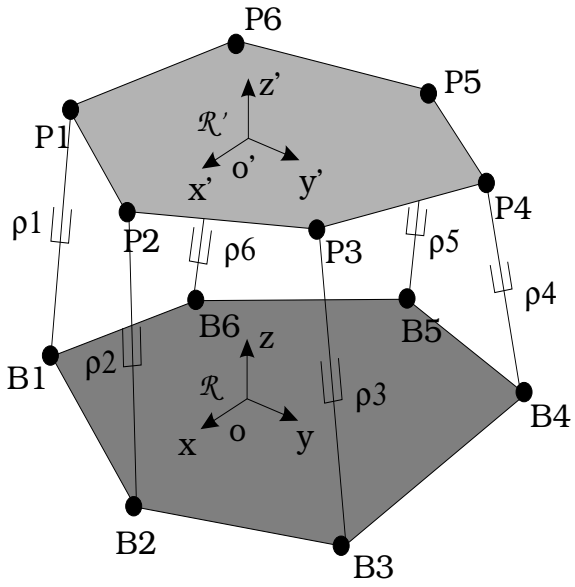

Figure 2.1: Notation used for the general Gough-Stewart platform.

base in frame $\mathcal{R}$ is denoted by vector $\mathbf{b}_i = [b_{ix}, b_{iy}, b_{iz}]^T$, $i = 1, \ldots, 6$, and the position of point P_i in frame $\mathcal{R}'$ is denoted by vector $\mathbf{p}'_i = [p'_{ix}, p'_{iy}, p'_{iz}]^T$, $i = 1, \ldots, 6$, which is constant in the mobile frame. Vector $\mathbf{s} = [x, y, z]^T$ denotes the coordinates of O' in the reference frame, vector $\boldsymbol{\omega}$ denotes the angular velocity of the mobile platform and matrix $\mathbf{Q}$ represents the rotation from the reference frame $\mathcal{R}$ to the mobile frame $\mathcal{R}'$.

The inverse kinematic problem of the general Gough-Stewart platform is readily solved, here a brief recall is presented. From the above notation, we know that the position vector of point P_i expressed in the reference frame $\mathcal{R}$ denoted by $\mathbf{p}_i$ is given by:

$$\mathbf{p}_i = \mathbf{s} + \mathbf{Q}\mathbf{p}'_i, \qquad i = 1, \ldots, 6 \tag{2.1}$$

Subtracting vector $\mathbf{b}_i$ from both sides of eq. (2.1), one obtains:

$$\mathbf{p}_i - \mathbf{b}_i = \mathbf{s} + \mathbf{Q}\mathbf{p}'_i - \mathbf{b}_i, \qquad i = 1, \ldots, 6 \tag{2.2}$$

where the left-hand side represents a vector connecting point B_i to point P_i, along the ith leg. Hence, taking the Euclidean norm of both sides of eq. (2.2) leads to:

$$\begin{aligned} \rho_i^2 &= \|\mathbf{p}_i - \mathbf{b}_i\|^2, \quad i = 1, \ldots, 6 \\ &= (\mathbf{s} + \mathbf{Q}\mathbf{p}'_i - \mathbf{b}_i)^T(\mathbf{s} + \mathbf{Q}\mathbf{p}'_i - \mathbf{b}_i), i = 1, \ldots, 6 \end{aligned} \tag{2.3}$$

Differentiating both sides of eq. (2.3) with respect to time, following the formalism proposed in Gosselin and Angeles [14] for parallel mechanisms, two Jacobian matrices

$\mathbf{A}$ and $\mathbf{B}$ are obtained and the velocity equation can be written as:

$$\mathbf{A}\mathbf{t} = \mathbf{B}\dot{\boldsymbol{\rho}} \tag{2.4}$$

where $\mathbf{t}$ is the six-dimensional twist of the platform and $\dot{\boldsymbol{\rho}}$ is the vector of joint velocities. These vectors are defined as:

$$\mathbf{t} = [\dot{\mathbf{s}}^T, \boldsymbol{\omega}^T]^T \tag{2.5}$$

$$\dot{\boldsymbol{\rho}} = [\dot{\rho}_1, \ldots, \dot{\rho}_6]^T \tag{2.6}$$

Hence, the aforementioned Jacobian matrices can be written as:

$$\mathbf{B} = \mathrm{diag}(\rho_1, \ldots, \rho_6) \tag{2.7}$$

and

$$\mathbf{A} = \begin{bmatrix} \mathbf{c}_1^T \\ \vdots \\ \mathbf{c}_6^T \end{bmatrix} \tag{2.8}$$

with

$$\mathbf{c}_i = [(\mathbf{p}_i - \mathbf{b}_i)^T, (\mathbf{Q}\mathbf{p}_i' \times (\mathbf{p}_i - \mathbf{b}_i))^T]^T, i = 1, \ldots, 6 \tag{2.9}$$

Finally, the rotation matrix $\mathbf{Q}$ representing the orientation of the platform with respect to the base can be written as a function of the well-known Euler angles [43]:

$$\mathbf{Q} = \begin{bmatrix} \cos\theta\cos\psi & (\cos\psi\sin\theta\sin\phi & (\cos\psi\sin\theta\cos\phi \\ & -\sin\psi\cos\phi) & +\sin\psi\sin\phi) \\ \cos\theta\sin\psi & (\sin\psi\sin\theta\sin\phi & (\sin\psi\sin\theta\cos\phi \\ & +\cos\psi\cos\phi) & -\cos\psi\sin\phi) \\ -\sin\theta & \cos\theta\sin\phi & \cos\theta\cos\phi \end{bmatrix}$$

where ψ, θ, ϕ are the three Euler angles defined according to the convention $(\mathbf{Q}_z, \mathbf{Q}_y, \mathbf{Q}_x)$, i.e., the mobile frame is derived from the reference frame by first a rotation around the z-axis with an angle ψ, then a rotation around the new y-axis with an angle θ, and finally a rotation around the new x-axis with an angle ϕ.

2.2.2 Singularity analysis

Considering the velocity equation obtained above in eq. (2.4), three types of singularities, each of which having a different physical interpretation, have been defined by

Gosselin and Angeles [14]. These singularities occur, respectively, when (1) matrix B is singular, (2) matrix A is singular or (3) the nonlinear kinematic constraints degenerate. As pointed out in [14], only the first type of singularity is possible for serial mechanisms. The physical interpretation of each of the three types of singularity is given in detail in the same reference. They are briefly repeated here for quick reference.

2.2.3 Singularity of type I

Referring to eq. (2.4), the singularity of type I occur when we have:

$$\det(\mathbf{B}) = 0$$

The corresponding configurations are located at the boundaries of the workspace of the mechanism or on the internal boundaries between regions of the workspace in which the number of solutions of the inverse kinematic problem is different. Moreover, since the nullspace of $\mathbf{B}$ is not empty, there exist nonzero input vectors which will result in a vanishing Cartesian velocity output. In other words, some velocities cannot be produced at the end-effector. This type of singularities leads to a simple expression that is easily obtained and avoided.

2.2.4 Singularity of type II

Referring to eq. (2.4) again, the singularities of type II occur when matrix $\mathbf{A}$ is rank-deficient:

$$\det(\mathbf{A}) = 0$$

As opposed to the singularities of type I, this type of singularity can occur inside the mechanism's Cartesian workspace and will correspond to the set of configurations for which two different branches of the direct kinematic problem meet. In fact, this is why this type of singularities cannot occur for serial mechanisms since the direct kinematic problem always leads to a unique solution. Since the nullspace of matrix $\mathbf{A}$ is not empty, there exist nonzero Cartesian output which will be mapped into a vanishing input. The corresponding configuration will be one in which an infinitesimal motion of the end-effector is possible even if the actuators are locked.

2.2.5 Singularity of type III

This type of singularity occur when both **A** and **B** become simultaneously singular. Such singularities will lead to configurations where a finite motion of the end effector is possible even if the actuators are locked or in situations where a finite motion of the actuators produces no motion of the end effector. In both cases, the mechanism cannot be controlled. This kind of singularity can be easily avoided as singularity of type I.

2.2.6 Constraint singularity

In [56], a new type of singularity was identified, which is called constraint singularity. As the constraint singularity analysis of a parallel mechanism is input independent, it can be performed before the kinematic analysis. A constraint singularity can occur only in a parallel mechanism with the degree of freedom of the platform, n, lower than the number of joints in any leg. In screw theory, the motion and constraints of a kinematic chain are represented by screw systems, which are termed as twist systems and wrench systems respectively. When a mechanism is at constraint singularities, the screw system of the constraint wrenches degenerates and becomes of a dimension lower than $6 - n$. As a result, the system of output freedoms instantaneously increases its dimension. Hence, both the mechanism as a whole and the platform have at least $n + 1$ DOF. The extra freedom of the platform may or may not be controlled by the actuators.

For the general Gough-Stewart platform, this type of singularity does not occur. The classification presented above is general and can be applied to any closed-loop mechanism. In this chapter and throughout this thesis, the singularities of type II, also called RO (Redundant Output) in Zlatanov, Fenton, Benhabib [55]— which corresponds to configurations in which the stiffness of the mechanism is locally lost— are the focus of our study.

2.3 Linear decomposition of the determinant

It is well known that a condition for a matrix to be singular is that its determinant be equal to zero. In this chapter this property will be used to obtain the algebraic condition for the Gough-Stewart platform to be in a singular configuration. To this end, a linear decomposition of the determinant will be used. In order to clearly illustrate the approach that is used to expand the determinant of the 6×6 Jacobian matrix $\mathbf{A}$, a simple 2×2 matrix $\mathbf{V}$ is first introduced. Let:

$$\mathbf{V} = \begin{bmatrix} (S_1 + x), & (T_1 x - S_1 y + z) \\ (S_2 + x), & (T_2 x - S_2 y + z) \end{bmatrix}$$

According to the method of linear decomposition of the determinant, an important property of the determinant is that it depends linearly on any of its columns [42]. This property is used here to expand the determinant of $\mathbf{V}$. First, matrix $\mathbf{V}$ is rewritten as:

$$\begin{aligned} \mathbf{V} &= [\,(\mathbf{s} + \mathbf{n}x), \quad (\mathbf{t}x - \mathbf{s}y + \mathbf{n}z)\,] \\ &= [\,\mathbf{v}_1, \quad \mathbf{v}_2\,] \end{aligned}$$

where vectors $\mathbf{s}$, $\mathbf{t}$ and $\mathbf{n}$ are defined as follows:

$$\begin{aligned} \mathbf{s} &= [\,S_1, \quad S_2\,]^T \\ \mathbf{t} &= [\,T_1, \quad T_2\,]^T \\ \mathbf{n} &= [\,1, \quad 1\,]^T \end{aligned}$$

Using this notation, the determinant of matrix $\mathbf{V}$ can be expanded as follows:

$$\begin{aligned} \det(\mathbf{V}) &= |\,\mathbf{v}_1 \quad \mathbf{v}_2\,| \\ &= |\,\mathbf{s} \quad \mathbf{t}x\,| + |\,\mathbf{s} \quad -\mathbf{s}y\,| + |\,\mathbf{s} \quad \mathbf{n}z\,| + |\,\mathbf{n}x \quad \mathbf{t}x\,| \\ &\quad + |\,\mathbf{n}x \quad -\mathbf{s}y\,| + |\,\mathbf{n}x \quad \mathbf{n}z\,| \\ &= |\mathbf{s} \quad \mathbf{t}|x - |\mathbf{s} \quad \mathbf{s}|y + |\mathbf{s} \quad \mathbf{n}|z + |\mathbf{n} \quad \mathbf{t}|x^2 \\ &\quad - |\mathbf{n} \quad \mathbf{s}|xy + |\mathbf{n} \quad \mathbf{n}|xz \end{aligned}$$

where $|\mathbf{s} \quad \mathbf{t}|$ stands for the determinant of the matrix formed with columns $\mathbf{s}$ and $\mathbf{t}$. Hence, the determinant of matrix $\mathbf{V}$ defined above is written as the sum of $2 \times 3 = 6$ determinants. By inspection of the above expression, it is clear that two of the determinants vanish, namely, $|\mathbf{n} \quad \mathbf{n}|xz$ and $|\mathbf{s} \quad \mathbf{s}|y$, since the two columns of the matrices are linearly dependent. Then, one has $\det(\mathbf{V}) = |\mathbf{s} \quad \mathbf{t}|x + |\mathbf{s} \quad \mathbf{n}|z + |\mathbf{n} \quad \mathbf{t}|x^2 - |\mathbf{n} \quad \mathbf{s}|xy = (S_1 T_2 - S_2 T_1)x + (S_1 - S_2)z + (T_2 - T_1)x^2 - (S_2 - S_1)xy$. Note that the order of the two columns in each determinant must be preserved.

Note 1: the determinant of matrix $\mathbf{V}$ defined above can be thought of as the direct multiplication of its two columns, namely, $(\mathbf{s}+\mathbf{n}x)$ and $(\mathbf{t}x-\mathbf{s}y+\mathbf{n}z)$. Therefore, $\det(\mathbf{V})$ can be written as the sum of $2 \times 3 = 6$ determinants.

Note 2: if any vector appears more than once in a determinant, then the determinant will vanish, because of the dependence of the columns, such as $|\mathbf{n} \quad \mathbf{n}|xz = 0$.

Note 3: in order to correctly expand the matrix, the order of the columns in each determinant must be preserved.

2.4 Expansion of matrix A of the general Gough-Stewart platform

The above approach is now applied to expand the determinant of the Jacobian matrix $\mathbf{A}$ of the general Gough-Stewart platform. Matrix $\mathbf{A}$ can be written in the following form according to eq. (2.8) and eq. (2.9):

$$\mathbf{A} = [\,\mathbf{e}_1 \quad \mathbf{e}_2 \quad \mathbf{e}_3 \quad \mathbf{e}_4 \quad \mathbf{e}_5 \quad \mathbf{e}_6\,] \tag{2.10}$$

where $\mathbf{e}_i$, $i = 1, \ldots, 6$, are the six columns of matrix $\mathbf{A}$, and they are constructed using the following vectors and scalars:

$$\begin{aligned}
\mathbf{e}_1 &= \mathbf{a}_1 q_{11} + \mathbf{a}_2 q_{12} + \mathbf{a}_3 q_{13} - \mathbf{d}_1 + \mathbf{u}x \\
\mathbf{e}_2 &= \mathbf{a}_1 q_{21} + \mathbf{a}_2 q_{22} + \mathbf{a}_3 q_{23} - \mathbf{d}_2 + \mathbf{u}y \\
\mathbf{e}_3 &= \mathbf{a}_1 q_{31} + \mathbf{a}_2 q_{32} + \mathbf{a}_3 q_{33} - \mathbf{d}_3 + \mathbf{u}z \\
\mathbf{e}_4 &= \mathbf{a}_1(zq_{21} - yq_{31}) + \mathbf{a}_2(zq_{22} - yq_{32}) + \mathbf{a}_3(zq_{23} - yq_{33}) \\
&\quad + \mathbf{a}_{51} q_{31} + \mathbf{a}_{52} q_{32} + \mathbf{a}_{53} q_{33} - \mathbf{a}_{61} q_{21} - \mathbf{a}_{62} q_{22} - \mathbf{a}_{63} q_{23} \\
\mathbf{e}_5 &= \mathbf{a}_1(xq_{31} - zq_{11}) + \mathbf{a}_2(xq_{32} - zq_{12}) + \mathbf{a}_3(xq_{33} - zq_{13}) \\
&\quad - \mathbf{a}_{41} q_{31} - \mathbf{a}_{42} q_{32} - \mathbf{a}_{43} q_{33} + \mathbf{a}_{61} q_{11} + \mathbf{a}_{62} q_{12} + \mathbf{a}_{63} q_{13} \\
\mathbf{e}_6 &= \mathbf{a}_1(yq_{11} - xq_{21}) + \mathbf{a}_2(yq_{12} - xq_{22}) + \mathbf{a}_3(yq_{13} - xq_{23}) \\
&\quad + \mathbf{a}_{41} q_{21} + \mathbf{a}_{42} q_{22} + \mathbf{a}_{43} q_{23} - \mathbf{a}_{51} q_{11} - \mathbf{a}_{52} q_{12} - \mathbf{a}_{53} q_{13}
\end{aligned}$$

where q_{ij} is the ijth element of matrix $\mathbf{Q}$ and where $\mathbf{a}_i$ and $\mathbf{d}_i$, $i = 1, 2, 3$, are 6×1 vectors of architectural parameters defined as:

$$\mathbf{a}_1 = [p'_{1x}, \quad p'_{2x}, \quad p'_{3x}, \quad p'_{4x}, \quad p'_{5x}, \quad p'_{6x}]^T$$

$$\mathbf{a}_2 = [p'_{1y}, \quad p'_{2y}, \quad p'_{3y}, \quad p'_{4y}, \quad p'_{5y}, \quad p'_{6y}]^T$$
$$\mathbf{a}_3 = [p'_{1z}, \quad p'_{2z}, \quad p'_{3z}, \quad p'_{4z}, \quad p'_{5z}, \quad p'_{6z}]^T$$
$$\mathbf{d}_1 = [b_{1x}, \quad b_{2x}, \quad b_{3x}, \quad b_{4x}, \quad b_{5x}, \quad b_{6x}]^T$$
$$\mathbf{d}_2 = [b_{1y}, \quad b_{2y}, \quad b_{3y}, \quad b_{4y}, \quad b_{5y}, \quad b_{6y}]^T$$
$$\mathbf{d}_3 = [b_{1z}, \quad b_{2z}, \quad b_{3z}, \quad b_{4z}, \quad b_{5z}, \quad b_{6z}]^T$$

Moreover, vectors $\mathbf{a}_{4i}$, $\mathbf{a}_{5i}$, $\mathbf{a}_{6i}$, $i = 1, 2, 3$, are vectors containing combinations of architectural parameters defined as:

$$\mathbf{a}_{41} = [p'_{1x}b_{1x}, \quad p'_{2x}b_{2x}, \quad p'_{3x}b_{3x}, \quad p'_{4x}b_{4x}, \quad p'_{5x}b_{5x}, \quad p'_{6x}b_{6x}]^T$$
$$\mathbf{a}_{42} = [p'_{1y}b_{1x}, \quad p'_{2y}b_{2x}, \quad p'_{3y}b_{3x}, \quad p'_{4y}b_{4x}, \quad p'_{5y}b_{5x}, \quad p'_{6y}b_{6x}]^T$$
$$\mathbf{a}_{43} = [p'_{1z}b_{1x}, \quad p'_{2z}b_{2x}, \quad p'_{3z}b_{3x}, \quad p'_{4z}b_{4x}, \quad p'_{5z}b_{5x}, \quad p'_{6z}b_{6x}]^T$$
$$\mathbf{a}_{51} = [p'_{1x}b_{1y}, \quad p'_{2x}b_{2y}, \quad p'_{3x}b_{3y}, \quad p'_{4x}b_{4y}, \quad p'_{5x}b_{5y}, \quad p'_{6x}b_{6y}]^T$$
$$\mathbf{a}_{52} = [p'_{1y}b_{1y}, \quad p'_{2y}b_{2y}, \quad p'_{3y}b_{3y}, \quad p'_{4y}b_{4y}, \quad p'_{5y}b_{5y}, \quad p'_{6y}b_{6y}]^T$$
$$\mathbf{a}_{53} = [p'_{1z}b_{1y}, \quad p'_{2z}b_{2y}, \quad p'_{3z}b_{3y}, \quad p'_{4z}b_{4y}, \quad p'_{5z}b_{5y}, \quad p'_{6z}b_{6y}]^T$$
$$\mathbf{a}_{61} = [p'_{1x}b_{1z}, \quad p'_{2x}b_{2z}, \quad p'_{3x}b_{3z}, \quad p'_{4x}b_{4z}, \quad p'_{5x}b_{5z}, \quad p'_{6x}b_{6z}]^T$$
$$\mathbf{a}_{62} = [p'_{1y}b_{1z}, \quad p'_{2y}b_{2z}, \quad p'_{3y}b_{3z}, \quad p'_{4y}b_{4z}, \quad p'_{5y}b_{5z}, \quad p'_{6y}b_{6z}]^T$$
$$\mathbf{a}_{63} = [p'_{1z}b_{1z}, \quad p'_{2z}b_{2z}, \quad p'_{3z}b_{3z}, \quad p'_{4z}b_{4z}, \quad p'_{5z}b_{5z}, \quad p'_{6z}b_{6z}]^T$$

and vector $\mathbf{u}$ is defined as:

$$\mathbf{u} = [1 \quad 1 \quad 1 \quad 1 \quad 1 \quad 1]^T$$

Expanding matrix $\mathbf{A}$ according to the linear decomposition presented in the previous section, there will be a sum of at least $5 \times 5 \times 5 \times 9 \times 9 \times 9 = 91125$ determinants. However, all the terms in which a column appears more than once will vanish. The challenge is to identify the nonzero determinants and to preserve the order of columns in each determinant automatically. In the following subsection, a simple example matrix $\mathbf{A}'$, with a form similiar to that of matrix $\mathbf{A}$ is used to illustrate the procedure employed to expand matrix $\mathbf{A}$.

2.4.1 Expansion algorithm

First, assume that matrix $\mathbf{A}'$ is a 3×3 matrix with the following form:

$$\mathbf{A}' = [\,\mathbf{e}_1' \quad \mathbf{e}_2' \quad \mathbf{e}_3'\,]$$

where $\mathbf{e}_i'$, $i = 1, 2, 3$, are the three columns of matrix $\mathbf{A}'$, and they are constructed using the following vectors and scalars:

$$\begin{aligned}
\mathbf{e}_1' &= -\mathbf{a}_2' \cos\theta \cos\psi + \mathbf{d}_1' x \cos\theta \sin\psi - \mathbf{a}_3' \sin\theta \\
\mathbf{e}_2' &= \mathbf{a}_3'(\cos\psi \sin\theta \sin\phi - \sin\psi \cos\phi) - \mathbf{a}_1'(\sin\psi \sin\theta \sin\phi + \cos\psi \cos\phi) \\
&\quad + \mathbf{d}_2' y \cos\theta \sin\phi \\
\mathbf{e}_3' &= \mathbf{d}_3' z(\cos\psi \sin\theta \cos\phi + \sin\psi \sin\theta) + \mathbf{a}_1'(\sin\psi \sin\theta \cos\phi - \cos\psi \cos\phi) \\
&\quad - \mathbf{a}_2' \cos\theta \cos\phi
\end{aligned}$$

where $\mathbf{a}_i'$ and $\mathbf{d}_{i-}$, $i = 1, 2, 3$, are 3×1 vectors of architectural parameters, and ψ, θ and ϕ are the three Euler angles.

A total of 6 steps will be used to illustrate how to expand matrix $\mathbf{A}'$.

Step 1: decompose each column of matrix $\mathbf{A}'$, $\mathbf{e}_i'$, into two parts, the vector part V_i and the scalar part S_i, as follows:

$$\begin{aligned}
\mathbf{e}_1' \longleftrightarrow \quad V_1 &= [-\mathbf{a}_2' \quad \mathbf{d}_1' \quad -\mathbf{a}_3'] \\
S_1 &= [\cos\theta \cos\psi \quad x \cos\theta \sin\psi \quad \sin\theta] \\
\mathbf{e}_2' \longleftrightarrow \quad V_2 &= [\mathbf{a}_3' \quad -\mathbf{a}_3' \quad -\mathbf{a}_1' \quad -\mathbf{a}_1' \quad \mathbf{d}_2'] \\
S_2 &= [\cos\psi \sin\theta \sin\phi \quad \sin\psi \cos\phi \quad \sin\psi \sin\theta \sin\phi \quad \cos\psi \cos\phi \\
&\quad y \cos\theta \sin\phi] \\
\mathbf{e}_3' \longleftrightarrow \quad V_3 &= [\mathbf{d}_3' \quad \mathbf{d}_3' \quad \mathbf{a}_1' \quad -\mathbf{a}_1' \quad -\mathbf{a}_2'] \\
S_3 &= [z \cos\psi \sin\theta \cos\phi \quad z \sin\psi \sin\theta \quad \sin\psi \sin\theta \cos\phi \quad \cos\psi \cos\phi \\
&\quad \cos\theta \cos\phi]
\end{aligned}$$

According to the foregoing example, there should be $3 \times 5 \times 5 = 75$ determinants when expanding matrix $\mathbf{A}'$, and some of them vanish because of the linear dependence of the columns.

Step 2: assign the following integer numbers to the vectors and scalars:

$$\mathbf{a}_1' \to 1, \quad \mathbf{a}_2' \to 2, \quad \mathbf{a}_3' \to 4,$$

$$\mathbf{d}_1{}' \to 8, \quad \mathbf{d}_2{}' \to 16, \quad \mathbf{d}_3{}' \to 32,$$

$$\sin\theta \to 1, \quad \cos\theta \to 10, \quad \sin\psi \to 100, \quad \cos\psi \to 1000,$$

$$\sin\phi \to 10000, \quad \cos\phi \to 100000,$$

$$x \to 1000000, \quad y \to 10000000, \quad z \to 100000000.$$

In other words, use the powers of 2 for the vectors and the powers of 10 for the scalars. The reasons for assigning the above numbers are:

1. For vectors, if we know the sum of the numbers associated with the vectors in a given combination, then the exact vectors can be identified. For example, if the sum is 21, then we immediately know that it is constituted by 1, 4, and 16. Hence, as shown in the following steps, if any two or more sums are the same, it is clear that the corresponding terms contain the same vectors, although maybe in different orders. This result will be helpful to simplify the final expression of the singularity locus.

2. For scalars, adding up the corresponding elements of the vector part in the scalar part allows the identification of the scalar expressions in the corresponding term. For example, if one of the determinants consists of three columns: the first column from the first element of V_1 is $-\mathbf{a}_2{}'$, the second column from the first element of V_2 is $\mathbf{a}_3{}'$, and the last column from the first element of V_3 is $\mathbf{d}_3{}'$, then, the scalar part on the same row is constructed by the sum of the first element of S_1, the first element of S_2 and the first element of S_3. The result is 100113012, which represents $z\cos\phi\sin\phi\cos^3\psi\cos\theta\sin^2\theta$, the latter expression being the proper scalar expression appearing in the determinant.

Step 3: construct Table 2.1, which consists of two parts: the V part (abbreviated from Vector part), and the S part (abbreviated from Scalar part).

1. V part:

   C_1, C_2, C_3: represent the integer number of the three vector columns of each determinant.

	V part					S part			
No.	C_1	C_2	C_3	$Check$	$Sum1$	C_1'	C_2'	C_3'	$Sum2$
1	-2	4	32	1	38	1010	11001	100101001	100113012
2	-2	4	32	1	38	1010	11001	100000101	100012112
3	-2	4	1	1	7	1010	11001	100101	112112
4	-2	4	-1	1	7	1010	11001	101000	113011
5	-2	4	-2	0					
6	-2	-4	32	1	38	1010	100100	100101001	100202111
7	-2	-4	32	1	38	1010	100100	100000101	100101211
8	-2	-4	1	1	7	1010	100100	100101	201211
9	-2	-4	-1	1	7	1010	100100	101000	202110
10	-2	-4	-2	0					
⋮									
74	-4	16	-1	1	21	1	10010010	101000	10111011
75	-4	16	-2	1	22	1	10010010	100010	10110021

Table 2.1: Expansion of the determinant of the matrix $\mathbf{A}'$ in assigned numbers.

$Check$: if there are two linearly dependent columns, then the determinant will be zero, if so this index is set to 0, otherwise it is 1.

$Sum1$: add up the absolute values of the three numbers in columns C_1, C_2 and C_3 in the V part.

2. S part:

   C_1', C_2', C_3': represent the corresponding three columns in the S part. If the number in the $Check$ column is 1, then add all the numbers on that row, otherwise omit these numbers.

   $Sum2$: add up the three numbers in the three columns of this part together. This number represents the combinations of the *sine* and *cosine* of Euler angles and position variables x, y and z.

Step 4: simplify the results in both the V and the S part, and construct Table 2.2.

1. V part:

Sign: is equal to $(-1)^{m+n}$ in which m denotes the number of negative numbers among the three columns and n denotes the number of permutations required to rearrange the three numbers in ascending order.

Eliminate all the rows for which the *Check* column is 0, then start from the second row to check if there are any rows that have the same $Sum1$ as row 1, if so then change the $\det \mathbf{M}_i$ column into the same order, that is $\det \mathbf{M}_1$. Then, define the nearest row, whose sum is different from row 1, as $\det \mathbf{M}_2$, and repeat the same process, until we have the smallest number of rows in the table, i.e.,

$$\begin{aligned} \det \mathbf{M}_1 &= \det([\mathbf{a}_2{}' \quad \mathbf{a}_3{}' \quad \mathbf{d}_3{}']) \\ \det \mathbf{M}_2 &= \det([\mathbf{a}_1{}' \quad \mathbf{a}_2{}' \quad \mathbf{a}_3{}']) \\ &\vdots \\ \det \mathbf{M}_{17} &= \det([\mathbf{a}_2{}' \quad \mathbf{a}_3{}' \quad \mathbf{d}_2{}']) \end{aligned}$$

2. S part: change all the $\sin\theta$, $\sin\psi$, $\sin\phi$ whose degrees are more than one into the corresponding $\cos\theta$, $\cos\psi$, $\cos\phi$, that is, $\sin^2\theta = 1 - \cos^2\theta$, $\sin^3\theta = \sin\theta - \sin\theta\cos^2\theta$, $\sin^2\psi = 1 - \cos^2\psi$, $\sin^3\psi = \sin\psi - \sin\psi\cos^2\psi$, $\sin^2\phi = 1 - \cos^2\phi$, $\sin^3\phi = \sin\phi - \sin\phi\cos^2\phi$, likewise for higher degrees of $\sin\theta$, $\sin\psi$ and $\sin\phi$. For example, in the first row in Table 2.1, the S part 100113012 is then changed to 100113010-100113030, which represents $z\cos\phi\sin\phi\cos^3\psi\cos\theta\sin^2\theta = z\cos\phi\sin\phi\cos^3\psi\cos\theta - z\cos\phi\sin\phi\cos^3\psi\cos^3\theta$, as shown in Table 2.2.

Step 5: check the S part of Table 2.2: if numbers have been rewritten in two parts, separate the parts and put the negative numbers before them in the *Sign* column to obtain Table 2.3.

Step 6: check in Table 2.3 to see if there are any rows having the same S part, if so regroup the identical terms as follows, $K_j = a \cdot \det \mathbf{M}_i + b \cdot \det \mathbf{M}_{i+1} + c \cdot \det \mathbf{M}_{i+2} \ldots$. ($a, b, c$ here are integer numbers, which may be positive or negative). Finally, the analytical expression of the expansion of the determinant of Jacobian matrix $\mathbf{A}'$ is obtained, which has the following form:

$$F = \sum_j K_j \cdot (S \text{ part})_j$$

$\det \mathbf{M}_i$	V part					S part
i	columns			$Sum1$	$Sign$	
1	$\mathbf{a}_2{}'$	$\mathbf{a}_3{}'$	$\mathbf{d}_3{}'$	38	-1	100113012=100113010-100113030
	2	4	32			$= z\cos\phi\sin\phi\cos^3\psi\cos\theta$
						$-z\cos\phi\sin\phi\cos^3\psi\cos^3\theta$
				38	-1	100012112=100012110-100012130
						$= z\sin\phi\cos^2\psi\sin\psi\cos\theta$
						$-z\sin\phi\cos^2\psi\sin\psi\cos^3\theta$
				38	1	$100202111=z\cos^2\phi\cos^2\psi\sin\psi\cos\theta\sin\theta$
				38	1	100101211=100101011-100103011
						$= z\cos\phi\cos\psi\cos\theta\sin\theta$
						$-z\cos\phi\cos^3\psi\cos\theta\sin\theta$
2	$\mathbf{a}_1{}'$	$\mathbf{a}_2{}'$	$\mathbf{a}_3{}'$	7	-1	112112=112110-112130
	1	2	4			$= \cos\phi\sin\phi\cos^2\psi\sin\psi\cos\theta$
						$-\cos\phi\sin\phi\cos^2\psi\sin\psi\cos^3\theta$
				7	1	$113011=\cos\phi\sin\phi\cos^3\psi\cos\theta\sin\theta$
				7	1	201211=201011-203011
						$= \cos^2\phi\cos\psi\cos\theta\sin\theta$
						$-\cos^2\phi\cos^3\psi\cos\theta\sin\theta$
				7	-1	$202110=\cos^2\phi\cos^2\psi\sin\psi\cos\theta$
...						
16	$\mathbf{a}_1{}'$	$\mathbf{a}_3{}'$	$\mathbf{d}_2{}'$	21	-1	10110112=10110110-10110130
	1	4	16			$= y\cos\phi\sin\phi\sin\psi\cos\theta$
						$-y\cos\phi\sin\phi\sin\psi\cos^3\theta$
				21	1	$10111011=y\cos\phi\sin\phi\cos\psi\cos\theta\sin\theta$
17	$\mathbf{a}_2{}'$	$\mathbf{a}_3{}'$	$\mathbf{d}_2{}'$	22	1	$10110021=y\cos\phi\sin\phi\cos^2\theta\sin\theta$
	2	4	16			

Table 2.2: All the determinants that are not equal to zero.

$\det \mathbf{M}_i$	V part					S part
i	columns			$Sum1$	$Sign$	
1	$\mathbf{a}_2{}'$ 2	$\mathbf{a}_3{}'$ 4	$\mathbf{d}_3{}'$ 32	38	-1	$100113010 = z\cos\phi\sin\phi\cos^3\psi\cos\theta$
				38	1	$100113030 = z\cos\phi\sin\phi\cos^3\psi\cos^3\theta$
					-1	$100012110 = z\sin\phi\cos^2\psi\sin\psi\cos\theta$
					1	$100012130 = z\sin\phi\cos^2\psi\sin\psi\cos^3\theta$
					1	$100202111 = z\cos^2\phi\cos^2\psi\sin\psi\cos\theta\sin\theta$
					1	$100101011 = z\cos\phi\cos\psi\cos\theta\sin\theta$
					-1	$100103011 = z\cos\phi\cos^3\psi\cos\theta\sin\theta$
2	$\mathbf{a}_1{}'$ 1	$\mathbf{a}_2{}'$ 2	$\mathbf{a}_3{}'$ 4	7	-1	$112110 = \cos\phi\sin\phi\cos^2\psi\sin\psi\cos\theta$
					1	$112130 = \cos\phi\sin\phi\cos^2\psi\sin\psi\cos^3\theta$
					1	$113011 = \cos\phi\sin\phi\cos^3\psi\cos\theta\sin\theta$
					1	$201011 = \cos^2\phi\cos\psi\cos\theta\sin\theta$
					-1	$203011 = \cos^2\phi\cos^3\psi\cos\theta\sin\theta$
					-1	$202110 = \cos^2\phi\cos^2\psi\sin\psi\cos\theta$
...						
16	$\mathbf{a}_1{}'$ 1	$\mathbf{a}_3{}'$ 4	$\mathbf{d}_2{}'$ 16	21	-1	$10110110 = y\cos\phi\sin\phi\sin\psi\cos\theta$
					1	$10110130 = y\cos\phi\sin\phi\sin\psi\cos^3\theta$
					1	$10111011 = y\cos\phi\sin\phi\cos\psi\cos\theta\sin\theta$
17	$\mathbf{a}_2{}'$ 2	$\mathbf{a}_3{}'$ 4	$\mathbf{d}_2{}'$ 16	22	1	$10110021 = y\cos\phi\sin\phi\cos^2\theta\sin\theta$

Table 2.3: Separation of the S part of Table2.

2.4.2 Application of the algorithm to the Jacobian matrix of the general Gough-Stewart platform

The procedure defined above can be used to expand the determinant of the Jacobian matrix $\mathbf{A}$ of the general Gough-Stewart platform. A total of 3981 different determinants are obtained, that is, $\det \mathbf{M}_i$, $i = 1, \ldots, 3981$. After checking the S part, the analytical expression of the singularity locus of the general Gough-Stewart platform with six variables is obtained, where x, y, z are at most of degree 3, $\sin\theta, \sin\psi, \sin\phi$ are at most of degree 1, $\cos\theta, \cos\psi, \cos\phi$ are at most of degree 3, and the highest total degree of all variables in one term $(x, y, z, \sin\theta, \sin\psi, \sin\phi, \cos\theta, \cos\psi, \cos\phi)$ is 11. The singularity locus equation is constructed with 2173 different terms, that is, K_j, $j = 1, \ldots, 2173$. This equation can be written as:

$$\begin{aligned} F(x, y, z, \phi, \theta, \psi) &= C_1x^3 + C_2x^2y + C_3x^2z + C_4x^2 + C_5y^2x + C_6xyz + C_7xy + C_8xz^2 \\ &\quad + C_9xz + C_{10}x + C_{11}y^3 + C_{12}y^2z + C_{13}y^2 + C_{14}yz^2 + C_{15}yz \\ &\quad + C_{16}y + C_{17}z^3 + C_{18}z^2 + C_{19}z + C_{20} = 0 \end{aligned} \tag{2.11}$$

where C_i $i = 1, \ldots, 20$ are functions of the architectural parameters and the Euler angles, which can be written as:

$$C_i = \sum_{j=0}^{3} D_{0j}^i (\cos\theta)^j + \sum_{j=0}^{3} E_{1j}^i \sin\theta (\cos\theta)^j$$

with

$$\begin{aligned} D_{0j}^i &= \sum_{k=0}^{3} F_{0j0k}^i (\cos\phi)^k + \sum_{k=0}^{3} L_{0j1k}^i \sin\phi (\cos\phi)^k \\ E_{1j}^i &= \sum_{k=0}^{3} M_{1j0k}^i (\cos\phi)^k + \sum_{k=0}^{3} N_{1j1k}^i \sin\phi (\cos\phi)^k \end{aligned}$$

where

$$\begin{aligned} F_{0j0k}^i &= \sum_{m=0}^{3} P_{0j0k0m}^i (\cos\psi)^m + \sum_{m=0}^{3} R_{0j0k1m}^i \sin\psi (\cos\psi)^m \\ L_{0j1k}^i &= \sum_{m=0}^{3} S_{0j1k0m}^i (\cos\psi)^m + \sum_{m=0}^{3} T_{0j1k1m}^i \sin\psi (\cos\psi)^m \\ M_{1j0k}^i &= \sum_{m=0}^{3} U_{1j0k0m}^i (\cos\psi)^m + \sum_{m=0}^{3} V_{1j0k1m}^i \sin\psi (\cos\psi)^m \\ N_{1j1k}^i &= \sum_{m=0}^{3} W_{1j1k0m}^i (\cos\psi)^m + \sum_{m=0}^{3} I_{1j1k1m}^i \sin\psi (\cos\psi)^m \end{aligned}$$

here D^i_{0j} and E^i_{1j} denote coefficients of $(\sin\theta)^0(\cos\theta)^j$ and $(\sin\theta)^1(\cos\theta)^j$ of C_i, respectively. F^i_{0j0k} and L^i_{0j1k} represent coefficients of $(\sin\theta)^0(\cos\theta)^j(\sin\phi)^0(\cos\phi)^k$ and $(\sin\theta)^0(\cos\theta)^j(\sin\phi)^1(\cos\phi)^k$ of C_i, respectively. S^i_{0j1k0m} and T^i_{0j1k1m} denote coefficients of $(\sin\theta)^0(\cos\theta)^j(\sin\phi)^1(\cos\phi)^k(\sin\psi)^0(\cos\psi)^m$ and $(\sin\theta)^0(\cos\theta)^j(\sin\phi)^1(\cos\phi)^k(\sin\psi)^1$ $(\cos\psi)^m$ of C_i, respectively. Likewise for the other coefficients shown above.

Note 1: for $i = 1, 2, 3, 5, 6, 8, 11, 12, 14$ and 17 — i.e., the coefficients of the terms in which the x, y, z degrees are 3 — the sums of the subscript six digit numbers are less than or equal to $11 - 3 = 8$, that is, for example, S^i_{0j1k0m}, $0 + j + 1 + k + 0 + m \leq 8$.

Note 2: for $i = 4, 7, 9, 13, 15, 18$ —i.e., the coefficients of the terms in which the degrees of x, y, z are 2 — the sums of the subscript six digit numbers are less than or equal to $11 - 2 = 9$, that is, for example, S^i_{0j1k0m}, $0 + j + 1 + k + 0 + m \leq 9$.

Note 3: for $i = 10, 16, 19$ — i.e., the coefficients of the terms in which the degrees of x, y, z are 1 — the sums of the subscript six digit numbers are less than or equal to $11 - 1 = 10$, this is, for example, S^i_{0j1k0m}, $0 + j + 1 + k + 0 + m \leq 10$.

Note 4: for $i = 20$, the sums of the subscript six digit numbers above are at most 11, that is, for example, S^i_{0j1k0m}, $0 + j + 1 + k + 0 + m \leq 11$.

From the above, it is clear that the terms in the expression of the determinant, namely, K_j, $j = 1, \ldots, 2173$, are combinations of $\det \mathbf{M}_i$, $i = 1, \ldots, 3981$, which are constructed by six vectors of architectural parameters and their combinations. For a given architecture, all matrices $\mathbf{M}_i$ are constants. The details are given in the Appendix A.

2.5 Representation of the singularity loci of the general Gough-Stewart platform

Since it is impossible to represent graphically the singularity locus in 6-D space, in this section, examples of singularity locus in 3-D are illustrated.

i	b_{ix}	b_{iy}	b_{iz}	p'_{ix}	p'_{iy}	p'_{iz}
1	92.58	99.64	20.10	30.00	73.00	-35.10
2	132.58	30.36	28.45	78.22	-10.52	-23.00
3	40.00	-120.00	31.18	48.22	-62.48	-33.60
4	-46.00	-130.00	3.10	-44.22	-56.48	-25.50
5	-130.0	23.36	13.48	-70.22	-20.52	-34.10
6	-82.58	89.77	8.76	-34.00	45.00	-39.00

Table 2.4: Geometric properties of a general Gough-Stewart platform (all lengths are given in mm).

The geometric parameters of a general Gough-Stewart platform are given in Table 2.4. To illustrate the singularity locus of this mechanism, in the following examples, the data of Table 2.4 is used.

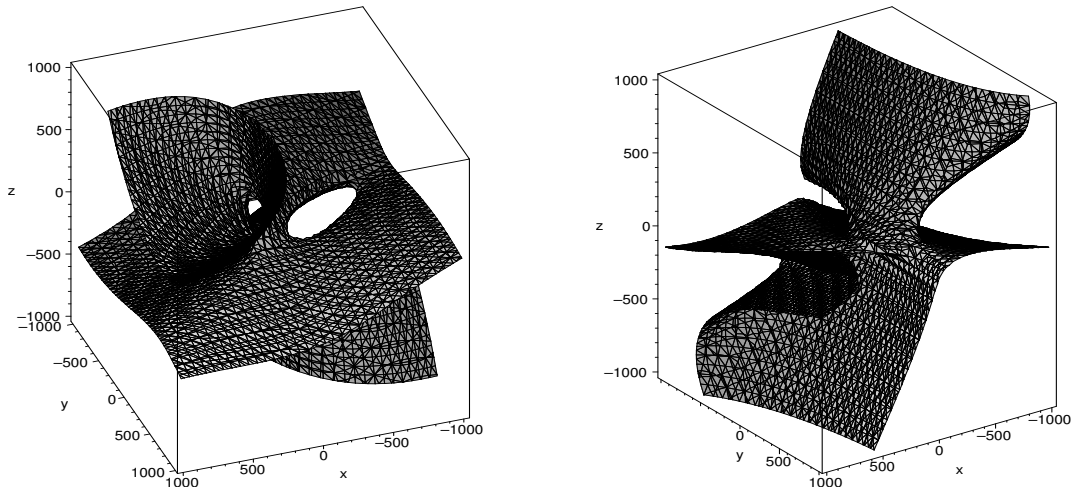

(a) $\phi = -2°$, $\theta = 30°$, $\psi = -87°$.

(b) $\phi = 30°$, $\theta = 30°$, $\psi = 30°$.

Figure 2.2: Singularity loci in 3-D Cartesian space with constant orientations (lengths are given in mm).

2.5.1 Case 1: Constant orientation

Fixing the orientation of the platform and applying eq. (2.11), the singularity locus equation is now the function of three position variables in the following form:

$$F_1(x, \quad y, \quad z) = 0 \tag{2.12}$$

the highest degrees of x, y and z in eq. (2.12) are 3, 3, 3, respectively.

Plots of singularity loci within $x, y, z \in [-1000, 1000]$ (all lengths are given in mm) with different orientations are illustrated in Figure 2.2. The resulting surfaces match the results previously obtained by Mayer St-Onge and Gosselin [33].

2.5.2 Case 2: Constant position

Fixing the position of the platform and applying eq. (2.11) again, the singularity locus equation is now the function of three Euler angles in the following form:

$$F_2(\theta, \quad \phi, \quad \psi) = 0 \tag{2.13}$$

the highest degrees of $\sin\theta$, $\sin\phi$ and $\sin\psi$ in eq. (5.13) are 1, 1, 1, repectively ,the highest degrees of $\cos\theta$, $\cos\phi$ and $\cos\psi$ in eq. (5.13) are 3, 3, 3, repectively. Plots of the singularity loci within $\theta, \phi, \psi \in [-\frac{\pi}{2}, \frac{\pi}{2}]$ with different positions are shown in Figure 2.3.

2.5.3 Case 3: Others

Fixing two of the three position varaibles and one of the three orientation variables and applying eq. (2.11) again, the singularity equation is now a function of one position variable and two Euler angles in the following form:

$$F_3(z, \quad \theta, \quad \psi) = 0 \tag{2.14}$$

the highest degree of z in eq. (2.14) is 3, the highest degrees of $\sin\theta, \sin\psi$, $\cos\theta$ and $\cos\psi$ are 1, 1, 3, 3, respectively. plots of the singularity loci within $\theta, \psi \in [-\frac{\pi}{2}, \frac{\pi}{2}]$ and $z \in [-1000, 1000]$ are shown in Figures 2.4 and 2.5 with different values of x, y and $\phi = 30°$, respectively.

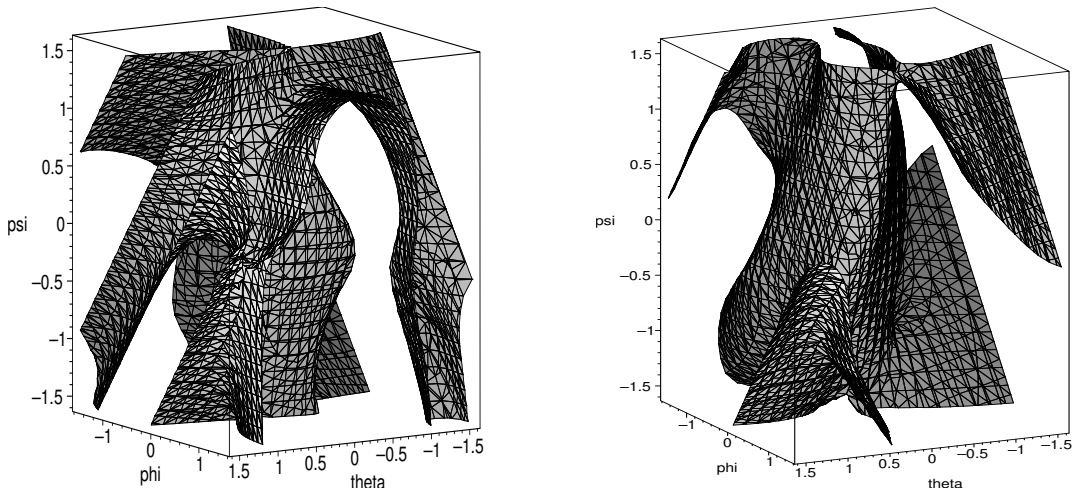

(a) $x = 0, y = 0, z = 0$.

(b) $x = 100, y = 100, z = 100$.

Figure 2.3: Singularity loci in 3-D Cartesian space with constant positions (lengths are given in mm).

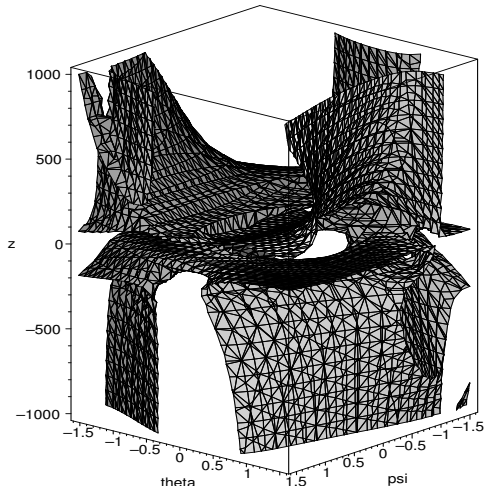

Figure 2.4: Singularity locus in 3-D Cartesian space with $\phi = 30°, x = 0, y = 0$ (lengths are given in mm).

Given two of the Euler angles, for example, θ and ψ and one of the three position variables, for example, z, applying the singularity locus equation (2.11) again, the singularity locus equation is now a function of one Euler angle ϕ and two position variables x and y, which can be expressed in the following form:

$$F_4(\phi, x, y) = 0 \tag{2.15}$$

the highest degrees of $\sin\phi$, $\cos\phi$, x and y in eq. (2.15) are 1, 3, 3 and 3, respectively,

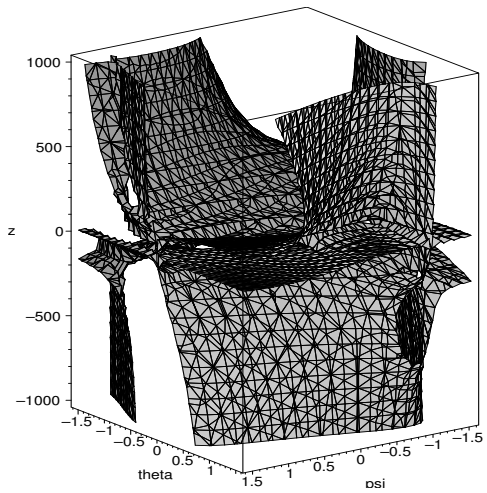

Figure 2.5: Singularity locus in 3-D Cartesian space with $\phi = 30°, x = 100, y = 100$ (lengths are given in mm).

Plots of the singularity locus within $\phi \in [-\frac{\pi}{2}, \frac{\pi}{2}]$, $x, y \in [-1000, 1000]$ (lengths are given in mm), are shown in Figures 2.6 and 2.7 with different values of ψ, $\theta = 30°$ and $z = 100$, respectively.

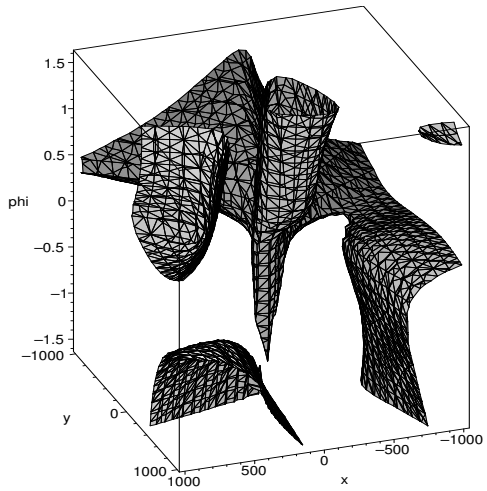

Figure 2.6: Singularity locus in 3-D Cartesian space with $\theta = 30°, \psi = -87°, z = 100$ (lengths are given in mm).

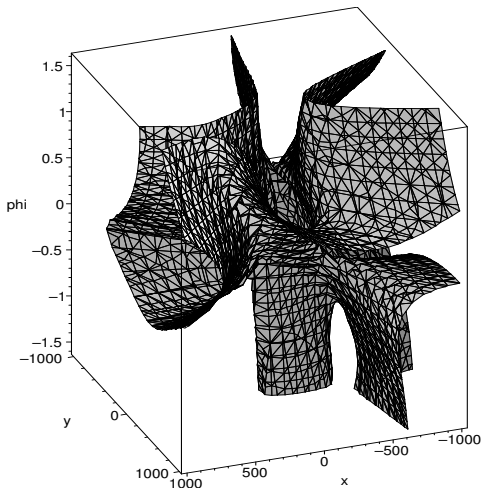

Figure 2.7: Singularity locus in 3-D Cartesian space with $\theta = 30°, \psi = 30°, z = 100$ (lengths are given in mm).

2.6 Computation time

Applying the geometric parameters of the general Gough-Stewart platform given in Table 2.4, we programmed with Maple 8 under Linux RedHat 9.0 and the CPU of the computer is a Pentium *IV* 2.4 GHz. It takes around 1 minute to derive the singularity locus equation. However, the time of the plotting of the curves for a given platform is obviously dependent on the resolution that one requires.

2.7 Conclusions

An analytical expression of the singularity locus of the general Gough-Stewart platform, which is in six variables (three position varaibles x, y and z and three orientation variables ϕ, θ and ψ) has been presented in this chapter for the first time. The method used here to obtain this expression is based on the cascaded expansion of the determinant of the Jacobian matrix of the mechanism. According to the method of linear decomposition of the determinant, the expansion of the direct kinematic matrix of the general Gough-Stewart platform will lead to a sum of $5 \times 5 \times 5 \times 12 \times 12 \times 12 = 216000$ determinants. After eliminating the determinants whose columns are dependent, a total of 3981 determinants are obtained, i.e., $\det \mathbf{M}_i$, $i = 1, \ldots, 3981$. After checking if there

are any identical *S part* in Table 2.3, 2173 terms are obtained, i.e., K_j, $j = 1, \ldots, 2173$, and the final analytical expression is written as: $F = \sum_j K_j \cdot (\text{S part})_j$, which is the function of $x, y, z, \phi, \theta, \psi$. This expression is then used to obtain a graphical representation of the singularity locus in 3-D Cartesian space for constant orientation, constant position or combinations of both.

In a context of design, it is of primary importance to determine whether there are singularities in a designated workspace. With the expression obtained here and a given set of structural parameters, the singularity locus can be obtained immediately. Although the expression is rather complicated, it is possible to obtain interactive graphical representations.

The singularity locus expression is applicable to all Gough-Stewart platform regardless of the geometric parameters. The expression developed here is of great interest for the design and analysis of Gough-Stewart platforms. It allows the designer to visualize interactively the singularity locus superimposed on the given workspace by fixing any three of the six variables.

Most importantly, the expression developed here will be used in Chapters 4 and 5 to determine singularity free regions in the workspace of the Gough-Stewart platform.

Chapter 3

Determination of Maximal Singularity-Free Zones in the Workspace of Planar 3-RPR Parallel Mechanisms

3.1 Introduction

Avoiding singularities within the workspace of a parallel mechanism has been addressed by several researchers. Bhattacharya, S., Hatwal, H. and Ghosh, A. [2] proposed an exact method and an approximate method to restructure the path which can avoid the singularity and remain close to the original prescribed path. In the exact method,

the leg force demand at the next goal point on the trajectory is continuously checked for possible violations of the preset limits as the mechanism moves close to a singular configurations. As soon as the force demand on any actuator crosses its preset limit, an optimization problem is solved to determine the alternative velocities leading to an alternate path on which the actuator forces would be constrained within limits. In the approximate method, a constraint on the determinant of the Jacobian matrix is applied as soon as the force demands on the next point exceeds the allowable limits. Consequently the parallel mechanism moves over a constant determinant manifold along a curve which is the weighted projection of the prescribed path of the device. The exact method always yields a minimum deviation of the parallel mechanism from the specified path but requires high computation time. On the other hand, although the approximate method sometimes fails to utilize the available forces in the leg maximally, it is time-efficient and therefore more suitable for most applications.

Merlet [32] presented an algorithm for solving the verification of a trajectory for a 6-DOF parallel mechanism with respect to the workspace, i.e., given two different postures for the end-effector, the algorithm determines whether the straight line joining these two points in the parameter space lies completely within the workspace. The algorithm is based on the analysis of algebraic inequalities describing the constraints on the workspace and provides a technique for computing those parts of the trajectory that lie outside the workspace. The constraints considered are limitations on the link interference. The method is found to be exact if the orientation of the end-effector is kept constant along the trajectory and approximate if the orientation is allowed to vary.

Dash et al. [7] presented a numerical technique for path planning inside the workspace of parallel mechanisms avoiding singularities. First, an approximate maximum workspace is found, which is then discretized into radial and equal area sectors and the exact workspace boundary is determined. Singularity points are determined inside this workspace following a numerical method. These points are grouped into several clusters by using a density based clustering algorithm and are modeled as obstacles. If any singularity point lies on or close to the path, the path is restructured to avoid that point till it again joins the original optimal path.

Three cases of singularity loci of the general Gough-Stewart platform within a given workspace were illustrated in the previous chapter. It is clear from these plots that the

singularity surfaces can be complex. From the design and control point of view, it is desirable to locate the singularity-free zones in the workspace. This is the main objective of this thesis and will be addressed in Chapters 4 and 5. The present chapter aims at introducing the general methodology proposed in this thesis using three-DOF problems in order to validate the concepts.

In this chapter, a procedure is introduced to determine the maximal singularity-free zones for three-degree-of-freedom workspaces corrresponding to the case 3 of section 2.5. First, planar 3-RPR parallel mechanisms, which have been studied in detail by several researchers (such as, [13], [44], [45]) are introduced. The kinematic and singularity analysis of the mechanisms are briefly recalled. According to the classification of singularities given by Gosselin and Angeles [14], the analytic expression of singularity of type II is obtained for this mechanism. Then, with the singularity equation obtained, a procedure is presented to locate maximal singularity-free zones within given ranges of the rotational variable. Contrary to the trajectory planning methods cited above, the algorithm presented here is a demonstration of the application of mathematical techniques in a trajectory planning context, which are easy to understand and use. Within the zones obtained, it is guaranteed that there exists no singularity, that means, the end-effector can move arbitrarily within these zones. This procedure is applicable to any mechanism with known singularity equation in 3-D Cartesian space. Finally, numerical examples are given to illustrate the application of the procedure to both the 3-RPR parallel mechanisms and the general Gough-Stewart platform while constraining three of the Cartesian degrees of freedom.

3.2 Kinematic analysis of the $3-RPR$ Planar Parallel Mechanism

A planar 3-RPR parallel mechanism with actuated prismatic joints is shown in Figure 1.2(a), which consists of a triangular mobile platform $P_1P_2P_3$ and a fixed triangle base $B_1B_2B_3$. P_i and B_i are connected via the actuated prismatic joints of variable length ρ_i, $i = 1, 2, 3$. Passive revolute joints are located at B_i and P_i and the mechanism has 3-DOFs. The moving platform can translate in the xy plane and rotate with respect to an axis perpendicular to the xy plane. The kinematic analysis of the mecha-

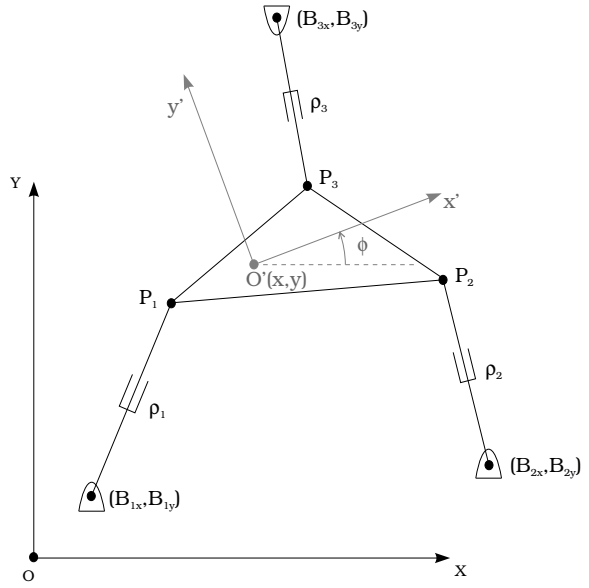

Figure 3.1: Notation used for the planar 3-DOF parallel mechanisms with actuated prismatic joints

nism is now briefly recalled, which consists of inverse kinematics, velocity equation and the singularity analysis.

3.2.1 Inverse kinematics and velocity equation

In Figure 3.1, a reference frame OXY is attached to the base and a mobile frame $O'X'Y'$ is attached to the moving platform. The position of point B_i on the base is denoted by vector $\mathbf{b}_i = [B_{ix}, B_{iy}]^T$ $(i = 1, 2, 3)$ in the fixed reference frame and the position of point P_i in the mobile frame is presented by vector $\mathbf{p}'_i = [P'_{ix}, P'_{iy}]^T$ $(i = 1, 2, 3)$, which is constant in the mobile frame. Let vector $\mathbf{s} = [x, y]^T$ denote the position of O' in the fixed reference frame and $\mathbf{Q}$ be the rotation matrix representing the rotation of the platform from frame OXY to frame $O'X'Y'$ with

$$\mathbf{Q} = \begin{bmatrix} \cos\phi & -\sin\phi \\ \sin\phi & \cos\phi \end{bmatrix}$$

From the above notation, we know that the position vector of point P_i expressed in the fixed reference frame by $\mathbf{p}_i = [P_{ix}, P_{iy}]^T$ is given by:

$$\mathbf{p}_i = \mathbf{s} + \mathbf{Q}\mathbf{p}'_i \tag{3.1}$$

The length of the ith leg ρ_i, which is the distance between points P_i and B_i, can be written as:

$$\rho_i{}^2 = (P_{ix} - B_{ix})^2 + (P_{iy} - B_{iy})^2, \qquad i = 1, 2, 3 \tag{3.2}$$

differentiating eq. (3.2) with respect to time, the velocity equation is obtained as follows:

$$\mathbf{A}\mathbf{t} = \mathbf{B}\dot{\boldsymbol{\rho}} \tag{3.3}$$

Here $\dot{\boldsymbol{\rho}} = [\dot{\rho_1}, \dot{\rho_2}, \dot{\rho_3}]^T$ denotes the actuator velocities, while $\mathbf{t} = [\dot{x}, \dot{y}, \dot{\phi}]^T$ denotes the Cartesian velocity vector of the platform and $\mathbf{A}$ and $\mathbf{B}$ are two Jacobian matrices written as:

$$\mathbf{B} = \begin{bmatrix} \rho_1 & 0 & 0 \\ 0 & \rho_2 & 0 \\ 0 & 0 & \rho_3 \end{bmatrix} \tag{3.4}$$

$$\mathbf{A} = \begin{bmatrix} a_{11} & a_{12} & a_{13} \\ a_{21} & a_{22} & a_{23} \\ a_{31} & a_{32} & a_{33} \end{bmatrix} \tag{3.5}$$

with

$$a_{i1} = x + P'_{ix}\cos\phi - P'_{iy}\sin\phi - B_{ix}, \qquad i = 1, 2, 3 \tag{3.6}$$

$$a_{i2} = y + P'_{ix}\sin\phi + P'_{iy}\cos\phi - B_{iy}, \qquad i = 1, 2, 3 \tag{3.7}$$

$$\begin{aligned} a_{i3} = {} & (P'_{iy}\sin\phi - x - P'_{ix}\cos\phi + B_{ix})(P'_{iy}\cos\phi + P'_{ix}\sin\phi) \\ & + (y + p'_{ix}\sin\phi + p'_{iy}\cos\phi - B_{iy})(P'_{ix}\cos\phi - P'_{iy}\sin\phi) \\ & i = 1, 2, 3 \end{aligned} \tag{3.8}$$

3.2.2 Singularity equation

According to the singularity classification of closed-loop mechanisms defined in [14], a total of three types of singularities are defined. Singularity of type I occur when matrix $\mathbf{B}$ is singular, which are located at the boundaries of the workspace of the mechanism. Singularity of type III occur when the nonlinear kinematic constraints degenerate. Both types of singularities can also be avoided easily. Zlatanov, Bonev and Gosselin [56] identified a particular kind of singularities, referred to as constraint singularity. Constraint singularities may occur even when both matrix $\mathbf{A}$ and matrix $\mathbf{B}$ are

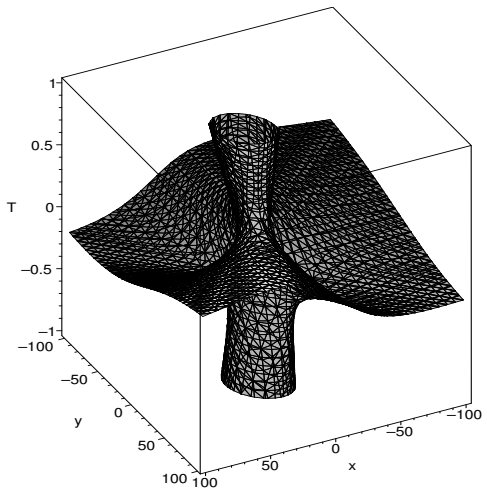

Figure 3.2: Singularity locus of a planar 3-RPR parallel mechanism within a region of the workspace limited by $x \in [-100, 100], y \in [-100, 100]$ and $T \in [-1, 1]$ (lengths are given in mm).

not singular, which is a complement to the singularity classification given by Gosselin and Angeles [14]. A constraint singularity can only occur in a parallel mechanism with a DOF of the platform, n, lower than the number of joints in any leg. For the 3-RPR parallel mechanisms, this type of singularity does not occur. The singularity of type II are also called RO (Redundant Output) in [55]. They correspond to configurations in which the stiffness of the mechanism is locally lost, which occurs when matrix $\mathbf{A}$ is singular, i.e., $\det(\mathbf{A}) = 0$. Expanding matrix $\mathbf{A}$ and applying the *tangent* of the half angle substitution, i.e, defining $T = \tan(\frac{\phi}{2})$, the singularity equation can be written as:

$$F(x, y, T) = F_0 + F_1 T + F_2 T^2 + F_3 T^3 + F_4 T^4 + F_5 T^5 + F_6 T^6 = 0 \tag{3.9}$$

with

$$F_i \;\; = \;\; F_{i0} + F_{i1} x + F_{i2} y + F_{i3} x^2 + F_{i4} xy + F_{i5} y^2 \tag{3.10}$$

where the coefficients F_{ij} $(i = 0, \ldots, 6)$ $(j = 0, \ldots, 5)$ are functions of the architectural parameters. For a given architecture, the latter coefficients F_{ij} are constants.

Using the above expression (3.9), it is possible to represent the singularity locus in the workspace of the mechanism. An example is given in Figure 3.2, where the singularity locus —a surface— is plotted in the (x, y, T) space. The geometric parameters used to generate this plot are those given in Table 3.1.

i	B_{ix}	B_{iy}	P'_{ix}	P'_{iy}
1	3.78	4.34	−4.83	−3.19
2	34.47	−3.78	12.04	−3.19
3	16.23	34.76	8.23	12.09

Table 3.1: Geometric parameters of a 3-RPR parallel mechanism (all lengths are given in mm).

3.3 Determination of maximal singularity-free zones

In a context of design and/or trajectory planning, an important problem is to find singularity-free zones in the workspace of the mechanism. In this section, a new procedure is introduced to address the following problem: **For a given rotational range of motion** $(T_{min} \leq T \leq T_{max})$ **and a given position** (x_o, y_o)**, find the largest singularity-free disk centered in** (x_o, y_o) **in the** xy **positioning workspace such that this disk will be free of singularities for any orientation within the prescribed range** $[T_{min}, T_{max}]$.

The above problem can be solved using the following procedure:

First, since $T = \tan(\frac{\phi}{2})$ is comprised in a finite interval, i.e., $T \in [T_{min}, T_{max}]$, it can be written as [32]:

$$T(\sin\alpha) = T_{min} + \frac{(T_{max} - T_{min})(1 + \sin\alpha)}{2} \tag{3.11}$$

With different prescribed ranges, T is only a function of $\sin\alpha$. If the range of T is symmetric with respect to zero, i.e., $T_{max} = -T_{min} = a$, then T can be simply written as:

$$T = a\sin\alpha \tag{3.12}$$

The latter special case (eq. (3.12)) is now assumed in order to simplify the derivation, keeping in mind that the more general case (eq. (3.11)) can also be solved using the same procedure.

Substituting eq. (3.12) into eq. (3.9), the singularity equation is now a function of $(x, y, \sin\alpha)$, which is rewritten as:

$$\begin{aligned} F(x, y, \sin\alpha) &= F_0 + F_1 a \sin\alpha + F_2 a^2 \sin^2\alpha + F_3 a^3 \sin^3\alpha + F_4 a^4 \sin^4\alpha + F_5 a^5 \sin^5\alpha \\ &\quad + F_6 a^6 \sin^6\alpha \end{aligned} \tag{3.13}$$

where the coefficients $F_i, i = 1, \ldots, 6$, have been defined in eq. (3.10).

3.3.1 Step 1: Formulation as a minimization problem

An alternative formulation for the problem stated above is the following: **Within the prescribed range of orientation, find the point on the singularity surface, which is the closest to the center point** (x_o, y_o). This problem can be written mathematically as a minimization problem, namely:

$$\min_{(x,y,\alpha,\lambda)} d \tag{3.14}$$

where

$$d = (x - x_o)^2 + (y - y_o)^2 + \lambda F(x, y, \sin\alpha) \tag{3.15}$$

where λ is a Lagrange multiplier used to transform the constrained problem into an unconstrained problem.

An extremum of function d will be obtained if the partial derivatives of d with respect to x, y, α and λ are equal to zero, namely,

$$\frac{\partial d}{\partial x} = 2(x - x_o) + \lambda \frac{\partial F}{\partial x} = 0 \tag{3.16}$$

$$\frac{\partial d}{\partial y} = 2(y - y_o) + \lambda \frac{\partial F}{\partial y} = 0 \tag{3.17}$$

$$\frac{\partial d}{\partial \alpha} = \lambda \frac{\partial F}{\partial \alpha} = 0 \tag{3.18}$$

$$\frac{\partial d}{\partial \lambda} = F(x, y, \sin\alpha) = 0 \tag{3.19}$$

which forms a system of four nonlinear equations in the four unknowns x, y, α and λ.

Eq. (3.18) can be rewritten in the following form:

$$\frac{\partial F}{\partial \alpha} = S \cos\alpha = 0 \tag{3.20}$$

where

$$S(x, y, \sin\alpha) = F_1 a + 2F_2 a^2 \sin\alpha + 3F_2 a^3 \sin^2\alpha + 4F_4 a^4 \sin^3\alpha + 5F_5 a^5 \sin^4\alpha + 6F_6 a^6 \sin^5\alpha$$

where the coefficients $F_i, i = 1, \ldots, 6$, have been defined in eq. (3.10).

3.3.2 Step 2: Solution of the nonlinear equations

It is readily observed that only eqs. (3.16) and (3.17) contain λ. Eliminating λ from these two equations leads to a new equation, which is a function of x, y, and $\sin\alpha$. We obtain a system of three equations and three variables x, y, and α. The new equation has the following form:

$$R_0 + R_1 \sin\alpha + R_2 \sin^2\alpha + R_3 \sin^3\alpha + R_4 \sin^4\alpha + R_5 \sin^5\alpha + R_6 \sin^6\alpha = 0 \quad (3.21)$$

where

$$R_i \;=\; R_{i0} + R_{i1}x + R_{i2}y + R_{i3}x^2 + R_{i4}xy + R_{i5}y^2 \quad , i = 0, \ldots, 6$$

where the coefficients $R_{iv} (i = 0, \ldots, 6)(v = 0, \ldots, 5)$ are only functions of the architectural parameters. For a given architecture, they are constants.

We now have three equations with three unknowns, x, y and α. As shown in eq. (3.20), eq. (3.18) can be factored. Hence the latter equation can be satisfied in the following cases:

$$S(x, y, \sin\alpha) = 0, \quad \text{or} \quad \cos\alpha = 0$$

which can be rewritten as:

$$S(x, y, \sin\alpha) = 0, \quad \sin\alpha = 1 \quad \text{or} \quad \sin\alpha = -1$$

If $S(x, y, \sin\alpha) = 0$, then the point on the singularity surface, which is the closest to the point (x_o, y_o), is located within the range of T, otherwise it is located on one of the two boundaries of the range of T. Hence, three cases of solutions are distinguished.

3.3.2.1 Case1: $S(x, y, \sin\alpha) = 0$

$S(x, y, \sin\alpha) = 0$ together with eq. (3.21) and eq. (3.19) form a system of three equations with three unknowns, i.e., x, y and $\sin\alpha$.

First, use the resultant [39] to eliminate one of the variables x or y from $S(x, y, \sin\alpha) = 0$, eq. (3.19) and eq. (3.21). For example, first eliminate x from equations $S(x, y, \sin\alpha) = 0$ and eq. (3.19), then eliminate x from $S(x, y, \sin\alpha) = 0$ and eq. (3.21). A new set of two equations is obtained with two variables y and $\sin\alpha$, which are written as:

$$f_1(y, \sin\alpha) = 0 \tag{3.22}$$

$$f_2(y, \sin\alpha) = 0 \tag{3.23}$$

The degrees of y and $\sin\alpha$ in eq. (3.22) are 4 and 22, respectively, while the degrees of y and $\sin\alpha$ in eq. (3.23) are 4 and 20, respectively.

Then, variable y is eliminated from eq. (3.22) and eq. (3.23) using the resultant a second time. A single equation with only one variable, $\sin\alpha$, is obtained and can be written as:

$$\sum_{i=0}^{168} D_i \sin^i\alpha = 0 \tag{3.24}$$

where the coefficients D_i are functions of the architectural parameters only. Finally, solve eq. (3.24) numerically and list all solutions for $\sin\alpha$. In the numerical solution of a given problem, there are usually only a few real solutions. Most of the solutions obtained are complex and are excluded in the procedure. Then, perform the back substitution using the following process:

1. Substitute the first solution of $\sin\alpha$ into eqs. (3.22) and (3.23). Now, these equations are only functions of y and can be solved independently. Solving these two equations for y, two groups of solutions of y are obtained. Among these two sets of solutions of y, if there is one common solution, then note it as y_1, otherwise, repeat with the following solution of $\sin\alpha$ until all solutions of $\sin\alpha$ are substituted. Finally, keep all groups of $\sin\alpha_i$ and corresponding y_i, i.e., $\sin\alpha = \sin\alpha_i$ and $y = y_i$.

2. Substitute each group of solution $(\sin\alpha, y)$ obtained in the first step into $S(x, y, \sin\alpha) = 0$, eq. (3.19) and eq. (3.21). Now, there are three new equations, which are only functions of x. Solving these three equations, three groups of solutions for x are obtained. If there is a common solution, denote it as $x = x_i$, with the same subscript as $\sin\alpha_i$ and y_i. This procedure is repeated with the next $\sin\alpha_i$ and the corresponding y_i. All groups of solutions for $\sin\alpha_i$, y_i and the corresponding x_i are then recorded.

3. Each of the solution sets x_i, y_i, $\sin\alpha_i$ obtained will satisfy eq. (3.19), i.e., all minima are located on the singularity manifold. Therefore, using eq. (3.15) on a solution set, one has:

$$d_i = (x_i - x_o)^2 + (y_i - y_o)^2$$

This index d_i is evaluated for all solution sets. The solution leading to the smallest value of d is the global minimum. The value of d is the square of the radius of the circle of the singularity-free zone and is recorded as:

$$r_1^2 = V_1$$

3.3.2.2 Case 2: $\sin\alpha = 1$

Substituting $\sin\alpha = 1$ into eq. (3.21) and eq. (3.19) leads to two equations that are only functions of x and y. The degrees of x, y in these equations are 2 and 2, respectively. Eliminate one of the variables, for example, y, then a single equation, which is only a function of x is obtained:

$$G_0 + G_1 x + G_2 x^2 + G_3 x^3 + G_4 x^4 = 0 \tag{3.25}$$

where the coefficients G_i $(i = 0, \ldots, 4)$ are only functions of architectural parameters. Solving this equation and listing all the solutions of x provides a set of potential solutions. Each solution x_i is back substituted in eq. (3.21) and eq. (3.19) and each of these equations is then solved for y. The common root of the two equaitons is noted y_i. Then for each real set x_i, y_i, compute $d_i = (x_i - x_o)^2 + (y_i - y_o)^2$. The solution leading to the minimum value of d_i is the global minimum. This value is noted as:

$$r_2^2 = V_2$$

3.3.2.3 Case 3: $\sin\alpha = -1$

Substituting $\sin\alpha = -1$ into eq. (3.21) and eq. (3.19) leads to two equations that are only funtions of x and y. The degrees of x, y in these equations are 2 and 2, respectively. Eliminating one of the variables, for example, y, then a single equation is obtained, which is only function of x, namely,

$$H_0 + H_1 x + H_2 x^2 + H_3 x^3 + H_4 x^4 = 0 \tag{3.26}$$

where the coefficients H_i $(i = 0, \ldots, 4)$ are only functions of the architectural parameters. Solving this equation and listing all solutions for x provides a set of potential solutions. Then, the back substitution process given above in case 2 is repeated and the smallest value d is noted as:

$$r_3^2 = V_3$$

3.3.3 Step 3: Geometric interpretation of the solution

Define a cylinder in the 3-D Cartesian (x, y, T) space whose axis is defined as $x = x_o, y = y_o$, in the following form:

$$\begin{aligned} (x - x_o)^2 + (y - y_o)^2 - r^2 &= 0 \\ T &\in [b \quad c] \\ b &\in (0 \quad 1] \\ c &\in (0 \quad 1] \\ b &< c \end{aligned} \tag{3.27}$$

where $r^2 = \min(r_1^2, r_2^2, r_3^2)$. Within this cylinder, it can be guaranteed that there is no singularity. In fact, for the prescribed range of orientation, this cylinder is the largest singularity-free cylinder centered in (x_o, y_o).

3.4 Application of the procedure to symmetric ranges of the orientation ϕ

In this section, several examples are illustrated with different ranges of T and the architectural parameters given in Table 3.1 are used. As indicated in eq. (3.24), the degree of $\sin\alpha$ is 168 for the first case of the solution. However, solving the equation numerically, only a few real solutions for $\sin\alpha$ are obtained. The other solutions are complex and are excluded from the procedure.

3.4.1 Maximal singularity-free cylinder with $\phi \in [-90^\circ \quad 90^\circ]$

The above procedure is now applied to the mechanism of the Table 3.1 with $x_o = 0$, $y_o = 20mm$ and $T_{max} \equiv -T_{min} = 1$, i.e., $\phi \in [-90^\circ, 90^\circ]$. From eq. (3.12), it is readily observed that $T = \sin\alpha$. The maximal singularity-free cylinder is shown in Figure 3.3. The portion of the singularity surface containing the point closest to the cylinder axis is at point $(x, y, \sin\alpha) = (0.64385, 19.84452, 1)$ and the radius square of the cylinder is equal to $0.43872mm^2$ (lengths are given in mm). In this case, it is clear that the critical point is located at one extremity of the cylinder, $\sin\alpha = 1$, i.e., $\phi = 90^\circ$. It is also observed that imposing a large range of rotation leads to a cylinder with a small radius, as expected.

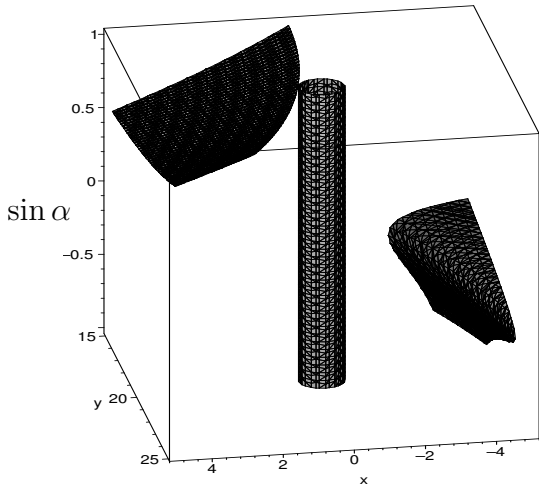

Figure 3.3: Maximal singularity-free cylinder with $\phi \in [-90^\circ, 90^\circ]$.

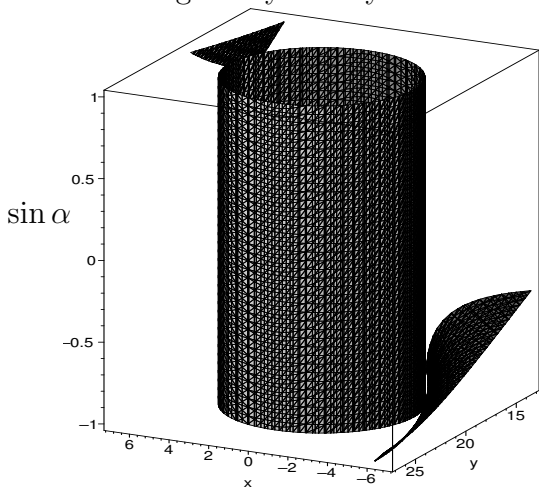

Figure 3.4: Maximal singularity-free cylinder with $\phi \in [-45^\circ, 45^\circ]$.

3.4.2 Maximal singularity-free cylinder with $\phi \in [-45°, 45°]$

Let now $x_o = 0$, $y_o = 20mm$ and $T_{max} \equiv -T_{min} = \tan(\frac{\pi}{8})$, i.e., $\phi \in [-45°, 45°]$. According to eq. (3.12), T is written as:

$$T = \tan(\frac{\pi}{8}) \sin\alpha$$

Applying the above procedure, the maximal singularity-free cylinder is shown in Figure 3.4. The portion of the singularity surface containing the point closest to the cylinder axis is at point $(x, y, \sin\alpha) = (-4.32334, 18.29473, -1)$ and the radius square of the cylinder is equal to $21.59913mm^2$ (lengths are given in mm). In this case, it is clear that the critical point is located at one extremity of the cylinder, $\sin\alpha = -1$, i.e., $\phi = -45°$. As expected, reducing the requested range of orientation significantly increases the radius of the cylinder.

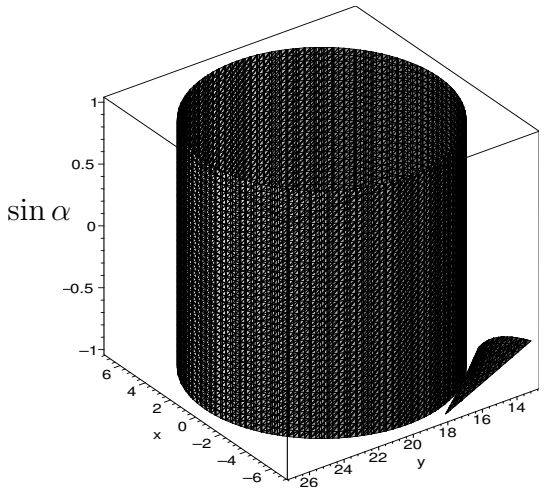

Figure 3.5: Maximal singularity-free cylinder with $\phi \in [-30°, 30°]$.

3.4.3 Maximal singularity-free cylinder with $\phi \in [-30°, 30°]$

Let now $x_o = 0$, $y_o = 20mm$ and $T_{max} \equiv -T_{min} = \tan(\frac{\pi}{12})$, i.e., $\phi \in [-30° \quad 30°]$. According to eq. (3.12), T is written as:

$$T = \tan(\frac{\pi}{12}) \sin\alpha$$

Applying the above procedure, the maximal singularity-free cylinder is shown in Figure 3.5. The portion of the singularity surface containing the point closest to the

cylinder axis is at point $(x, y, \sin\alpha) = (-5.17655, 15.67384, -1)$ and the radius square of the cylinder is equal to $45.51273mm^2$ (lengths are given in mm). In this case, it is clear that the critical point is located at one extremity of the cylinder, $\sin\alpha = -1$, i.e., $\phi = -30°$. Again, a reduction of the requested range of orientation increases significantly the radius of the singularity-free cylinder. In all cases presented above, it can be guaranteed that the cylinder does not contain any singular configuration. Finally, it is also noted that in all cases, the global minimum was located at one end of the cylinder. This is often (although not always) the case and leads to very stable numerical solutions since in these cases (cases 2 and 3 of section 3.3.2) the solutions are obtained from simple quadric equations.

3.5 Application of the procedure to asymmetric ranges of the orientation ϕ

As shown in eq. (3.11), with different ranges of T, T is only function of α. A plot of the singularity loci eq. (3.9) in 3-D space within $x \in [-100, 100], y \in [-100, 100]$ and $T \in [0, 1]$ is illustrated in Figure 3.6. In the following examples, the above procedure is applied with asymmetric ranges of T.

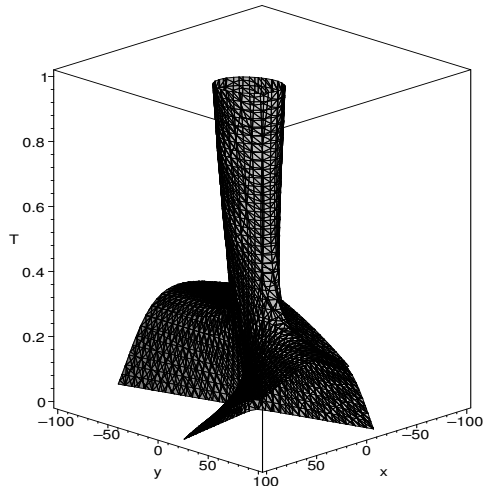

Figure 3.6: Singularity locus of the planar 3-RPR parallel mechanism of Table 3.1 within a region of the workspace limited by $x \in [-100, 100]$, $y \in [-100, 100]$ and $T \in [0, 1]$ (lengths are given in mm).

3.5.1 Maximal singularity-free cylinder with $\phi \in [0, 90°]$

For $T \in [0, 1]$, i.e., $\phi \in [0, 90°]$, according to eq. (3.11), T is written as:

$$\begin{aligned} T &= 0 + \frac{(1 + \sin\alpha)(1 - 0)}{2} \\ &= \frac{(1 + \sin\alpha)}{2} \end{aligned}$$

Applying the above procedure with $x_o = 0$, $y_o = 20mm$. The maximal singularity-free cylinder obtained is shown in Figure 3.7. The portion of the singularity surface containing the point closest to the cylinder axis is at point $(x, y, \sin\alpha) = (0.64385, 19.84445, 1)$ and the radius square of the cylinder is equal to $0.43872mm^2$ (lengths are given in mm). In this case, it is clear that the critical point is located at one extremity of the cylinder, $\sin\alpha = 1$, i.e., $\phi = 90°$. It can be observed that the result obtained is exactly the same as the one obtained with the symmetric range $\phi \in [-90°, 90°]$ in the previous section. This is consistent with the fact that the most critical orientation in this case is $\phi = 90°$.

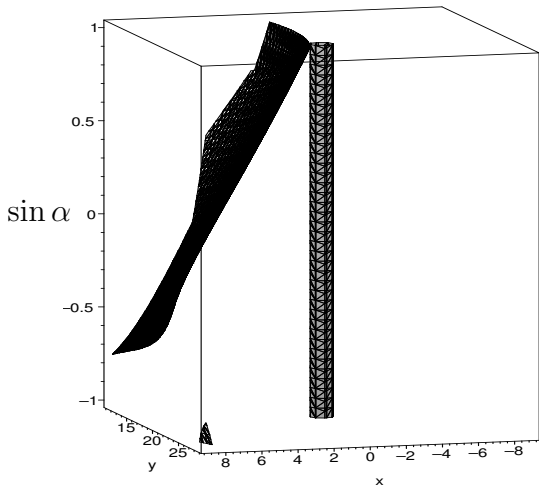

Figure 3.7: Maximal singularity-free cylinder with $\phi \in [0, 90°]$.

3.5.2 Maximal singularity-free cylinder with $\phi \in [0, 60°]$

For $T \in [0, \frac{\sqrt{3}}{3}]$, i.e., $\phi \in [0, 60°]$, according to eq. (3.11), T is written as:

$$T = 0 + \frac{(1 + \sin\alpha)(\frac{\sqrt{3}}{3} - 0)}{2}$$

$$= \frac{\sqrt{3}}{6}(1+\sin\alpha)$$

Applying the above procedure with $x_o = 0$, $y_o = 20mm$, the maximal singularity-free cylinder obtained is shown in Figure 3.8. The portion of the singularity surface containing the point closest to the cylinder axis is at point $(x, y, \sin\alpha) = (4.87016, 18.50795, 1)$ and the radius square of the cylinder is equal to $25.94473mm^2$ (lengths are given in mm). In this case, it is clear that the critical point is located at one extremity of the cylinder, $\sin\alpha = 1$, i.e., $\phi = 60°$.

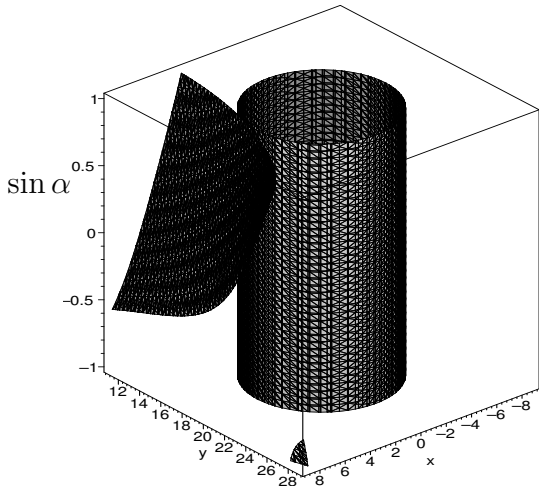

Figure 3.8: Maximal singularity-free cylinder with $\phi \in [0, 60°]$.

3.5.3 Maximal singularity-free cylinder with $\phi \in [0, 30°]$

For $T \in [0, \tan(\frac{\pi}{12})]$, i.e., $\phi \in [0, 30°]$, according to eq. (3.11), T is written as:

$$\begin{aligned} T &= 0 + \frac{(1+\sin\alpha)(\tan(\frac{\pi}{12}) - 0)}{2} \\ &= \frac{1}{2}\tan(\frac{\pi}{12})(1+\sin\alpha) \end{aligned}$$

Applying the above procedure with $x_o = 0$, $y_o = 20mm$, the maximal singularity-free cylinder obtained is shown in Figure 3.9. The portion of the singularity surface containing the point closest to the cylinder axis is at point $(x, y, \sin\alpha) = (8.28005, 18.19334, 1)$ and the radius square of the cylinder is equal to $71.83043mm^2$ (lengths are given in mm). In this case, it is clear that the critical point is located at one extremity of the cylinder, $\sin\alpha = 1$, i.e., $\phi = 30°$. It is interesting to note that, in this case, the result

obtained is different from the one obtained in the previous section with the symmetric range $\phi \in [-30°, 30°]$. This is because in the previous optimization, the most critical orientation was $\phi = -30°$, which is now excluded from the range of motion.

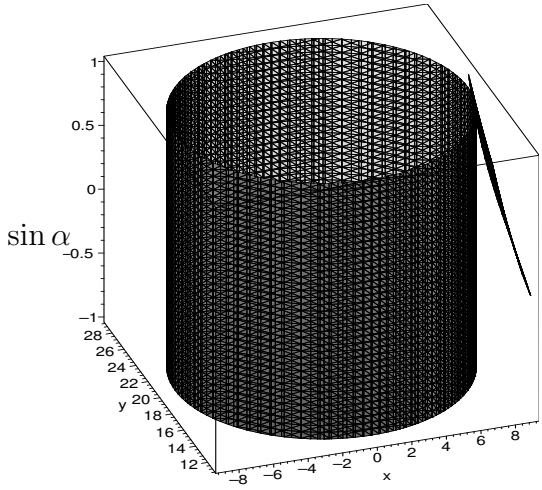

Figure 3.9: Maximal singularity-free cylinder with $\phi \in [0, 30°]$.

3.6 Computation time

The above examples were programmed with Maple 8 under Linux RedHat 9.0 and the CPU of the computer is a Pentium *IV* 2.4 GHz. For case 1 of the procedure, the highest degree of $\sin\alpha$ in eq. (3.24) is 168. Solving the equation and listing all the real solutions of $\sin\alpha$ requires approximately 82s. In cases 2 and 3, the highest degrees of x in eqs. (3.25) and (3.26) are 4. Hence, the computation time is much shorter. As shown in the process illustrated in **Step2**, back substitution is carried out to find the other variable y in each case. The computation time is not easy to determine, since it is dependent on the numerical example. However, since the degrees of the equations used in the back substitution are not high compared to eq. (3.24), obtaining the final result is fast and requires a total of approximately 2 minutes.

In a context of design, this computation time is acceptable, but it is prohibitive in a context of trajectory planning. However, it should be noted that a hard coded implementation of the procedure would be significantly faster than the Maple version and could very well be fast enough for trajectory planning applications.

i	b_{ix}	b_{iy}	b_{iz}	p'_{ix}	p'_{iy}	p'_{iz}
1	92.58	99.64	23.10	30.00	73.00	-37.10
2	132.58	30.36	23.10	78.22	-10.52	-37.10
3	40.00	-130.00	23.10	48.22	-62.48	-37.10
4	-40.00	-130.00	23.10	-48.22	-62.48	-37.10
5	-132.58	30.36	23.10	-78.22	-10.52	-37.10
6	-92.58	99.64	23.10	-30.00	73.00	-37.10

Table 3.2: Geometric properties of the INRIA prototype (all lengths are given in mm).

3.7 Application of the procedure to the general Gough-Stewart platform

As an introduction to the upcoming chapters, the above procedure can be applied to the Gough-Stewart platform by constraining its motion to three degrees of freedom. The singularity locus equation of the general Gough-Stewart platform has been obtained in the previous chapter as a function of six variables (three position variables x, y, z and three Euler angles ϕ, θ and ψ). Fixing two of the three Euler angles and one of the position variables, the general Gough-Stewart platform has 3-DOFs, i.e., the translation in one plane and rotation with respect to an axis, which is similar to that of the $3-RPR$ planar parallel mechanisms. For example, fixing one of three position variables and two of the three Euler angles, the singularity equation is a function of x, y and ϕ. Using the half angle substitution formulation, i.e., $\tan(\phi/2) = T$, the singularity equation can be written in the following form:

$$E(x, y, T) = 0$$

where the degrees of x, y and T are 3, 3 and 6, respectively. The geometric parameters of a parallel mechanism designed and built at INRIA based on a Gough-Stewart platform are given in Table 3.2. In the following examples of the general Gough-Stewart platform, the data of Table 3.2 is used.

3.7.1 Symmetric ranges of orientation

In this section, fixing the position variable at $z = 1dm$ and two orientation variables at $\theta = 30^\circ$ and $\psi = 30^\circ$, examples with symmetric ranges of ϕ are presented as follows:

3.7.1.1 Maximal singularity-free cylinder with $\phi \in [-90^\circ, 90^\circ]$

For $T \in [-1 \quad 1]$, i.e., $\phi \in [-90^\circ, 90^\circ]$, according to eq. (3.12), T is written as:

$$T = \sin\alpha$$

A plot of the singularity locus of the platform within the given workspace is shown in Figure 3.10, as shown in the figure, there exists complicated singularities inside the given workspace. Applying the above procedure with $x_o = 0$, $y_o = 0$, the maximal singularity-free cylinder is shown in Figure 3.11. The portion of the singularity surface containing the point closest to the cylinder axis is at point $(x, y, \sin\alpha) = (0.28823, -0.24019, -0.05402)$ and the radius square of the cylinder is equal to $0.14077dm^2$ (lengths are given in dm). In this case, it is clear that the critical point is located between the two extremities of the cylinder, $\sin\alpha = -0.05402$, i.e., $\phi = -6.19325^\circ$. Therefore, in this example, the minimum solution was found using the case 1 of the procedure.

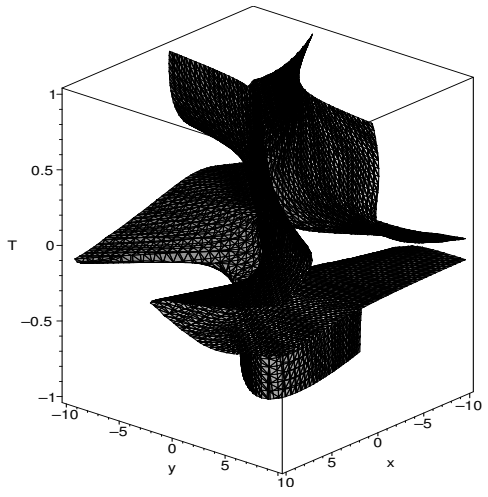

Figure 3.10: The singularity locus of the general Gough-Stewart platform with $x \in [-10, 10]$, $y \in [-10, 10]$ and $T \in [-1, 1]$ (all lengths are given in dm).

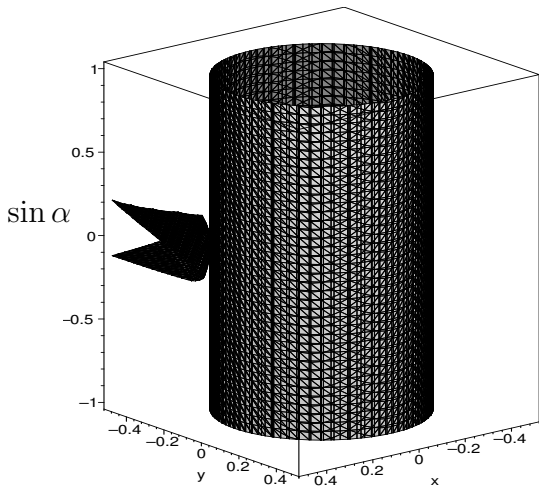

Figure 3.11: Maximal singularity-free cylinder with $\phi \in [-90°, 90°]$.

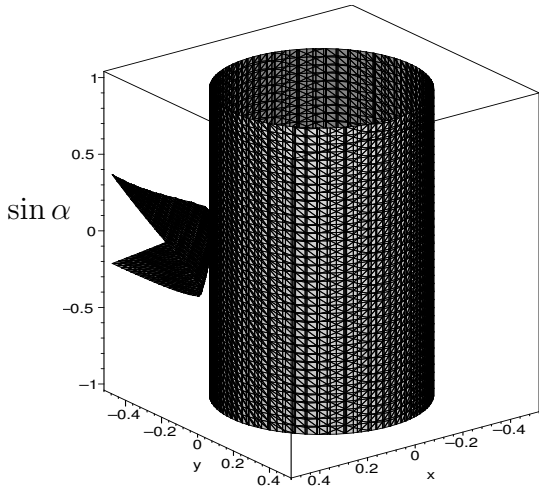

Figure 3.12: Maximal singularity-free cylinder with $\phi \in [-60°, 60°]$.

3.7.1.2 Maximal singularity-free cylinder with $\phi \in [-60°, 60°]$

For $T \in [-\frac{\sqrt{3}}{3}, \frac{\sqrt{3}}{3}]$, i.e., $\phi \in [-60°, 60°]$, according to eq. (3.12), T is written as:

$$T = \frac{\sqrt{3}}{3} \sin \alpha$$

Applying the above procedure with $x_o = 0$, $y_o = 0$. The maximal singularity-free cylinder is shown in Figure 3.12. The portion of the singularity surface containing the point closest to the cylinder axis is at point $(x, y, \sin \alpha) = (0.28823, -0.24019, -0.09357)$ and the radius square of the cylinder is equal to $0.14077 dm^2$ (lengths are given in dm). In this case, it is clear that the critical point is located between the two extremities of the cylinder, $\sin \alpha = -0.09357$, i.e., $\phi = -6.19325°$. As expected, a reduction of the

range of rotation did not affect the radius of the singularity-free cylinder because the critical orientation is included in both ranges.

3.7.2 Asymmetric ranges of orientation

3.7.2.1 Maximal singularity-free cylinder with $\phi \in [0, 90°]$

For $T \in [0, 1]$, i.e., $\phi \in [0, 90°]$, according to eq. (3.11), T is written as:

$$\begin{aligned} T &= 0 + \frac{(1 + \sin\alpha)(1 - 0)}{2} \\ &= \frac{(1 + \sin\alpha)}{2} \end{aligned}$$

Applying the above procedure with $x_o = 0$ and $y_o = 1dm$, the maximal singularity-free cylinder is shown in Figure 3.13. The portion of the singularity surface containing the point closest to the cylinder axis is at point $(x, y, \sin\alpha) = (0.77975, 0.18039, -1)$ and the radius square of the cylinder is equal to $1.27978dm^2$ (lengths are given in dm). In this case, it is clear that the critical point is located at one extremity of the cylinder, $\sin\alpha = -1$, i.e., $\phi = 0°$.

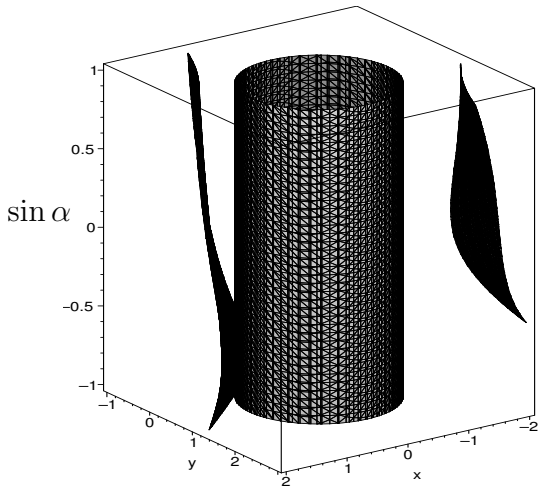

Figure 3.13: Maximal singularity-free cylinder with $\phi \in [0, 90°]$.

3.7.2.2 Maximal singularity-free cylinder with $\phi \in [30°, 90°]$

For $T \in [\tan\frac{\pi}{12}, 1]$, i.e., $\phi \in [30°, 90°]$, according to eq. (3.11), T is written as:

$$\begin{aligned} T &= \tan(\frac{\pi}{12}) + \frac{(1+\sin\alpha)(1-\tan(\frac{\pi}{12}))}{2} \\ &= \tan(\frac{\pi}{12}) + \frac{1}{2}(1-\tan(\frac{\pi}{12}))(1+\sin\alpha) \end{aligned}$$

Applying the above procedure with $x_o = 0$ and $y_o = 1dm$, the maximal singularity-free cylinder is shown in Figure 3.14. The portion of the singularity surface containing the point closest to the cylinder axis is at point $(x, y, \sin\alpha) = (1.09849, 0.23651, -1)$ and the radius square of the cylinder is equal to $1.78961dm^2$ (lengths are given in dm). In this case, it is clear that the critical point is located at one extremity of the cylinder, $\sin\alpha = -1$, i.e., $\phi = 30°$.

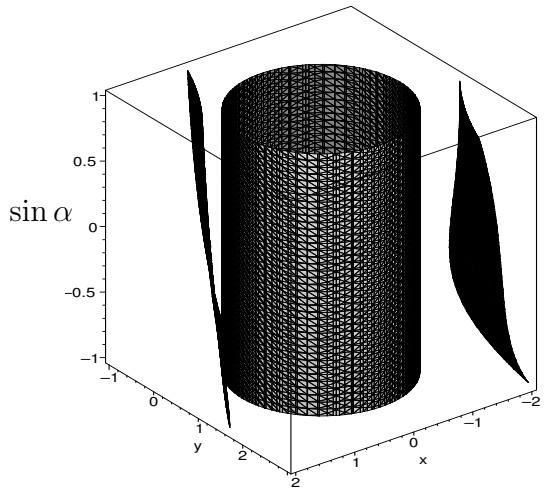

Figure 3.14: Maximal singularity-free cylinder with $\phi \in [30°, 90°]$.

3.7.2.3 Maximal singularity-free cylinder with $\phi \in [60°, 90°]$

For $T \in [\frac{\sqrt{3}}{3}, 1]$, i.e., $\phi \in [60°, 90°]$, according to eq. (3.11), T is written as:

$$\begin{aligned} T &= \frac{\sqrt{3}}{3} + \frac{(1+\sin\alpha)(1-\frac{\sqrt{3}}{3})}{2} \\ &= \frac{\sqrt{3}}{3} + \frac{1}{2}(1-\frac{\sqrt{3}}{3})(1+\sin\alpha) \end{aligned}$$

Applying the above procedure with $x_o = 0$ and $y_o = 1dm$, the maximal singularity-free cylinder is shown in Figure 3.15. The portion of the singularity surface containing the

point closest to the cylinder axis is also shown, which is located at one extremity of the cylinder with $(x, y, \sin\alpha) = (1.23967, 0.17505, -1)$ with the radius square of the cylinder is equal to $2.21730dm^2$ (lengths are given in dm), i.e., $\phi = 60°$.

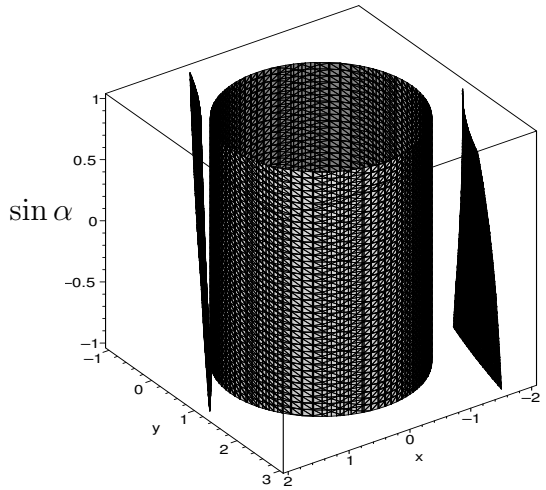

Figure 3.15: Maximal singularity-free cylinder with $\phi \in [60°, 90°]$.

3.8 Conclusions

A procedure for the determination of maximal singularity-free zones of a planar $3-RPR$ parallel mechanism with given center has been developed in this chapter. The procedure is based on a Lagrange multiplier method with the known singularity equation. The origin of the circle generating the cylinder, which is denoted as (x_o, y_o), is the center of the planned workspace. Applying this procedure, graphical representations of the singularity-free cylinders for different ranges of ϕ are obtained automatically. When a singularity-free cylinder is obtained using the optimization procedure, the most critical orientation is also obtained. Therefore, it is possible to increase the radius of the singularity-free cylinder by reducing the orientation range so as to exclude the most critical orientation. This information, obtained as a byproduct of the procedure, is also very useful in a context of design.

The procedure is effective and feasible, and does not rely on any special assumption on the geometry of the mechanism. Therefore, the procedure can be used to locate singularity-free zones for mechanisms in 3-D Cartesian space. It is a useful tool for the design and trajectory planning of a mechanism with known singularity equation.

Finally, the procedure was shown to be applicable to Gough-Stewart platforms when the latter are restricted to a specific 3-DOF motion system (two translations and one orientation). Although this application is rather academic, it serves as an introduction to the next chapters.

Chapter 4

Maximal Singularity-Free Zones of the General Gough-Stewart Platform for Constant Orientation or Position

4.1 Introduction

In Chapter 3, a procedure was introduced to determine maximal singularity-free zones for the planar 3-RPR parallel mechanisms. The procedure was also applied to the general Gough-Stewart platform for a specific similar 3-DOF motion system, that is, the platform can translate in the xy plane and rotate with respect to the axis perpendicular

to the xy plane. In practice, it is generally more useful to study the motion of the Gough-Stewart platform when either its orientation or its position is fixed.

In this chapter, inspired by the principle of the procedure of Chapter 3, two procedures are introduced to locate maximal singularity-free zones of the general Gough-stewart platform when either the orientation or the position is fixed. The results lead to singularity-free zones in the three-dimensional position workspace for a prescribed orientation or to singularity-free zones in the three-dimensional orientation workspace for a prescribed position. Both types of results are very useful in a context of design or trajectory planning.

This chapter is organized as follows: First, using the analytical form of the singularity locus equation of the general Gough-Stewart platform obtained in Chapter 2, the singularity equations for constant orientation or position are briefly recalled. Then, two procedures based on Lagrange multipliers are presented to locate maximal singularity-free zones with a prescribed center: one for constant orientation and the other for constant position. The singularity-free zones obtained are spheres tangent to the singularity locus in a 3-D position or orientation Cartesian space. Finally, numerical values are used to graphically illustrate both cases in order to demonstrate the effectiveness of the procedures. The procedures can be applied to analyze other similar parallel mechanisms with known singularity equations.

4.2 Singularity equations for constant orientation or position

The analytical singularity locus expression of the general Gough-Stewart platform obtained in Chapter 2 is a function of six variables, i.e., three position variables, x, y, z, and three orientation variables, ϕ, θ, ψ. Using this expression, first, fix the orientation and the singularity equation is then only function of x, y, z, in which the highest degree of x, y, z is 3. The resulting expression can be written in this form:

$$\begin{aligned} F_1(x,y,z) \;=\; & f_1x^3 + f_2x^2y + f_3x^2z + f_4x^2 + f_5y^2x + f_6xyz + f_7xy + f_8xz^3 + f_9xz \\ & + f_{10}x + f_{11}y^3 + f_{12}y^2z + f_{13}y^2 + f_{14}yz^2 + f_{15}yz + f_{16}y + f_{17}z^3 + f_{18}z^2 \\ & + f_{19}z + f_{20} = 0 \end{aligned} \tag{4.1}$$

where f_i, $i = 1, \ldots, 20$ are only functions of the architectural parameters for a given orientation. For a given architecture, the coefficients are constants. In fact, eq. (4.1) is the constant-orientation singularity locus presented in [34].

Similarly, it is possible to start from the general singularity locus equation of Chapter 2 and to fix the position. Then, applying the *tangent* of the half angle substitution on the Euler angles, that is, $T_1 = \tan(\frac{\theta}{2})$, $T_2 = \tan(\frac{\phi}{2})$ and $T_3 = \tan(\frac{\psi}{2})$, the singularity equation becomes a function of T_1, T_2 and T_3 for given position, which is written as:

$$F_2(T_1, T_2, T_3) = r_6 {T_1}^6 + r_5 {T_1}^5 + r_4 {T_1}^4 + r_3 {T_1}^3 + r_2 {T_1}^2 + r_1 T_1 + r_0 \tag{4.2}$$

where

$$r_i = s_6 {T_2}^6 + s_5 {T_2}^5 + s_4 {T_2}^4 + s_3 {T_2}^3 + s_2 {T_2}^2 + s_1 T_2 + s_0, \quad i = 0, ..., 6$$

where

$$s_i = w_6 {T_3}^6 + w_5 {T_3}^5 + w_4 {T_3}^4 + w_3 {T_3}^3 + w_2 {T_3}^2 + w_1 T_3 + w_0, \quad i = 0, ..., 6$$

where $w_i, i = 0, \ldots, 6$ are only functions of the architectural parameters for a given position. For a given architecture, these coefficients are constants.

4.3 Singularity-free zones in the constant-orientation workspace of the general Gough-Stewart platform

In this section, a new procedure is introduced to address the following problem: **For a given center of position (x_o, y_o, z_o) within the given workspace and for a prescribed orientation of the platform, find the largest singularity-free sphere in the (x, y, z) position workspace of the general Gough-Stewart platform**. For constant position of the general Gough-Stewart platform, another procedure is developed to address the following problem: **For a given center of orientation (T_{1o}, T_{2o}, T_{3o}) within the given workspace, find the largest singularity-free zone in (T_1, T_2, T_3) orientation space for the prescribed position**.

Applying the given architectural parameters given in Table 3.2, plots of the singularity loci eq. (4.1) with constant orientations within the given workspaces, $x, y, z \in [-10, 10]$, are presented in Figure 4.1. It is clear that the singularity manifolds are rather complex.

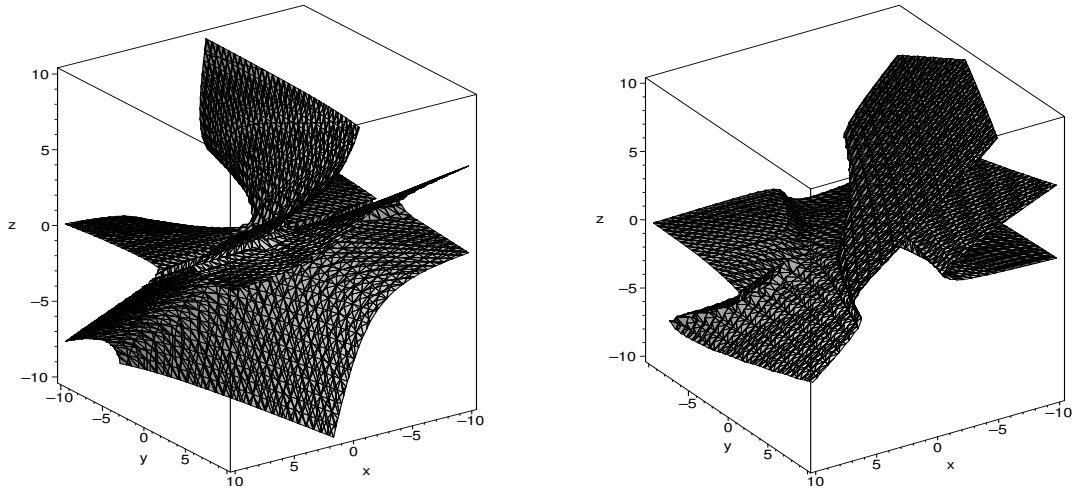

(a) $\phi = -2°$, $\theta = 30°$, $\psi = -87°$.

(b) $\phi = 30°$, $\theta = 30°$, $\psi = 30°$.

Figure 4.1: Singularity loci in 3-D Cartesian space with constant orientations (lengths are given in dm).

4.3.1 Mathematical formulation

The above constant orientation problem of the general Gough-Stewart platform can be solved using the following procedure:

Step 1: Choose a point (x_o, y_o, z_o) in 3-D Cartesian position space, which will be used as the center of the planned workspace. The point must not lie on the singularity surface. That is, when $x = x_o, y = y_o$ and $z = z_o$ are substituted into eq. (4.1), the result must be different from zero.

An alternative formulation for the problem stated above is the following: **For a given orientation, find the point on the singularity surface which is the closest to the center point** (x_o, y_o, z_o). This formulation can be written mathematically

as a minimization problem, namely:

$$\min_{(x,y,z,\lambda_1)} d_1 \tag{4.3}$$

where

$$d_1 = (x - x_o)^2 + (y - y_o)^2 + (z - z_o)^2 + \lambda_1 F_1(x, y, z) \tag{4.4}$$

where λ_1 is a Lagrange multiplier used to transform the constrained problem into an unconstrained problem. The above problem amounts to finding the largest possible sphere, centered at (x_o, y_o, z_o), which does not contain any singularity.

Step 2: An extremum of function of d_1 will be obtained if the partial derivatives of d_1 with respect to x, y, z and λ_1 are equal to zero, namely,

$$\frac{\partial d_1}{\partial x} = 2(x - x_o) + \lambda_1 \frac{\partial F_1}{\partial x} = 0 \tag{4.5}$$

$$\frac{\partial d_1}{\partial y} = 2(y - y_o) + \lambda_1 \frac{\partial F_1}{\partial y} = 0 \tag{4.6}$$

$$\frac{\partial d_1}{\partial z} = 2(z - z_o) + \lambda_1 \frac{\partial F_1}{\partial z} = 0 \tag{4.7}$$

$$\frac{\partial d_1}{\partial \lambda_1} = F_1(x, y, z) = 0 \tag{4.8}$$

which forms a system of four nonlinear equations in four unknowns x, y, z and λ_1.

Step 3: The above four equations are then solved to obtain a single equation with one unknown. It is readily observed that eqs. (4.5)— (4.7) contain λ_1. First, λ_1 can be eliminated from these three equations. For example, first, solving eq. (4.5) for λ_1 and substituting the result into eq. (4.6) leads to eq. (4.9), in which the degrees of x, y and z are 3, 3 and 2, respectively. Then, substituting the expression of λ_1 obtained from eq. (4.5) into eq. (4.7) leads to eq. (4.10), in which the degrees of x, y and z are 3, 2 and 3, respectively. Eqs. (4.9) and (4.10) together with eq. (4.8) form a system of three equations in three unknowns x, y and z. Eqs. (4.9) and (4.10) are written in the following form:

$$g_1(x, y, z) = 0 \tag{4.9}$$

$$g_2(x, y, z) = 0 \tag{4.10}$$

The resultant [39] is used to eliminate z from eqs. (4.9) and (4.10) leading to eq. (4.11), in which the degrees of x and y are 7 and 9, respectively. Then the elimination of z

from eqs. (4.9) and (4.8) leads to eq. (4.12), in which the degrees of x and y are 9 and 9, respectively. Eq. (4.11) and eq. (4.12) form a system of two equations in two unknowns, namely:

$$g_3(x, y) = 0 \tag{4.11}$$

$$g_4(x, y) = 0 \tag{4.12}$$

Finally, one of the two variables left are eliminated from eqs. (4.11) and (4.12) using again the resultant. For example, eliminating y, a single equation with only one variable, x, is obtained and can be written as:

$$\sum_{i=1}^{81} D_i x^i = 0 \tag{4.13}$$

where the coefficients D_i are the functions of architectural parameters for a constant orientation. For a given architecture, they are constants.

Step 4: Solve eq. (4.13) numerically and list all the real solutions of x, then, perform the back substitution using the following process:

1. Substitute the first solution of x, i.e., $x = x_1$ into eqs. (4.11) and (4.12). Now, these equations are only functions of y and can be solved independently. Solving the two equations for y, two groups of solutions of y are obtained. Among these two sets of solutions of y, if there is one common solution, it is then noted as y_1. Otherwise, repeat with the following solution of x until all solutions of x are substituted. Finally, keep all groups of solutions of x and the corresponding solutions of y, i.e., x_i and y_i.

2. Substitute each group of solution (x_i, y_i) obtained in the first step into eqs. (4.8), (4.9) and (4.10), now there are three equations, which are only functions of z. Solving these three equations independently, three groups of solutions of z are obtained. Among the three groups of solutions of z, if there is a common solution, denote it as z_i with the same subscript as x_i and y_i. This procedure is repeated with the next group of (x_i, y_i). All groups of solutions for x, y and corresponding z are then recorded.

3. Each of the solution sets x_i, y_i, z_i obtained will satisfy eq. (4.8) and are therefore located on the singularity manifold, as it should. Hence, referring to eq. (4.4),

the performance index d can be written, for a solution set as:

$$d_i = (x_i - x_o)^2 + (y_i - y_o)^2 + (z_i - z_o)^2$$

This index d_i is computed for all solution sets. The solution leading to the smallest value of d is the global minimum. The value of d is the square of the radius of the sphere corresponding to the singularity-free zone.

Step 5: Define a sphere in the 3-D Cartesian (x, y, z) space centered at the point (x_o, y_o, z_o). The sphere can be written in the following form:

$$(x - x_o)^2 + (y - y_o)^2 + (z - z_o)^2 - r^2 = 0 \tag{4.14}$$

where r^2 is the smallest value of d calculated above. Within this sphere, it can be guaranteed that there is no singularity. In fact, for the prescribed orientation, this sphere is the largest singularity-free sphere centered in (x_o, y_o, z_o).

4.3.2 Examples

Two examples are now given and the results are illustrated graphically. The architectural parameters given in Table 3.2 are used.

4.3.2.1 Example of constant orientation with $\phi = -2°$, $\theta = 30°$, and $\psi = -87°$

Assuming the given constant orientation: $\phi = -2°$, $\theta = 30°$, and $\psi = -87°$, the above procedure is applied. The maximal singularity-free spheres of the Gough-Stewart platform of Table 3.2 with different centers are shown in Figure 4.2. In Figure 4.2(a), the sphere is tangent to the singularity locus at point $(x, y, z) = (0.01029, -0.04536, 0.03765)$ and the radius square of the sphere is equal to $0.00358dm^2$ in the 3-D (x, y, z) position space. In Figure 4.2(b), the sphere is tangent to the singularity locus at point $(x, y, z) = (-1.12570, -1.23297, -0.44768)$ and the radius square of the sphere is equal to $0.37513dm^2$ in the 3-D (x, y, z) position space. In Figure 4.2(c), the sphere is tangent to the singularity locus at point $(x, y, z) = (1.03826, 1.07729, 0.87862)$ (lengths are given in dm) and the radius square of the sphere is equal to $0.02217dm^2$ in the 3-D (x, y, z) position space.

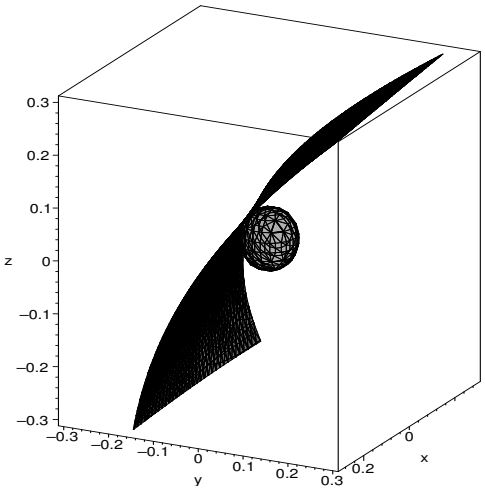

(a) Centered in $(0, 0, 0)$.

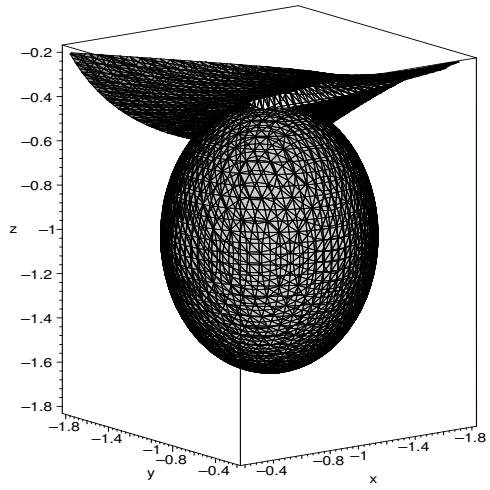

(b) Centered in $(-1, -1, -1)$.

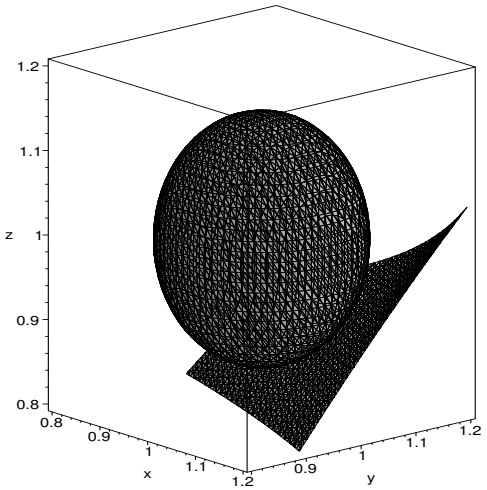

(c) Centered in $(1, 1, 1)$.

Figure 4.2: Maximal singularity-free spheres of the general Gough-Stewart platform with $\phi = -2°$, $\theta = 30°$, and $\psi = -87°$ (lengths are given in dm).

4.3.2.2 Example of constant orientation with $\phi = 30°$, $\theta = 30°$, and $\psi = 30°$

Assuming the given constant orientation: $\phi = 30°$, $\theta = 30°$, and $\psi = 30°$, the above procedure is applied. The maximal singularity-free spheres of the Gough-Stewart platform of Table 3.2 with different centers are shown in Figure 4.3. In Figure 4.3(a), the sphere is tangent to the singularity locus at point $(x, y, z) = (0.00274, 0.05376, -0.11597)$ and the radius square of the sphere is equal to $0.01635dm^2$ in the 3-D (x, y, z) posi-

tion space. In Figure 4.3(b), the sphere is tangent to the singularity locus at point $(x, y, z) = (-0.98278, -1.11353, -0.40626)$ and the radius square of the sphere is equal to $0.36571dm^2$ in the 3-D (x, y, z) position space. In Figure 4.3(c), the sphere is tangent to the singularity locus at point $(x, y, z) = (1.27398, 0.82637, 1.25696)$ (lengths are given in dm) and the radius square of the sphere is equal to $0.17124dm^2$ in the 3-D (x, y, z) position space.

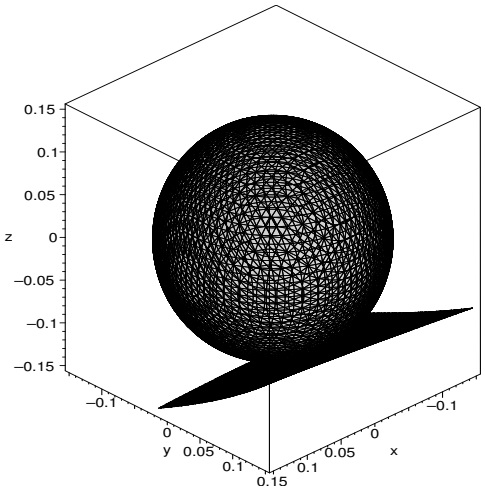

(a) Centered in $(0, 0, 0)$.

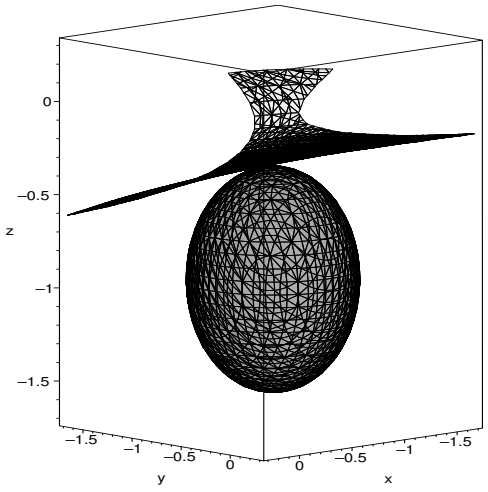

(b) Centered in $(-1, -1, -1)$.

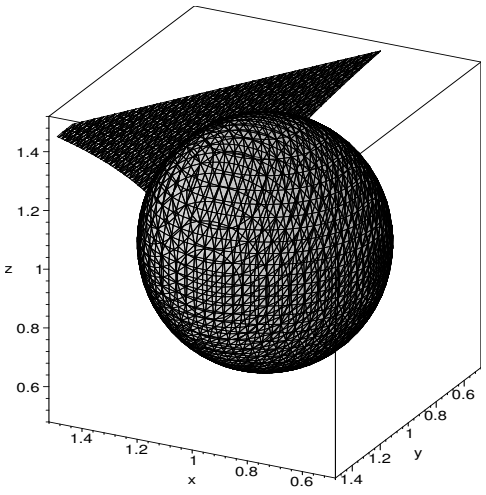

(c) Centered in $(1, 1, 1)$.

Figure 4.3: Maximal singularity-free spheres of the general Gough-Stewart platform with $\phi = 30°$, $\theta = 30°$, and $\psi = 30°$ (lengths are given in dm).

As a byproduct of the procedure, the most critical position on the surface of the

sphere (point of tangent contact with the singularity locus) is also obtained. Therefore, it could be possible to increase the size of the singularity-free zone by moving the center of the sphere in a direction opposite to the tangent point and repeating the procedure. For example, for the constant orientation with $\phi = -2°$, $\theta = 30°$ and $\psi = -87°$, if the center of the singularity-free sphere is chosen as the point $(-0.1, 0.44082, -0.36589)$, and repeat the procedure, as shown in Figure 4.4, the singularity-free sphere whose radius square is equal to $0.20447dm^2$ in the 3-D (x, y, z) position space (bigger than $0.00358dm^2$ as shown in Figure 4.2(a)) is obtained. The sphere is tangent to the singularity locus at point $(x, y, z) = (-.29451, 0.18059, -0.68040)$, instead of the point $(x, y, z) = (0.01029, -0.04536, 0.03765)$. The reason for this change is that the distance from the point $(-0.1, 0.44082, -0.36589)$ to the point $(-.29451, 0.18059, -0.68040)$ is shorter than to the point $(0.01029, -0.04536, 0.03765)$.

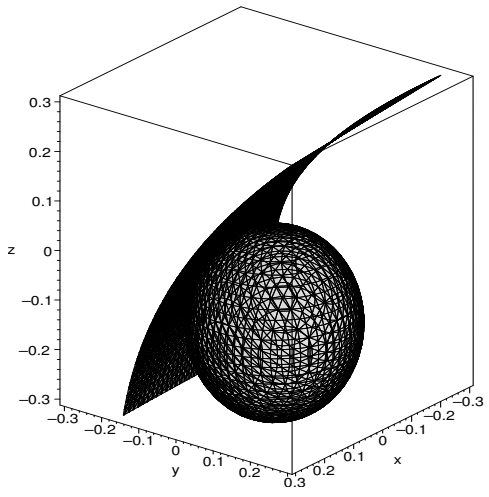

Figure 4.4: The maximal singularity-free zone of the general Gough-Stewart platform with $\phi = -2°$, $\theta = 30°$, and $\psi = -87°$ centered at $(-0.1, 0.44082, -0.36589)$ (lengths are given in dm).

4.4 Singularity-free zones in the constant-position workspace of the general Gough-Stewart platform

In this section, a procedure is introduced to address the following problem: **For a given central orientation** (T_{1o}, T_{2o}, T_{3o}) **within the given workspace and for a**

prescribed position of the platform, find the largest singularity-free sphere centered in (T_{1o}, T_{2o}, T_{3o}) in the (T_1, T_2, T_3) orientation workspace of the general Gough-Stewart platform.

Using the singularity locus eq. (4.2) and the architectural parameters given in Table 3.2, the constant position singularity loci of the Gough-Stewart platform with different constant positions are given in Figure 4.5. The singularity manifold are rather complex. Furthermore, the geometric interpretation of the (T_1, T_2, T_3) space is not intuitive. In fact, it is not possible to define a metric in the latter space. Nevertheless, a continuous region in this space will correspond to a continuous set of orientation. Therefore, by identifying a singularity-free region in this space, a continuous set of singularity-free orientations will be obtained.

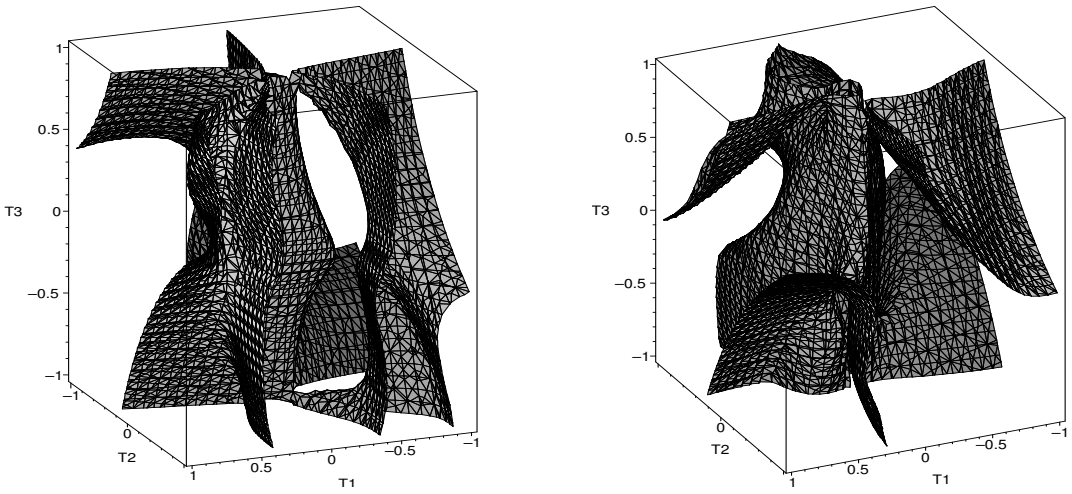

(a) $x = 0, y = 0, z = 0$.

(b) $x = 1, y = 1, z = 1$.

Figure 4.5: Singularity loci in 3-D Cartesian space with constant positions (lengths are given in dm).

4.4.1 Mathematical formulation

Since the highest degrees of T_1, T_2 and T_3 in equation (4.2) are 6, respectively, it is difficult to follow the procedure used in the previous section for the constant-orientation to combine the four equations into a single equation. Therefore, in this section, the

constant-position problem is solved using the following procedure, based on an alternative solution:

Step 1: Choose a point (T_{1o}, T_{2o}, T_{3o}) in 3-D Cartesian orientation workspace, which will be used as the center of the planned workspace. The point must not lie on the singularity locus, that is, substituting $T_1 = T_{1o}$, $T_2 = T_{2o}$, $T_3 = T_{3o}$ and the given architecture parameters into eq. (4.2), the result must not be equal to zero.

The formulation now proposed can be stated as follows: **Find the point on the singularity surface which is the closest to the center point (T_{1o}, T_{2o}, T_{3o})**. The formulation can be written mathematically as a minimization problem, namely:

$$\min_{(T_1,T_2,T_3,\lambda_2)} d_2 \tag{4.15}$$

where

$$d_2 = (T_1 - T_{1o})^2 + (T_2 - T_{2o})^2 + (T_3 - T_{3o})^2 + \lambda_2 F_2(T_1, T_2, T_3) \tag{4.16}$$

where λ_2 is a Lagrange multiplier used to transform the constrained problem into an unconstrained problem.

Step 2: An extremum of d_2 will be obtained if the partial derivatives of d_2 with respect to T_1, T_2, T_3 and λ_2 are equal to zero, namely:

$$\frac{\partial d_2}{\partial T_1} = 2(T_1 - T_{1o}) + \lambda_2 \frac{\partial F_2}{\partial T_1} = 0 \tag{4.17}$$

$$\frac{\partial d_2}{\partial T_2} = 2(T_2 - T_{2o}) + \lambda_2 \frac{\partial F_2}{\partial T_2} = 0 \tag{4.18}$$

$$\frac{\partial d_2}{\partial T_3} = 2(T_3 - T_{3o}) + \lambda_2 \frac{\partial F_2}{\partial T_3} = 0 \tag{4.19}$$

$$\frac{\partial d_2}{\partial \lambda_2} = F_2(T_1, T_2, T_3) = 0 \tag{4.20}$$

which forms a system of four nonlinear equations in four unkowns T_1, T_2, T_3 and λ_2.

Step 3: The degree of the above nonlinear equations is much higher than in the constant-orientation problem. Therefore, it is not possible to eliminate variables and reduce the problem to a single equation in one unknown. Instead, the above system of equations is solved numerically using, for instance, continuation methods [1] or the Newton-Raphson algorithm [38]. In principle, continuation methods allow all the roots

of a nonlinear system of equations to be found, however, no matter what methods will be used, the solutions obtained are further tested in order to ensure that the global minimization is found.

To this end, all the solutions of T_1, T_2, T_3 and corresponding λ_2 obtained numerically are first recorded. Then each group of solutions of T_1, T_2, T_3 and the corresponding λ_2 are substituted into (4.16) and the value of d_2 is calculated. The solution leading to the smallest value of d_2 is the global minimum. Denote the solution of T_1, T_2, T_3 corresponding to the smallest d_2 as ${T_1}^n$, ${T_2}^n$ and ${T_3}^n$, respectively. This solution is further investigated in the next step.

Step 4: In order to verify the above point (${T_1}^n$, ${T_2}^n$, ${T_3}^n$) is the point on the singularity locus closest to the point (T_{1o}, T_{2o}, T_{3o}), first, one of the three values of T_1, T_2 or T_3, i.e., $T_1 = {T_1}^n$, $T_2 = {T_2}^n$ or $T_3 = {T_3}^n$, is substituted into eq. (4.16). For example, substitute $T_1 = {T_1}^n$ into eq. (4.16), an extremum of d_2 will be obtained if the partial derivatives of d_2 with respect to T_2, T_3 and λ_2 are equal to zero, namely:

$$2(T_2 - T_{2o}) + \lambda_2 \frac{\partial F_2}{\partial T_2} = 0 \tag{4.21}$$

$$2(T_3 - T_{3o}) + \lambda_2 \frac{\partial F_2}{\partial T_3} = 0 \tag{4.22}$$

$$F_2(T_2, T_3) = 0 \tag{4.23}$$

which forms a system of three equations in three unknowns T_2, T_3 and λ_2.

The above three equations can now be reduced to one equation with one variable. First, eliminate λ_2 from eqs. (4.21) and (4.22). An equation in T_2 and T_3 is obtained:

$$h(T_2, T_3) = 0 \tag{4.24}$$

Now, there are two equations eq. (4.23) and eq. (4.24) in two unknowns T_2 and T_3. Second, eliminate one of the two left unknowns T_2 or T_3, for example, eliminate T_2 from eq. (4.23) and eq. (4.24) using the resultant. A single equation is obtained which is only function of T_3:

$$\sum_{i=1}^{84} E_i {T_3}^i = 0 \tag{4.25}$$

This equation can then be solved and all the real solutions of T_3 are obtained. Then, the back substitution can be performed using the following process:

1. Substitute the first solution of T_3, i.e., $T_3 = T_{31}$ into eqs. (4.23) and (4.24). Now, these equations are only functions of T_2 and can be solved independently. Solve the two equations for T_2, two groups of solutions of T_2 are obtained. Among these two sets of solutions of T_2, if there is one common solution, then noted as T_{21}. Repeat with the following solution of T_3 until all solutions of T_3 are substituted. Finally, keep all groups of solutions of T_3 and corresponding solutions of T_2, i.e., T_{3i} and T_{2i}.

2. Substitute each group of solutions for T_3, T_2 and $T_1 = {T_1}^n$ into eq. (4.16), knowing that at a solution, the last term of eq. (4.16) is equal to zero. Record the value of d_2 obtained for each solution. The solution with the minimum value of d_2 is the global minimum and should lead to $T_2 = {T_2}^n$ and $T_3 = {T_3}^n$

The process described above is used in order to further verify that the solution ${T_1}^n$, ${T_2}^n$, ${T_3}^n$ obtained numerically and corresponding to the smallest d_2 is the global minimum, i.e., the point of the singularity manifold closest to the point (T_{1o}, T_{2o}, T_{3o}) in the 3-D Cartesian (T_1, T_2, T_3) space. This verification can also be repeated by first letting $T_2 = {T_2}^n$ and then with $T_3 = {T_3}^n$. However, if a continuation method is used to solve numerically for the global minimum, this verification may be superfluous. The solution can also be verified graphically by plotting the resulting sphere and the singularity locus, as will be shown in the examples.

Step 5: Define a sphere whose center is located at (T_{1o}, T_{2o}, T_{3o}) in the 3-D Cartesian (T_1, T_2, T_3) space in the following form:

$$(T_1 - T_{1o})^2 + (T_2 - T_{2o})^2 + (T_3 - T_{3o})^2 - {r_T}^2 = 0 \tag{4.26}$$

where ${r_T}^2$ is the smallest value of d_2 calculated above. Within this zone, it can be guaranteed that there is no singularity. As mentioned above, the geometric interpretation of a sphere in the (T_1, T_2, T_3) space is not obvious. Nevertheless, it represents a continuous simply connected region of the space of orientations.

4.4.2 Examples

In the following examples, the singularity locus and the singularity-free zones of the general Gough-Stewart platform with different constant positions are given, in which

the centers of the singularity-free zones are at point $(0, 0, 0)$.

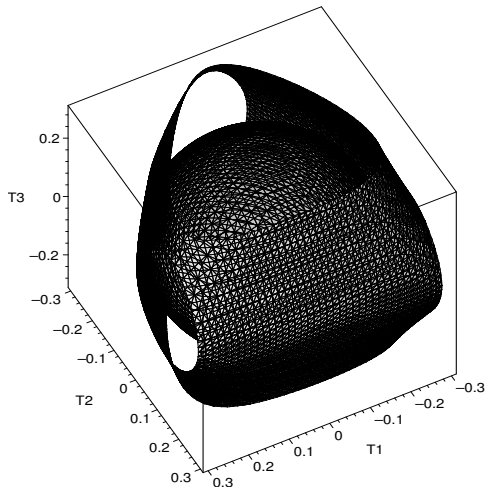

(a) in 3-D orientation space.

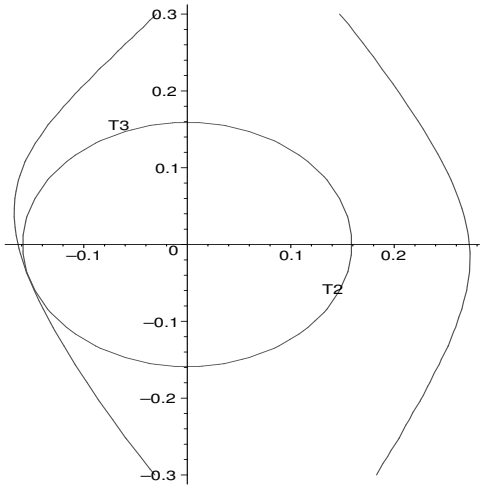

(b) in T_2T_3 plane with $T_1 = -0.21290$.

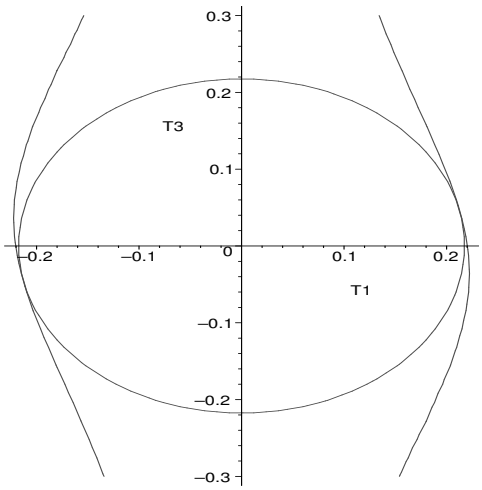

(c) in T_1T_3 plane with $T_2 = -0.15228$.

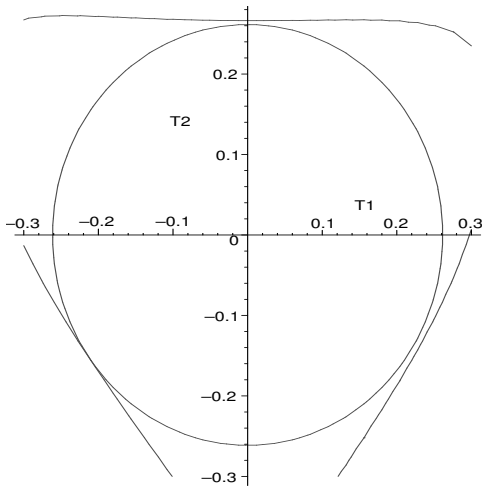

(d) in T_1T_2 plane with $T_3 = -0.04671$.

Figure 4.6: Maximal singularity-free zones of constant position with $x = 0, y = 0$ and $z = 0$ in 3-D orientation space and different planes (lengths are given in dm).

4.4.2.1 Example of constant position with $x = 0, y = 0$ and $z = 0$

With the constant position of the platform: $x = 0, y = 0$ and $z = 0$ and the Gough-Stewart platform of Table 3.2, the above procedure is applied. The maximal singularity-

free zone of the general Gough-Stewart platform in 3-D Cartesian orientation space is as shown in Figure 4.6(a). The sphere obtained is tangent to the singularity locus at point $(T_1, T_2, T_3) = (-0.21290, -0.15228, -0.04671)$ and the radius square of the sphere is equal to 0.07070. The zone obtained is free from singularities and that the minimum obtained is effectively the global minimum. The figures of the sections in the planes corresponding to $T_1 = -0.21290$, $T_2 = -0.15228$ and $T_3 = -0.04671$ are illustrated in Figures 4.6(b)–4.6(d), respectively.

4.4.2.2 Example of constant position with $x = 1, y = 1$ and $z = 1$

With the constant position of the platform: $x = 1, y = 1$ and $z = 1$ (lengths are given in dm), and the architectural parameters of Table 3.2, the singularity locus within the given workspace is illustrated in Figure 4.5(b). The above procedure is then applied and the maximal singularity-free zone of the platform in 3-D Cartesian orientation space is as shown in Figure 4.7. The sphere obtained is tangent to the singularity locus at point $(T_1, T_2, T_3) = (-0.05987, 0.03557, 0.00013)$ and the radius square of the sphere is equal to 0.00485.

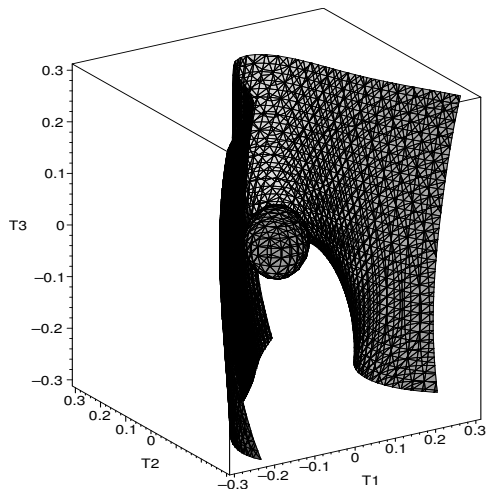

Figure 4.7: The maximal singularity-free zone of constant position with $x = 1, y = 1$ and $z = 1$ (lengths are given in dm).

4.5 Conclusions

In this chapter, two new procedures were presented to determine maximal singularity-free zones with given centers for constant orientation or constant position of the general Gough-Stewart platform, respectively. The procedures are based on a Lagrange multiplier method and the singularity equations developed in Chapter 2. The centers of the zones, which are the centers of the planned workspaces should be chosen properly. Applying the procedures, graphical representations of the singularity-free zones for different constant orientations or positions are obtained automatically.

Both procedures are feasible and easy to handle numerically. Since no assumption is made on the geometry of the mechanism, the procedures can be used to determine singularity-free zones for mechanisms with 3-DOF pure translations or rotations. It is an useful tool for analysis and the trajectory planning of mechanisms with known singularity equations.

Chapter 5

Maximal Singularity-free Zones of the General Gough-Stewart Platform in the Six-dimensional Cartesian Space

5.1 Introduction

In Chapter 2, the analytical expression of the singularity locus of the general Gough-Stewart platform, which is in six variables $(x, y, z, \phi, \theta, \psi)$ has been obtained. As the complete workspace of the general Gough-Stewart platform is a six-dimensional entity, which is impossible to visualize, algorithms for *constant-orientation workspace* and

constant-position workspace, which are 3-D workspaces have been proposed by several researchers ([25], [36], [12], [30], [16], [29], [4], [40]). In this chapter, for purposes of simplicity, we assume that the workspace of the general Gough-Stewart platform is known, and is given with proper ranges of the six variables in 6-D space.

In Chapters 3 and 4, procedures locating singularity-free zones for both $3-RPR$ planar parallel mechanisms and the general Gough-Stewart platform have been developed. Inspired by this approach and the results obtained, in this chapter, procedures for locating the maximal singularity-free zones in 6-D space are introduced. Indeed, although the results of Chapters 3 and 4 are of great interest, in a practical design, both positions and orientations must be varied simultaneously in order to obtain a more accurate account of the kinematic behavior of the mechanism in its 6-D workspace. However, when dealing with the 6-D workspace, graphical verifications are no longer possible. This is why graphical illustrations were provided in previous chapters, in order to gain confidence in the proposed approach.

In this chapter, three new procedures are introduced. Using a weighting factor, the three procedures are formulated with a common mathematical framework. The first procedure aims at locating maximal singularity-free zones in the 3-D position space, which are free from singularity for any orientation within given ranges. This procedure is more general than the procedure introduced in the preceding chapter since the latter assumed a constant orientation. The second procedure aims at determining maximal singularity-free zones in the 3-D orientation space, which are free from singularity for any position within given ranges. Again, this procedure is more general than the one introduced in the preceding chapter since the latter assumed a constant position. Finally, another procedure is developed to determine the maximal singularity-free zones in the 6-D workspace. Because of the complexity of the singularity equation of the general Gough-Stewart platform, a simple singularity equation having a form similar to that of the general Gough-Stewart platform is first used to illustrate the procedures. Then, the procedure are applied to the singularity equation of the general Gough-Stewart platform, and graphic illustrations of the maximal singularity-free zones are presented.

5.2 Simplified singularity equation

In order to illustrate the procedures, let us first assume that there exists a 6-DOF parallel mechanism, whose singularity locus can be expressed as an implicit function of the position variables x, y and z and the three Euler angles ϕ, θ and ψ, using the *tangent* half angle substitution, i.e., $T_1 = \tan(\frac{\theta}{2})$, $T_2 = \tan(\frac{\phi}{2})$ and $T_3 = \tan(\frac{\psi}{2})$, this singularity equation can be written in this form:

$$\begin{aligned} F(x, y, z, T_1, T_2, T_3) &= x^2 + y^2 + z^2 + e_1 x + e_2 y + e_3 z + {T_1}^2 + {T_2}^2 + {T_3}^2 \\ &\quad + e_4 T_1 + e_5 T_2 + e_6 T_3 + e_7 = 0 \end{aligned} \tag{5.1}$$

where $e_i, i = 1, \ldots, 7$, are constants.

Second, let us assume that workspaces of both this parallel mechanism and the general Gough-Stewart platform are known, and are comprised of two parts, a location part (a box in the 3-D position (x, y, z) space) and an orientation part (a box in the 3-D orientation (T_1, T_2, T_3) space), which define a hyper-box in the 6-D workspace of the mechanisms. This hyper-box is limited by

$$x \in [x_{min}, x_{max}], \quad y \in [y_{min}, y_{max}], \quad z \in [z_{min}, z_{max}]$$

$$T_1 \in [T_{1min}, T_{1max}], \quad T_2 \in [T_{2min}, T_{2max}], \quad T_3 \in [T_{3min}, T_{3max}]$$

The ranges of both the position variables and the orientation variables can be adjusted for different architectures and applications. The latter assumption is reasonable since, for design purposes, a rough estimate of the workspace is generally assumed and the precise boundaries of the actual workspace need not be considered in the first design stage.

In the next section, the mathematical formulation of the new procedures will be given and applied to the simplified singularity equation for illustration purposes.

5.3 Mathematical formulation

For a 6-DOF mechanism with a known singularity equation, the following problem is now addressed: **For a given center pose** $(x_o, y_o, z_o, T_{1o}, T_{2o}, T_{3o})$**, find the largest**

singularity-free 'hyper-sphere' in the 6-dimensional workspace, centered in $(x_o, y_o, z_o, T_{1o}, T_{2o}, T_{3o})$**, which is free from singularities**. An alternative formulation of this problem is: **Find the point on the singularity manifold (in 6-D), which is the closest to the center point** $(x_o, y_o, z_o, T_{1o}, T_{2o}, T_{3o})$. This problem can be written mathematically as a minimization problem, namely:

$$\min_{(x,y,z,T_1,T_2,T_3,\lambda)} D \tag{5.2}$$

where

$$\begin{aligned} D &= (x-x_o)^2 + (y-y_o)^2 + (z-z_o)^2 + (T_1-T_{1o})^2 + (T_2-T_{2o})^2 + (T_3-T_{3o})^2 \\ &\quad + \lambda F(x, y, z, T_1, T_2, T_3) \end{aligned} \tag{5.3}$$

where λ is a Lagrange multiplier used to transform the constrained problem into an unconstrained problem, and where F is the singularity manifold.

However, the above formulation poses the problem of defining a distance in the 6-D workspace in order to find the 'closest', point on the singularity manifold. Clearly, an Euclidean distance cannot be defined in this space since it is composed of mixed dimensions (position coordinates and orientation coordinates). Therefore, the above index D cannot be called a distance in the mathematical sense of the term and the singularity-free region obtained cannot formally be termed a 'hyper-sphere'.

However, the zone obtained, although not formally a 'hyper-sphere', is still a continuous singularity-free zone in the 6-D workspace, which is very useful in the context of design. Moreover, the designer may want to favour either the position workspace or the orientation workspace. To this end, a weighting coefficient is introduced, which can be adjusted by the designer. With the introduction of the weighting coefficient W, eq. (5.3) can be rewritten as:

$$\begin{aligned} D &= W((x-x_o)^2 + (y-y_o)^2 + (z-z_o)^2) + (1-W)((T_1-T_{1o})^2 + (T_2-T_{2o})^2 \\ &\quad + (T_3-T_{3o})^2) + \lambda F \end{aligned} \tag{5.4}$$

where $W \in [0 \quad 1]$. For different values of W within the given range, three procedures are proposed. These three procedures all rest on the same mathematical formulation.

5.3.1 Case 1, $W = 1$: Prescribed ranges of orientation

In this case, eq. (5.4) is rewritten as:

$$D_1 = (x - x_o)^2 + (y - y_o)^2 + (z - z_o)^2 + \lambda_1 F_1(x, y, z, T_1, T_2, T_3) \tag{5.5}$$

The above problem is now transformed into the following: **For a given rotational range of motion (**$(T_{1min} \leq T_1 \leq T_{1max})$**,** $(T_{2min} \leq T_2 \leq T_{2max})$ **and** $(T_{3min} \leq T_3 \leq T_{3max})$**) and a given center of position** (x_o, y_o, z_o)**, find the largest singularity-free sphere in the 3-D position workspace, which is free from singularities for any orientation in the given ranges**.

A geometric interpretation of this problem is as follows: for each orientation in the prescribed range, a singularity manifold can be plotted in the (x, y, z) space. Find the manifold that contains a point closest to the center (x_o, y_o, z_o) and locate this point on the manifold.

The following procedure is proposed to solve this problem:

Step 1: Introducing three new angles α_1, β_1 and μ_1, T_1, T_2 and T_3 within the given ranges can be written as [32]:

$$\begin{aligned} T_1 &= T_{1min} + (\frac{1 + \sin\alpha_1}{2})(T_{1max} - T_{1min}) \\ T_2 &= T_{2min} + (\frac{1 + \sin\beta_1}{2})(T_{2max} - T_{2min}) \\ T_3 &= T_{3min} + (\frac{1 + \sin\mu_1}{2})(T_{3max} - T_{3min}) \end{aligned}$$

where

$$\sin\alpha_1 \in [-1, 1], \quad \sin\beta_1 \in [-1, 1], \quad \sin\mu_1 \in [-1, 1]$$

For the sake of simplifying the derivation, the ranges of T_1, T_2 and T_3 are assumed to be symmetric with respect to zero, i.e., defining $T_{1max} = -T_{1min} = a$, with $a \in (0, 1]$ and likewise for the ranges of T_2 and T_3, i.e., $T_{2max} = -T_{2min} = b$ with $b \in (0, 1]$, $T_{3max} = -T_{3min} = c$ with $c \in (0, 1]$, then the above expressions of T_1, T_2 and T_3 can be rewitten as:

$$T_1 = a\sin\alpha_1, \quad T_2 = b\sin\beta_1, \quad T_3 = c\sin\mu_1$$

substituting the above expressions into eq. (5.1), the singularity equation is rewritten as:

$$\begin{aligned} F_1(x, y, z, \sin\alpha_1, \sin\beta_1, \sin\mu_1) &= x^2 + y^2 + z^2 + e_1 x + e_2 y + e_3 z + a^2 \sin^2\alpha_1 \\ &\quad + b^2 \sin^2\beta_1 + c^2 \sin^2\mu_1 + e_4 a \sin\alpha_1 \\ &\quad + e_5 b \sin\beta_1 + e_6 c \sin\mu_1 + e_7 = 0 \end{aligned} \tag{5.6}$$

Step 2: An extremum of function D_1 will be obtained if the partial derivatives of D_1 with respect to $x, y, z, \lambda_1, \alpha_1, \beta_1$ and μ_1 are equal to zero, namely,

$$\frac{\partial D_1}{\partial x} = 2(x - x_o) + \lambda_1(e_1 + 2x) = 0 \tag{5.7}$$

$$\frac{\partial D_1}{\partial y} = 2(y - y_o) + \lambda_1(e_2 + 2y) = 0 \tag{5.8}$$

$$\frac{\partial D_1}{\partial z} = 2(z - z_o) + \lambda_1(e_3 + 2z) = 0 \tag{5.9}$$

$$\frac{\partial D_1}{\partial \lambda_1} = F_1(x, y, z, \sin\alpha_1, \sin\beta_1, \sin\mu_1) = 0 \tag{5.10}$$

$$\frac{\partial D_1}{\partial \alpha_1} = (2a \sin\alpha_1 + e_4) a \cos\alpha_1 = A_1 a \cos\alpha_1 = 0 \tag{5.11}$$

$$\frac{\partial D_1}{\partial \beta_1} = (2b \sin\beta_1 + e_5) b \cos\beta_1 = B_1 b \cos\beta_1 = 0 \tag{5.12}$$

$$\frac{\partial D_1}{\partial \mu_1} = (2c \sin\mu_1 + e_6) c \cos\mu_1 = C_1 c \cos\mu_1 = 0 \tag{5.13}$$

where

$$\begin{aligned} A_1 &= 2a \sin\alpha_1 + e_4 \\ B_1 &= 2b \sin\beta_1 + e_5 \\ C_1 &= 2c \sin\mu_1 + e_6 \end{aligned}$$

in which a, b, c, x_o, y_o and z_o are constants, which are prescribed by the designer. For the simplified singularity equation, eqs. (5.11)— (5.13) are only functions of the Euler angles. However, for general cases, because of the coupling of the position variables and orientation variables, these equations are functions of all six variables, i.e., x, y, z, α_1, β_1 and μ_1. It will be shown that the procedure can be extended to the general case.

Now, there are a total of 7 equations, i.e., eqs. (5.7)— (5.13) and 7 variables, i.e., $x, y, z, \sin\alpha_1, \sin\beta_1, \sin\mu_1$ and λ_1.

Eqs. (5.11), (5.12) and (5.13) are satisfied in the following cases (a, b and c are not equal to zero):

$$A_1 = 0 \quad \text{or} \quad \cos\alpha_1 = 0$$
$$B_1 = 0 \quad \text{or} \quad \cos\beta_1 = 0$$
$$C_1 = 0 \quad \text{or} \quad \cos\mu_1 = 0$$

which represent:

$$A_1 = 0, \quad \sin\alpha_1 = 1, \quad \sin\alpha_1 = -1$$
$$B_1 = 0, \quad \sin\beta_1 = 1, \quad \sin\beta_1 = -1$$
$$C_1 = 0, \quad \sin\mu_1 = 1, \quad \sin\mu_1 = -1$$

As shown in Table 5.1, there are a total of $3 \times 3 \times 3 = 27$ combinations of cases satisfying eqs. (5.11), (5.12) and (5.13) . With the given ranges of the orientation variables, the orientation workspace of the mechanism is a box in 3-D (T_1, T_2, T_3) space. If $A_1 = 0$, $B_1 = 0$ and $C_1 = 0$, then the orientation part of the point (x, y, z, T_1, T_2, T_3) on the singularity surface, which is the closest to the point (x_o, y_o, z_o), i.e., (T_1, T_2, T_3), is located within the ranges of T_1, T_2 and T_3, which is inside the box. If any two of $A_1 = 0$, $B_1 = 0$ and $C_1 = 0$ are satisfied, for example, $A_1 = 0$ and $B_1 = 0$ together with $\sin\mu_1 = 1$, the orientation part of the point on the singularity surface, which is closest to the point (x_o, y_o, z_o) is located on one of the surfaces of the box. If any one of $A_1 = 0$, $B_1 = 0$ and $C_1 = 0$ is satisfied, for example, $A_1 = 0$ together with $\sin\beta_1 = 1$ and $\sin\mu_1 = 1$, the orientation part of the point on the singularity surface, which is closest to the point (x_o, y_o, z_o) is located on one of the edges of the box. Otherwise, it is located on one of the 8 vertices of the box. Hence, four cases of solutions are distinguished.

Step 3: Solve each of the combination listed in Table 5.1 together with eqs. (4.7)—(4.10). In other words, there are 27 independent series of computations.

In order to find the point (x, y, z, T_1, T_2, T_3) on the singularity locus, which is the closest to the given position in 6-D space, in the following sections, analytical solutions of the above four cases are presented. For the first case, i.e., $A_1 = 0$, $B_1 = 0$ and

Combination i	C_1	C_2	C_3
1	$A_1 = 0$	$B_1 = 0$	$C_1 = 0$
2	$A_1 = 0$	$B_1 = 0$	$\sin\mu_1 = 1$
3	$A_1 = 0$	$B_1 = 0$	$\sin\mu_1 = -1$
4	$A_1 = 0$	$\sin\beta_1 = 1$	$C_1 = 0$
5	$A_1 = 0$	$\sin\beta_1 = 1$	$\sin\mu_1 = 1$
6	$A_1 = 0$	$\sin\beta_1 = 1$	$\sin\mu_1 = -1$
7	$A_1 = 0$	$\sin\beta_1 = -1$	$C_1 = 0$
8	$A_1 = 0$	$\sin\beta_1 = -1$	$\sin\mu_1 = 1$
9	$A_1 = 0$	$\sin\beta_1 = -1$	$\sin\mu_1 = -1$
10	$\sin\alpha_1 = 1$	$B_1 = 0$	$C_1 = 0$
11	$\sin\alpha_1 = 1$	$B_1 = 0$	$\sin\mu_1 = 1$
12	$\sin\alpha_1 = 1$	$B_1 = 0$	$\sin\mu_1 = -1$
13	$\sin\alpha_1 = 1$	$\sin\beta_1 = 1$	$C_1 = 0$
14	$\sin\alpha_1 = 1$	$\sin\beta_1 = 1$	$\sin\mu_1 = 1$
15	$\sin\alpha_1 = 1$	$\sin\beta_1 = 1$	$\sin\mu_1 = -1$
16	$\sin\alpha_1 = 1$	$\sin\beta_1 = -1$	$C_1 = 0$
17	$\sin\alpha_1 = 1$	$\sin\beta_1 = -1$	$\sin\mu_1 = 1$
18	$\sin\alpha_1 = 1$	$\sin\beta_1 = -1$	$\sin\mu_1 = -1$
19	$\sin\alpha_1 = -1$	$B_1 = 0$	$C_1 = 0$
20	$\sin\alpha_1 = -1$	$B_1 = 0$	$\sin\mu_1 = 1$
21	$\sin\alpha_1 = -1$	$B_1 = 0$	$\sin\mu_1 = -1$
22	$\sin\alpha_1 = -1$	$\sin\beta_1 = 1$	$C_1 = 0$
23	$\sin\alpha_1 = -1$	$\sin\beta_1 = 1$	$\sin\mu_1 = 1$
24	$\sin\alpha_1 = -1$	$\sin\beta_1 = 1$	$\sin\mu_1 = -1$
25	$\sin\alpha_1 = -1$	$\sin\beta_1 = -1$	$C_1 = 0$
26	$\sin\alpha_1 = -1$	$\sin\beta_1 = -1$	$\sin\mu_1 = 1$
27	$\sin\alpha_1 = -1$	$\sin\beta_1 = -1$	$\sin\mu_1 = -1$

Table 5.1: The 27 cases of combinations of eq. (5.11), eq. (5.12) and eq. (5.13).

$C_1 = 0$, solve eqs. (5.7)— (5.10) together with $A_1 = 0$, $B_1 = 0$ and $C_1 = 0$ for $x, y, z, \lambda_1, \sin\alpha_1, \sin\beta_1$ and $\sin\mu_1$. The analytical solutions are:

$$\begin{aligned} x &= \frac{2x_o - e_1\lambda_1}{2(1+\lambda_1)} \\ y &= \frac{2y_o - e_2\lambda_1}{2(1+\lambda_1)} \\ z &= \frac{2z_o - e_3\lambda_1}{2(1+\lambda_1)} \\ \lambda_1 &= \frac{-s_1 \pm \sqrt{s_1^2 - s_1 s_2}}{s_1} \\ \sin\alpha_1 &= \frac{-e_4}{2a} \\ \sin\beta_1 &= \frac{-e_5}{2b} \\ \sin\mu_1 &= \frac{-e_6}{2c} \end{aligned}$$

where

$$\begin{aligned} s_1 &= {e_1}^2 + {e_2}^2 + {e_3}^2 + m_1 \\ s_2 &= -4{x_o}^2 - 4{y_o}^2 - 4{z_o}^2 - 4e_1x_o - 4e_2y_o - 4e_3z_o + m_1 \\ m_1 &= {e_4}^2 + {e_5}^2 + {e_6}^2 - 4e_7 \end{aligned}$$

There are two potential groups of solutions of the seven variables.

Each of the solution sets x, y, z, $\sin\alpha_1$, $\sin\beta_1$, $\sin\mu_1$ obtained will satisfy eq. (5.10), i.e., all minima are located on the singularity manifold. Therefore, using eq. (5.5) on a solution set, one has:

$$D_1 = (x - x_o)^2 + (y - y_o)^2 + (z - z_o)^2 \tag{5.14}$$

This index D_1 is evaluated for the two solution sets. The solution leading to the smaller value of D_1 is defined as r_{s1} and the corresponding values of the six variables noted as $x = x_1, y = y_1, z = z_1, \sin\alpha_1 = \sin\alpha_{11}, \sin\beta_1 = \sin\beta_{11}$ and $\sin\mu_1 = \sin\mu_{11}$ are recorded.

For the second case, i.e., any two of $A_1 = 0$, $B_1 = 0$ and $C_1 = 0$ are satisfied, for example, $A_1 = 0$, $B_1 = 0$ and $\sin\mu_1 = 1$, substituting $\sin\mu_1 = 1$ into eqs. (5.7)— (5.10), in our case, only substitute into eq. (5.10), together with $A_1 = 0$, $B_1 = 0$, there

are a total of six variables $(x, y, z, \lambda_1, \sin\alpha_1, \sin\beta_1)$ and six equations. Solving the six equations at the same time, the following solutions are obtained:

$$\begin{aligned} x &= \frac{2x_o - e_1\lambda_1}{2(1+\lambda_1)} \\ y &= \frac{2y_o - e_2\lambda_1}{2(1+\lambda_1)} \\ z &= \frac{2z_o - e_3\lambda_1}{2(1+\lambda_1)} \\ \lambda_1 &= \frac{-s_3 \pm \sqrt{s_3^2 - s_3 s_4}}{s_3} \\ \sin\alpha_1 &= \frac{-e_4}{2a} \\ \sin\beta_1 &= \frac{-e_5}{2b} \\ \sin\mu_1 &= 1 \end{aligned}$$

where

$$\begin{aligned} s_3 &= {e_1}^2 + {e_2}^2 + {e_3}^2 + {e_4}^2 + {e_5}^2 - m_2 \\ s_4 &= -4{x_o}^2 - 4{y_o}^2 - 4{z_o}^2 - 4e_1x_o - 4e_2y_o - 4e_3z_o + {e_4}^2 + {e_5}^2 - m_2 \\ m_2 &= 4e_7 + 4c^2 + 4e_6c \end{aligned}$$

There are two potential groups of solutions of $x, y, z, \lambda_1, \sin\alpha_1$ and $\sin\beta_1$. Each of the solution sets x, y, z, $\sin\alpha_1$, $\sin\beta_1$, $\sin\mu_1$ obtained will satisfy eq. (5.10), i.e., all minima are located on the singularity manifold. Therefore, using eq. (5.5) on a solution set, eq. (5.14) is obtained. D_1 is evaluated for the two solution sets and the smaller result is noted as r_{s2} and the corresponding values of the six variables as $x = x_2, y = y_2, z = z_2, \sin\alpha_1 = \sin\alpha_{12}, \sin\beta_1 = \sin\beta_{12}$, $\sin\mu_1 = 1$ are recorded.

For the third case, i.e., any one of $A_1 = 0$, $B_1 = 0$ and $C_1 = 0$ are satisfied, for example, $A_1 = 0$, $\sin\beta_1 = 1$ and $\sin\mu_1 = 1$, substitute $\sin\beta_1 = 1$ and $\sin\mu_1 = 1$ into eqs. (5.7)— (5.10), in our case, only substitute them in eq. (5.10), together with $A_1 = 0$, there are a total of five variables $(x, y, z, \lambda_1, \sin\alpha_1)$ and five equations. Solving the five equations at the same time, the following solutions are obtained:

$$\begin{aligned} x &= \frac{2x_o - e_1\lambda_1}{2(1+\lambda_1)} \\ y &= \frac{2y_o - e_2\lambda_1}{2(1+\lambda_1)} \\ z &= \frac{2z_o - e_3\lambda_1}{2(1+\lambda_1)} \end{aligned}$$

$$\begin{aligned}
\lambda_1 &= \frac{-s_5 \pm \sqrt{s_5^2 - s_5 s_6}}{s_5} \\
\sin\alpha_1 &= \frac{-e_4}{2a} \\
\sin\beta_1 &= 1 \\
\sin\mu_1 &= 1
\end{aligned}$$

where

$$\begin{aligned}
s_5 &= {e_1}^2 + {e_2}^2 + {e_3}^2 + {e_4}^2 - m_3 \\
s_6 &= -4{x_o}^2 - 4{y_o}^2 - 4{z_o}^2 - 4e_1x_o - 4e_2y_o - 4e_3z_o + {e_4}^2 - m_3 \\
m_3 &= 4b^2 + 4c^2 + 4e_5b + 4e_6c + 4e_7
\end{aligned}$$

There are two potential groups of solutions of x, y, z, λ_1 and one solution for $\sin\alpha_1$. Each of the solution sets x, y, z, $\sin\alpha_1$, $\sin\beta_1$, $\sin\mu_1$ obtained will satisfy eq. (5.10), i.e., all minima are located on the singularity manifold. Therefore, using eq. (5.5) on a solution set, eq. (5.14) is obtained. D_1 is evaluated for the two solution sets and the smaller result is noted as r_{s3} the corresponding values of the six variables are recorded as $x = x_3, y = y_3, z = z_3$, $\sin\alpha_1 = \sin\alpha_{13}$, $\sin\beta_1 = 1$ and $\sin\mu_1 = 1$.

For the fourth case, none of $A_1 = 0$, $B_1 = 0$ and $C_1 = 0$ is satisfied. For example, $\sin\alpha_1 = 1$, $\sin\beta = 1$ and $\sin\mu_1 = 1$. Substitute $\sin\alpha_1 = 1$, $\sin\beta_1 = 1$ and $\sin\mu_1 = 1$ into eqs. (5.7)— (5.10), in our case, only substitute them into eq. (5.10), there are a total of four variables (x, y, z, λ_1) and four equations. Solving the four equations at the same time, the following solutions are obtained:

$$\begin{aligned}
x &= \frac{2x_o - e_1\lambda_1}{2(1+\lambda_1)} \\
y &= \frac{2y_o - e_2\lambda_1}{2(1+\lambda_1)} \\
z &= \frac{2z_o - e_3\lambda_1}{2(1+\lambda_1)} \\
\lambda_1 &= \frac{-s_8 \pm \sqrt{s_8^2 - s_8 s_9}}{s_8} \\
\sin\alpha_1 &= 1 \\
\sin\beta_1 &= 1 \\
\sin\mu_1 &= 1
\end{aligned}$$

where

$$s_8 = -{e_1}^2 - {e_2}^2 - {e_3}^2 + 4m_4$$

$$\begin{aligned} s_9 &= 4({x_o}^2 + {y_o}^2 + {z_o}^2 + e_1 x_o + e_2 y_o + e_3 z_o + m_4) \\ m_4 &= a^2 + b^2 + c^2 + e_4 a + e_5 b + e_6 c + e_7 \end{aligned}$$

There are two potential groups of solutions of x, y, z, λ_1. Each of the solution sets x, y, z, $\sin\alpha_1$, $\sin\beta_1$, $\sin\mu_1$ obtained will satisfy eq. (5.10), i.e., all minima are located on the singularity manifold. Therefore, using eq. (5.5) on a solution set, eq. (5.14) is obtained. D_1 is evaluated for the two solution sets and the smaller result is noted as r_{s4}, the corresponding values of the six variables are recorded as $x = x_4, y = y_4, z = z_4$, $\sin\alpha_1 = 1$, $\sin\beta_1 = 1$, $\sin\mu_1 = 1$.

Likewise for the other 23 combinations, the smaller distance noted as $r_{si}, i = 1, \ldots, 27$ and the corresponding values of the six variables, i.e., $x = x_i, y = y_i, z = z_i, \sin\alpha_1 = \sin\alpha_{1i}, \sin\beta_1 = \sin\beta_{1i}$ and $\sin\mu_1 = \sin\mu_{1_i}, i = 1, \ldots, 27$, are recorded. Among $r_{si}, i = 1, \ldots, 27$, the smallest value of r_{si} is the global minimum, which is the square of the radius of the singularity-free zone.

Step 4: Define a sphere in the 3-D Cartesian (x, y, z) space whose center is defined as $x = x_o, y = y_o$ and $z = z_o$, in the following form:

$$(x - x_o)^2 + (y - y_o)^2 + (z - z_o)^2 - r^2 = 0 \tag{5.15}$$

where $r^2 = \min(r_{si}), i = 1, \ldots, 27$. Within this zone, it can be guaranteed that there is no singularity for any orientation in the prescribed ranges.

5.3.1.1 Example for a prescribed ranges of orientation

Let $e_1 = -1$, $e_2 = -3$, $e_3 = -5$, $e_4 = e_5 = e_6 = 0$, $e_7 = -6$, the singularity equation (5.1) is rewritten as:

$$F_1(x, y, z, T_1, T_2, T_3) = x^2 + y^2 + z^2 - x - 3y - 5z + {T_1}^2 + {T_2}^2 + {T_3}^2 - 6 = 0 \tag{5.16}$$

Applying the above procedure with the singularity equation (5.16), the maximal singularity-free spheres are shown in Figure 5.1 with different ranges of three Euler angles, ϕ, θ and ψ.

For ϕ, θ and $\psi \in [-\frac{\pi}{2}, \frac{\pi}{2}]$, the fourth case solution mentioned above is obtained, where $\sin\alpha_1 = \sin\beta_1 = \sin\mu_1 = -1$, i.e, $\phi = \theta = \psi = -\frac{\pi}{2}$, that means the orientation

part of the critical point on the singularity surface is on one of the eight vertices of the given orientation workspace box. As shown in 5.1(a), the singularity-free sphere is tangent to the singularity manifold at point $(x, y, z) = (-0.13705, -0.23823, -0.39704)$ in 3-D (x, y, z) space and the radius square of the singularity-free sphere is equal to $0.22070mm^2$ (lengths are given in mm).

For ϕ, θ and $\psi \in [-\frac{\pi}{3}, \frac{\pi}{3}]$, the fourth case solution mentioned above is obtained, where $\sin\alpha_1 = \sin\beta_1 = \sin\mu_1 = -1$, i.e, $\phi = \theta = \psi = -\frac{\pi}{3}$, that means the orientation part of the critical point on the singularity surface is on one of the eight vertices of the given orientation workspace box. As shown in 5.1(b), the singularity-free sphere is tangent to the singularity manifold at point $(x, y, z) = (-0.20227, -0.38035, -0.63392)$ in 3-D (x, y, z) and the radius square of the singularity-free sphere is equal to $0.56259mm^2$ (lengths are given in mm).

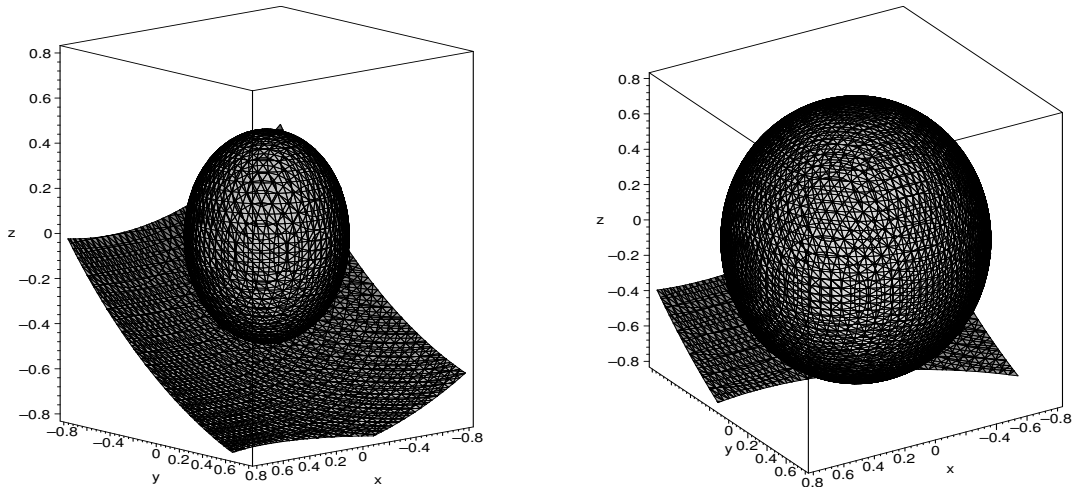

(a) ϕ, θ and $\psi \in [-\frac{\pi}{2}, \frac{\pi}{2}]$ (b) ϕ, θ and $\psi \in [-\frac{\pi}{3}, \frac{\pi}{3}]$

Figure 5.1: Maximal singularity-free zones in the 3-D position space for the most critical orientation (lengths are given in mm).

5.3.2 Case 2, $W = 0$: prescribed ranges of position

In this case, eq. (5.4) is rewritten as:

$$D_2 = (T_1 - T_{1o})^2 + (T_2 - T_{2o})^2 + (T_3 - T_{3o})^2 + \lambda_2 F_2 \tag{5.17}$$

The above problem now is transformed into the following: **For given positioning ranges of motion ($(x_{min} \leq x \leq x_{max})$, $(y_{min} \leq y \leq y_{max})$ and $(z_{min} \leq z \leq z_{max})$) and a given center of orientation (T_{1o}, T_{2o}, T_{3o}), find the largest singularity-free sphere in the 3-dimensional orientation workspace, which is free from singularities for any position in the given ranges**.

Again, a geometric interpretation of this problem can be given: for each position with the prescribed range, a singularity manifold can be plotted in the (T_1, T_2, T_3) space. The above problem amounts to finding the manifold that contains the point closest to the center (T_{1o}, T_{2o}, T_{3o}) and to identifying this point.

This problem is solved using the following procedure similar to the one described in the previous section:

Step 1: Introducing three new angles α_2, β_2 and μ_2, variables x, y and z within the given ranges can be written as [32]:

$$\begin{aligned} x &= x_{min} + (\frac{1+\sin\alpha_2}{2})(x_{max} - x_{min}) \\ y &= y_{min} + (\frac{1+\sin\beta_2}{2})(y_{max} - y_{min}) \\ z &= z_{min} + (\frac{1+\sin\mu_2}{2})(z_{max} - z_{min}) \end{aligned}$$

where

$$\sin\alpha_2 \in [-1, 1], \quad \sin\beta_2 \in [-1, 1], \quad \sin\mu_2 \in [-1, 1]$$

Again, for a simple derivation, the above given ranges of x, y and z are given symmetrically, i.e., $x_{max} = -x_{min} = a'$, with $a' \in (0, \infty)$. Likewise for the ranges of y and z, i.e., $y_{max} = -y_{min} = b'$ with $b' \in (0, \infty)$, $z_{max} = -z_{min} = c'$ with $c' \in (0, \infty)$. Then, the above expressions of x, y and z can be rewitten as:

$$x = a'\sin\alpha_2, \quad y = b'\sin\beta_2, \quad z = c'\sin\mu_2$$

Substituting the expression of x, y and z into eq. (5.1), the singularity equation is rewritten as:

$$\begin{aligned} F_2(\sin\alpha_2, \sin\beta_2, \sin\mu_2, T_1, T_2, T_3) &= a'^2\sin^2\alpha_2 + b'^2\sin^2\beta_2 + c'^2\sin^2\mu_2 + e_1a'\sin\alpha_2 \\ &\quad + e_2a'\sin\beta_2 + e_3a'\sin\mu_2 + {T_1}^2 + {T_2}^2 + {T_3}^2 \\ &\quad + e_4T_1 + e_5T_2 + e_6T_3 + e_7 \end{aligned} \tag{5.18}$$

Step 2: An extremum of D_2 will be obtained if the parital derivatives of D_2 with respect to $T_1, T_2, T_3, \lambda_2, \sin\alpha_2, \sin\beta_2$ and $\sin\mu_2$ are equal to zero, namely,

$$\frac{\partial D_2}{\partial T_1} = 2(T_1 - T_{1o}) + \lambda_2(e_4 + 2T_1) = 0 \tag{5.19}$$

$$\frac{\partial D_2}{\partial T_2} = 2(T_2 - T_{2o}) + \lambda_2(e_5 + 2T_2) = 0 \tag{5.20}$$

$$\frac{\partial D_2}{\partial T_3} = 2(T_3 - T_{3o}) + \lambda_2(e_6 + 2T_3) = 0 \tag{5.21}$$

$$\frac{\partial D_2}{\partial \lambda_2} = F_2(\sin\alpha_2, \sin\beta_2, \sin\mu_2, T_1, T_2, T_3) = 0 \tag{5.22}$$

$$\frac{\partial D_2}{\partial \alpha_2} = (2a'\sin\alpha_2 + e_1)a'\cos\alpha_2 = A_2 a'\cos\alpha_2 = 0 \tag{5.23}$$

$$\frac{\partial D_2}{\partial \beta_2} = (2b'\sin\beta_2 + e_2)b'\cos\beta_2 = B_2 b'\cos\beta_2 = 0 \tag{5.24}$$

$$\frac{\partial D_2}{\partial \mu_2} = (2c'\sin\mu_2 + e_3)c'\cos\mu_2 = C_2 c'\cos\mu_2 = 0 \tag{5.25}$$

where

$$\begin{aligned} A_2 &= 2a'\sin\alpha_2 + e_1 \\ B_2 &= 2b'\sin\beta_2 + e_2 \\ C_2 &= 2c'\sin\mu_2 + e_3 \end{aligned}$$

Eqs. (5.23), (5.24) and (5.25) are satisfied in the following cases (a', b' and c' are not equal to zero):

$$\begin{aligned} A_2 = 0 \quad &\text{or} \quad \cos\alpha_2 = 0 \\ B_2 = 0 \quad &\text{or} \quad \cos\beta_2 = 0 \\ C_2 = 0 \quad &\text{or} \quad \cos\mu_2 = 0 \end{aligned}$$

which represent:

$$\begin{aligned} A_2 = 0, \quad \sin\alpha_2 = 1, \quad \sin\alpha_2 = -1 \\ B_2 = 0, \quad \sin\beta_2 = 1, \quad \sin\beta_2 = -1 \\ C_2 = 0, \quad \sin\mu_2 = 1, \quad \sin\mu_2 = -1 \end{aligned}$$

Similarly to case 1 mentioned above, there are a total of $3\times3\times3 = 27$ combinations of cases satisfying eqs. (5.22), (5.23) and (5.24), a table similar to Table 5.1 is obtained

as shown in Table 5.2, in this case, $A_1, B_1, C_1, \sin\alpha_1, \sin\beta_1$ and $\sin\mu_1$ are replaced by $A_2, B_2, C_2, \sin\alpha_2, \sin\beta_2$ and $\sin\mu_2$, respectively.

With the given ranges of the position variables, the position workspace of the mechanism is a box in 3-D (x, y, z) space. If $A_2 = 0$, $B_2 = 0$ and $C_2 = 0$, then the position part of the point (x, y, z, T_1, T_2, T_3) on the singularity manifold, which is the closest to the point (T_{1o}, T_{2o}, T_{3o}), is located within the ranges of x, y and z, which is inside the box. If any two of $A_2 = 0$, $B_2 = 0$ and $C_2 = 0$ are satisfied, for example, $A_2 = 0$ and $B_2 = 0$ together with $\sin\mu_2 = 1$, the position part of the point on the singularity manifold, which is closest to the point (T_{1o}, T_{2o}, T_{3o}) is located on one of the surfaces of the box. If any one of $A_2 = 0$, $B_2 = 0$ and $C_2 = 0$ is satisfied, for example, $A_2 = 0$ together with $\sin\beta_2 = 1$ and $\sin\mu_2 = 1$, the position part of the point on the singularity manifold, which is closest to the point (T_{1o}, T_{2o}, T_{3o}) is located on one of the edges of the box. Otherwise, it is located on one of the 8 vertices of the box. Hence, four cases of solutions are distinguished.

Step 3: Solve each of the combination listed in Table 5.2 together with eqs. (4.19)—(4.22). In other words, there are 27 independent series of computations.

As shown in eqs.(5.19)—(5.25), the analytical expressions of the four cases of solutions are given as follows:

For the first case, i.e., $A_2 = 0$, $B_2 = 0$ and $C_2 = 0$, solve eqs. (5.19)— (5.22) together with $A_2 = 0$, $B_2 = 0$ and $C_2 = 0$ for $T_1, T_2, T_3, \lambda_2, \sin\alpha_2, \sin\beta_2$ and $\sin\mu_2$. The analytical solutions are:

$$\begin{aligned}
T_1 &= \frac{2T_{1o} - e_4\lambda_2}{2(1+\lambda_2)} \\
T_2 &= \frac{2T_{2o} - e_5\lambda_2}{2(1+\lambda_2)} \\
T_3 &= \frac{2T_{3o} - e_6\lambda_2}{2(1+\lambda_2)} \\
\lambda_2 &= \frac{-t_1 \pm \sqrt{{t_1}^2 - t_1 t_2}}{t_1} \\
\sin\alpha_2 &= \frac{-e_1}{2a'} \\
\sin\beta_2 &= \frac{-e_2}{2b'}
\end{aligned}$$

Combination i	C_1	C_2	C_3
1	$A_2 = 0$	$B_2 = 0$	$C_2 = 0$
2	$A_2 = 0$	$B_2 = 0$	$\sin\mu_2 = 1$
3	$A_2 = 0$	$B_2 = 0$	$\sin\mu_2 = -1$
4	$A_2 = 0$	$\sin\beta_2 = 1$	$C_2 = 0$
5	$A_2 = 0$	$\sin\beta_2 = 1$	$\sin\mu_2 = 1$
6	$A_2 = 0$	$\sin\beta_2 = 1$	$\sin\mu_2 = -1$
7	$A_2 = 0$	$\sin\beta_2 = -1$	$C_2 = 0$
8	$A_2 = 0$	$\sin\beta_2 = -1$	$\sin\mu_2 = 1$
9	$A_2 = 0$	$\sin\beta_2 = -1$	$\sin\mu_2 = -1$
10	$\sin\alpha_2 = 1$	$B_2 = 0$	$C_2 = 0$
11	$\sin\alpha_2 = 1$	$B_2 = 0$	$\sin\mu_2 = 1$
12	$\sin\alpha_2 = 1$	$B_2 = 0$	$\sin\mu_2 = -1$
13	$\sin\alpha_2 = 1$	$\sin\beta_2 = 1$	$C_2 = 0$
14	$\sin\alpha_2 = 1$	$\sin\beta_2 = 1$	$\sin\mu_2 = 1$
15	$\sin\alpha_2 = 1$	$\sin\beta_2 = 1$	$\sin\mu_2 = -1$
16	$\sin\alpha_2 = 1$	$\sin\beta_2 = -1$	$C_2 = 0$
17	$\sin\alpha_2 = 1$	$\sin\beta_2 = -1$	$\sin\mu_2 = 1$
18	$\sin\alpha_2 = 1$	$\sin\beta_2 = -1$	$\sin\mu_2 = -1$
19	$\sin\alpha_2 = -1$	$B_2 = 0$	$C_2 = 0$
20	$\sin\alpha_2 = -1$	$B_2 = 0$	$\sin\mu_2 = 1$
21	$\sin\alpha_2 = -1$	$B_2 = 0$	$\sin\mu_2 = -1$
22	$\sin\alpha_2 = -1$	$\sin\beta_2 = 1$	$C_2 = 0$
23	$\sin\alpha_2 = -1$	$\sin\beta_2 = 1$	$\sin\mu_2 = 1$
24	$\sin\alpha_2 = -1$	$\sin\beta_2 = 1$	$\sin\mu_2 = -1$
25	$\sin\alpha_2 = -1$	$\sin\beta_2 = -1$	$C_2 = 0$
26	$\sin\alpha_2 = -1$	$\sin\beta_2 = -1$	$\sin\mu_2 = 1$
27	$\sin\alpha_2 = -1$	$\sin\beta_2 = -1$	$\sin\mu_2 = -1$

Table 5.2: The 27 cases of combinations of eq. (5.22), eq. (5.23) and eq. (5.24).

$$\sin\mu_2 = \frac{-e_3}{2c'}$$

where

$$\begin{aligned} t_1 &= {e_4}^2 + {e_5}^2 + {e_6}^2 + n_1 \\ t_2 &= -4{T_{1o}}^2 - 4{T_{2o}}^2 - 4{T_{3o}}^2 - 4e_4T_{1o} - 4e_5T_{2o} - 4e_6T_{3o} + n_1 \\ n_1 &= {e_1}^2 + {e_2}^2 + {e_3}^2 - 4e_7 \end{aligned}$$

There are two potential groups of solutions of the seven variables T_1, T_2, T_3, λ_2, $\sin\alpha_2$, $\sin\alpha_2$ and $\sin\beta_2$. Each of the solution sets T_1, T_2, T_3, $\sin\alpha_2$, $\sin\beta_2$, $\sin\mu_2$ obtained will satisfy eq. (5.22), i.e., all minima are located on the singularity manifold. Therefore, using eq. (5.17) on a solution set, one has:

$$D_2 = (T_1 - T_{1o})^2 + (T_2 - T_{2o})^2 + (T_3 - T_{3o})^2 \tag{5.26}$$

This index D_2 is evaluated for the two solution sets. The solution leading to the smaller value of D_2 is defined as r_{t1} and the corresponding values of the six variables noted as $T_1 = T_{11}, T_2 = T_{21}, T_3 = T_{31}, \sin\alpha_2 = \sin\alpha_{21}, \sin\beta_2 = \sin\beta_{21}$ and $\sin\mu_2 = \sin\mu_{21}$ are recorded.

For the second case, i.e., any two of $A_2 = 0$, $B_2 = 0$ and $C_2 = 0$ are satisfied, for example, $A_2 = 0$, $B_2 = 0$ and $\sin\mu_2 = 1$, substituting $\sin\mu_2 = 1$ into eqs. (5.19)—(5.22), in our case, only substitute it into eq. (5.22), together with $A_2 = 0$, $B_2 = 0$, there are a total of six variables $(T_1, T_2, T_3, \lambda_2, \sin\alpha_2, \sin\beta_2)$ and six equations. Solving the six equations at the same time, the following solutions are obtained:

$$\begin{aligned} T_1 &= \frac{2T_{1o} - e_4\lambda_2}{2(1+\lambda_2)} \\ T_2 &= \frac{2T_{2o} - e_5\lambda_2}{2(1+\lambda_2)} \\ T_3 &= \frac{2T_{3o} - e_6\lambda_2}{2(1+\lambda_2)} \\ \lambda_2 &= \frac{t_3 \pm \sqrt{{t_3}^2 - t_3t_4}}{t_3} \\ \sin\alpha_2 &= \frac{-e_1}{2a'} \\ \sin\beta_2 &= \frac{-e_2}{2b'} \\ \sin\mu_2 &= 1 \end{aligned}$$

where

$$\begin{aligned} t_3 &= {e_1}^2 + {e_2}^2 + {e_4}^2 + {e_5}^2 + {e_6}^2 - n_2 \\ t_4 &= -4{T_{1o}}^2 - 4{T_{2o}}^2 - 4{T_{3o}}^2 - 4e_4T_{1o} - 4e_5T_{2o} - 4e_6T_{3o} + {e_1}^2 + {e_2}^2 - n_2 \\ n_2 &= 4c'^2 + 4c'e_3 + 4e_7 \end{aligned}$$

There are two potential groups of solutions of T_1, T_2, T_3, λ_2, $\sin\alpha_2$ and $\sin\beta_2$. Each of the solution sets T_1, T_2, T_3, $\sin\alpha_2$ and $\sin\beta_2$ obtained will satisfy eq. (5.22), i.e., all minima are located on the singularity manifold. Therefore, using eq. (5.17), eq. (5.26) is obtained. D_2 is evaluated for the two solution sets and the smaller result is noted as r_{t2} and the corresponding values of the six variables as $T_1 = T_{12}, T_2 = T_{22}, T_3 = T_{32}, \sin\alpha_2 = \sin\alpha_{22}$ and $\sin\beta_2 = \sin\beta_{22}$ are recorded.

For the third case, i.e., any one of $A_2 = 0$, $B_2 = 0$ and $C_2 = 0$ are satisfied, for example, $A_2 = 0$, $\sin\beta_2 = 1$ and $\sin\mu_2 = 1$, substitute $\sin\beta_2 = 1$ and $\sin\mu_2 = 1$ into eqs. (5.19)— (5.22), in our case, only substitute them into eq. (5.22), together with $A_2 = 0$, there are a total of five variables $(T_1, T_2, T_3, \lambda_2, \sin\alpha_2)$ and five equations. Solving the five equations at the same time, the following solutions are obtained:

$$\begin{aligned} T_1 &= \frac{2T_{1o} - e_4\lambda_2}{2(1+\lambda_2)} \\ T_2 &= \frac{2T_{2o} - e_5\lambda_2}{2(1+\lambda_2)} \\ T_3 &= \frac{2T_{3o} - e_6\lambda_2}{2(1+\lambda_2)} \\ \lambda_2 &= \frac{-t_5 \pm \sqrt{{t_5}^2 - t_5t_6}}{t_5} \\ \sin\alpha_2 &= \frac{-e_1}{2a'} \\ \sin\beta_2 &= 1 \\ \sin\mu_2 &= 1 \end{aligned}$$

where

$$\begin{aligned} t_5 &= {e_4}^2 + {e_5}^2 + {e_6}^2 + {e_1}^2 - n_3 \\ t_6 &= -4{T_{1o}}^2 - 4{T_{2o}}^2 - 4{T_{3o}}^2 - 4e_4T_{1o} - 4e_5T_{2o} - 4e_6T_{3o} + {e_1}^2 - n_3 \\ n_3 &= 4b'^2 + 4c'^2 + 4e_2b' + 4e_3c' + 4e_7 \end{aligned}$$

There are two potential groups of solutions of T_1, T_2, T_3, λ_2 and $\sin\alpha_2$. Each of the solution sets T_1, T_2, T_3 and $\sin\alpha_2$ obtained will satisfy eq. (5.22), i.e., all minima

are located on the singularity manifold. Therefore, using eq. (5.17) on a solution set, eq. (5.26) is obtained. D_2 is evaluated for the two solution sets and the smaller result is noted as r_{t3} the corresponding values of the six variables are recorded as $T_1 = T_{13}, T_2 = T_{23}, T_3 = T_{33}, \sin\alpha_2 = \sin\alpha_{23}$, $\sin\beta_2 = 1$ and $\sin\mu_2 = 1$.

For the fourth case, i.e., none of $A_2 = 0$, $B_2 = 0$ and $C_2 = 0$ is satisfied, for example, $\sin\alpha_2 = 1$, $\sin\beta_2 = 1$ and $\sin\mu_2 = 1$, substitute them into eqs. (5.19)—(5.22), in our case, only substitute them into eq. (5.22), there are a total of four variables $(T_1, T_2, T_3, \lambda_2)$ and four equations. Solving the four equations at the same time, the following solutions are obtained:

$$\begin{aligned}
T_1 &= \frac{2T_{1o} - e_4\lambda_2}{2(1+\lambda_2)} \\
T_2 &= \frac{2T_{2o} - e_5\lambda_2}{2(1+\lambda_2)} \\
T_3 &= \frac{2T_{3o} - e_6\lambda_2}{2(1+\lambda_2)} \\
\lambda_2 &= \frac{-t_7 \pm \sqrt{{t_7}^2 - t_7 t_8}}{t_7} \\
\sin\alpha_2 &= 1 \\
\sin\beta_2 &= 1 \\
\sin\mu_2 &= 1
\end{aligned}$$

where

$$\begin{aligned}
t_7 &= {e_4}^2 + {e_5}^2 + {e_6}^2 - n_4 \\
t_8 &= -4{T_{1o}}^2 - 4{T_{2o}}^2 - 4{T_{3o}}^2 - 4e_4T_{1o} - 4e_5T_{2o} - 4e_6T_{3o} - n_4 \\
n_4 &= 4a'^2 + 4b'^2 + 4c'^2 + 4e_1a' + 4e_2b' + 4e_3c' + 4e_7
\end{aligned}$$

There are two potential groups of solutions of T_1, T_2, T_3 and λ_2. Each of the solution sets T_1, T_2 and T_3 obtained will satisfy eq. (5.22), i.e., all minima are located on the singularity manifold. Therefore, using eq. (5.17) on a solution set, eq. (5.26) is obtained. D_2 is evaluated for the two solution sets and the smaller result is noted as r_{t4} the corresponding values of the six variables are recorded as $T_1 = T_{14}, T_2 = T_{24}, T_3 = T_{34}, \sin\alpha_2 = 1$, $\sin\beta_2 = 1$ and $\sin\mu_2 = 1$.

Likewise for the other 23 combinations, the smaller distance is recorded as $r_{ti}, i = 1, \ldots, 27$ and the corresponding values of the six variables, i.e., $T_1 = T_{1i}, T_2 = T_{2i}, T_3 =$

$T_{3i}, \sin\alpha_2 = \sin\alpha_{2i}, \sin\beta_2 = \sin\beta_{2i}$ and $\sin\mu_2 = \sin\mu_{2i}, i = 1, \ldots, 27$. Among $r_{ti}, i = 1, \ldots, 27$, the smallest value of r_{ti} is the global minimum, which is the square of the radius of the singularity-free zone.

Step 4: Define a sphere in the 3-D Cartesian (T_1, T_2, T_3) space whose center is defined as $T_1 = T_{1o}, T_2 = T_{2o}$ and $T_3 = T_{3o}$, in the following form:

$$(T_1 - T_{1o})^2 + (T_2 - T_{2o})^2 + (T_3 - T_{3o})^2 - r^2 = 0 \tag{5.27}$$

where $r^2 = \min(r_{ti}), i = 1, \ldots, 27$. Within this zone, it can be guaranteed that there is no singularity for any position in the prescribed range.

5.3.2.1 Example of for prescribed ranges of position

Let $T_{1o} = 0, T_{2o} = 0$, and $T_{3o} = 0$, $a = b = c = 1$, $e_1 = e_2 = e_3 = 0$, $e_4 = -1$, $e_5 = -0.5$, $e_6 = -0.7$ and $e_7 = -1.8$, the singularity equation, eq. (5.1), is rewritten as:

$$\begin{aligned} F(x, y, z, T_1, T_2, T_3) &= x^2 + y^2 + z^2 + {T_1}^2 + {T_2}^2 + {T_3}^2 \\ &\quad - T_1 - 0.5T_2 - 0.7T_3 - 1.8 = 0 \end{aligned} \tag{5.28}$$

Applying the above procedure with the singularity equation (5.28) and with $(T_{1o}, T_{2o}, T_{3o}) = (0, 0, 0)$, the maximal singularity-free spheres are shown in Figure 5.2 with different ranges of x, y and z.

For x, y and $z \in [-1, 1]$, the third case solution mentioned above is obtained, where $\sin\alpha_2 = \sin\beta_2 = -1$ and $\sin\mu_2 = 0$, i.e, $x = y = -1$ and $z = 0$, that means the position part of the critical point on the singularity manifold is on one of the edges of the given position workspace box. As shown in Figure 5.2(a), the singularity-free sphere is tangent to the singularity manifold at point $(T_1, T_2, T_3) = (0.13250, 0.06625, 0.09275)$ in 3-D (T_1, T_2, T_3) space and the radius square of the singularity-free sphere is equal to 0.03055.

For x, y and $z \in [-\frac{\sqrt{3}}{2}, \frac{\sqrt{3}}{2}]$, the fourth case solution mentioned above is obtained, where $\sin\alpha_2 = \sin\beta_2 = \sin\mu_2 = -1$, i.e., $x = y = z = -\frac{\sqrt{3}}{2}$, that means the position part of the critical point on the singularity manifold is on one of the eight vertices of the given position workspace box. As shown in Figure 5.2(b), the singularity-free sphere is tangent to the singularity manifold at point $(T_1, T_2, T_3) = (-0.34248, -0.17124, -0.23974)$

in 3-D (T_1, T_2, T_3) space and the radius square of the singularity-free sphere is equal to 0.20409.

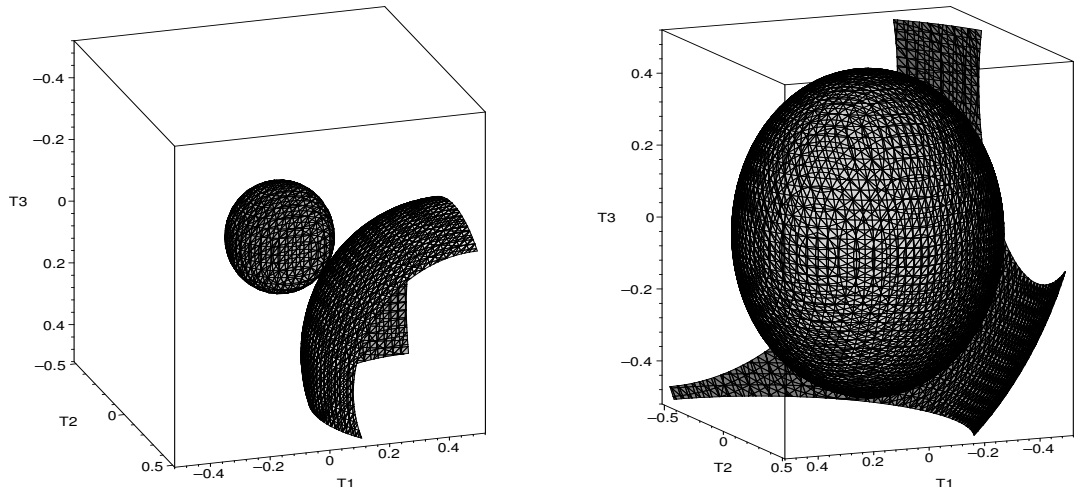

(a) x, y, and $z \in [-1, 1]$.

(b) x, y and $z \in [-\frac{\sqrt{3}}{2}, \frac{\sqrt{3}}{2}]$.

Figure 5.2: Maximal singularity-free zones in the 3-D orientation space for the most critical position (lengths are given in mm).

5.3.3 Case 3, $W \in (0, 1)$: singularity-free zones in the 6-D workspace

In this case, the problem addressed is stated as follows: **For a given position and orientation center in the 6-D space** $(x_o, y_o, z_o, T_{1o}, T_{2o}, T_{3o})$**, find the largest 'hyper-sphere' which is free from singularity**. By changing the value of W, the singularity-free zone will be distorted to favor either the positions or the orientations. The mathematical formulation of the problem is given by eqs. (5.2) and (5.4) and amounts to finding the point on the 6-D singularity manifold which is 'closest' to the center configuration $(x_o, y_o, z_o, T_{1o}, T_{2o}, T_{3o})$.

The solution procedure is now given:

Step 1: An extremum of function D will be obtained if the partial derivatives of

D with respect to x, y, z, T_1, T_2, T_3 and λ are equal to zero, namely,

$$\frac{\partial D}{\partial x} = 2W(x - x_o) + \lambda(2x + e_1) = 0 \quad (5.29)$$

$$\frac{\partial D}{\partial y} = 2W(y - y_o) + \lambda(2y + e_2) = 0 \quad (5.30)$$

$$\frac{\partial D}{\partial x} = 2W(z - z_o) + \lambda(2z + e_3) = 0 \quad (5.31)$$

$$\frac{\partial D}{\partial \lambda} = F = 0 \quad (5.32)$$

$$\frac{\partial D}{\partial T_1} = 2(1 - W)(T_1 - T_{1o}) + \lambda(2T_1 + e_4) = 0 \quad (5.33)$$

$$\frac{\partial D}{\partial T_2} = 2(1 - W)(T_2 - T_{2o}) + \lambda(2T_1 + e_5) = 0 \quad (5.34)$$

$$\frac{\partial D}{\partial T_3} = 2(1 - W)(T_3 - T_{3o}) + \lambda(2T_1 + e_6) = 0 \quad (5.35)$$

which forms a system of seven equations in seven unknowns.

Step 2: Solving the above seven equations simultaneously, several groups of solution of $x, y, z, \lambda, T_1, T_2$ and T_3 can be obtained. In general, these solutions will have to be obtained numerically. Substituting each group of solution into eq. (5.4) and calculating D, the smallest value of D denoted as D_s is the global minimum, which is the square of the radius of the singularity-free zone. The solution for $x, y, z, \lambda, T_1, T_2$ and T_3 corresponding to the smallest D is recorded, for example, $x = x_s$, $y = y_s$, $z = z_s$, $T_1 = T_{1s}$, $T_2 = T_{2s}$ and $T_3 = T_{3s}$.

Step 3: Defining a 'hyper-sphere' in the 6-D (x, y, z, T_1, T_2, T_3) space with the weighting coefficient, we have the following form:

$$W((x - x_o)^2 + (y - y_o)^2 + (z - z_o)^2) + (1 - W)((T_1 - T_{1o})^2 + (T_2 - T_{2o})^2 + (T_3 - T_{3o})^2) - r^2 = 0 \quad (5.36)$$

where $r^2 = D_s$. Within this zone, it can be guaranteed that there is no singularity.

5.3.3.1 Example: 6-D singularity-free 'hyper-sphere' for the simplified singularity locus

Since it is impossible to illustrate the singularity-free zones graphically in 6-D space, in the following examples, graphical illustrations are given in both 3-D position space and 3-D orientation space, respectively. For the graphical representations in the 3-D

position space, we substitute the given weighting coefficient, D_s and the corresponding $T_1 = T_{1s}$, $T_2 = T_{2s}$ and $T_3 = T_{3s}$ into eq. (5.36) and plot it in the 3-D position space. For presenting the figures in 3-D orientation space, substitute the given weight coefficients, D_s and the corresponding $x = x_s$, $y = y_s$, $z = z_s$ into eq. (5.36) and plot it in 3-D orientation space.

With $e_1 = -1$, $e_2 = -3$, $e_3 = -5$, $e_4 = -1$, $e_5 = -0.5$, $e_6 = -0.7$ and $e_7 = -3$, the singularity eq. (5.1) is rewritten as:

$$\begin{aligned} F(x, y, z, T_1, T_2, T_3) &= x^2 + y^2 + z^2 - x - 3y - 5z + {T_1}^2 + {T_2}^2 + {T_3}^2 \\ &\quad - T_1 - 0.5T_2 - 0.7T_3 - 3 = 0 \end{aligned} \tag{5.37}$$

Applying the above procedure with the singularity equation (5.37), the maximal singularity-free spheres in 3-D position and orientation space are shown in Figures 5.3— 5.5 with different weighting coefficients. The centers of the singularity-free zones in both 3-D position and orientation space are at the point $(0, 0, 0)$.

For $W = 0.1$, the critical point on the singularity manifold is $(x, y, z, T_1, T_2, T_3) = (-0.075895, -0.22768, -0.37947, -0.07589, -0.03795, -0.05313)$ in 6-D (x, y, z, T_1, T_2, T_3) space. As shown in Figure 5.5, in 3-D (x, y, z) position space, the radius square of the singularity-free sphere is $0.21885mm^2$ and in 3-D (T_1, T_2, T_3) orientation space, the radius square of the singularity-free sphere is equal to 0.00093.

For $W = 0.5$, the critical point on the singularity manifold is $(x, y, z, T_1, T_2, T_3) = (-0.075895, -0.22768, -0.37947, -0.07589, -0.03795, -0.05313)$ in 6-D (x, y, z, T_1, T_2, T_3) space. As shown in Figure 5.4, in 3-D (x, y, z) position space, the radius square of the singularity-free sphere is $0.20160mm^2$ and in 3-D (T_1, T_2, T_3) orientation space, the radius square of the singularity-free sphere is equal to 0.01002.

For $W = 0.9$, the critical point on the singularity manifold is $(x, y, z, T_1, T_2, T_3) = (-0.03312, -0.09935, -0.16559, -0.63399, -0.31699, -0.44379)$ in 6-D (x, y, z, T_1, T_2, T_3) space. As shown in Figure 5.3, in 3-D (x, y, z) position space, the radius square of the singularity-free sphere is $0.03839mm^2$ and in 3-D (T_1, T_2, T_3) orientation space, the radius square of the singularity-free sphere is equal to 0.69938.

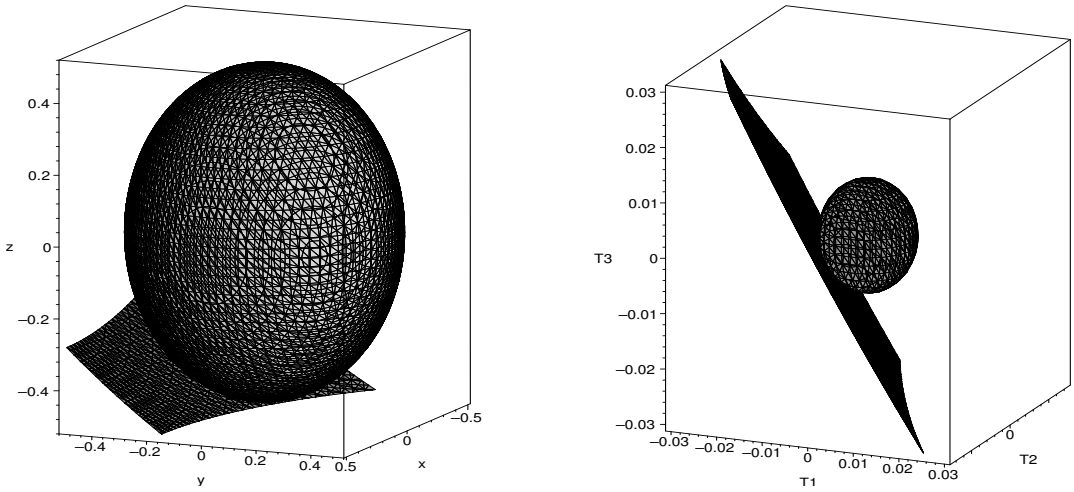

(a) In 3-D position space (b) In 3-D orientation space

Figure 5.3: Maximal singularity-free 'hyper-sphere' for the simplified singularity equation with $W = 0.1$ (lengths are given in mm).

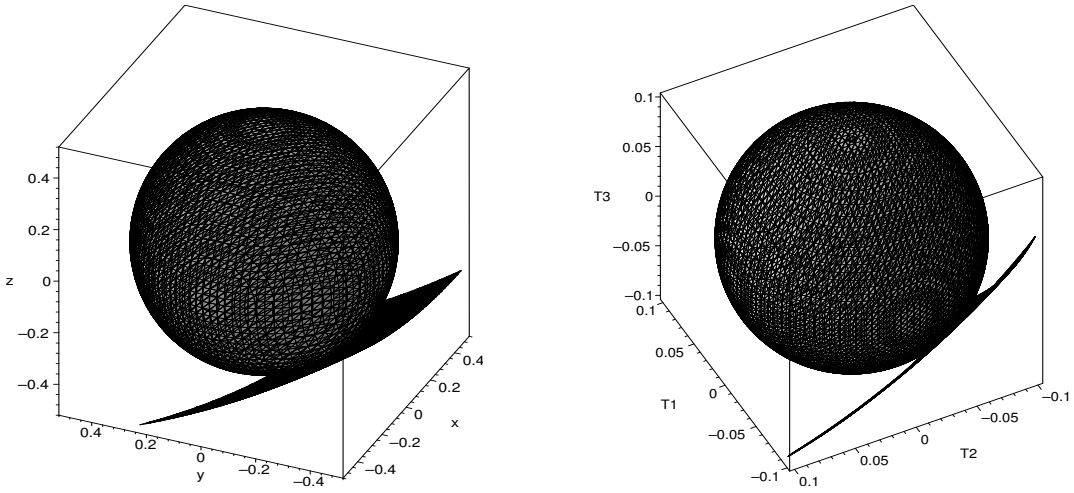

(a) In 3-D position space (b) In 3-D orientation space

Figure 5.4: Maximal singularity-free 'hyper-sphere' for the simplified singularity equation with $W = 0.5$ (lengths are given in mm).

5.4 Application to the general Gough-Stewart platform

The procedures illustrated above using the simplified singularity equation can be directly applied to the Gough-Stewart platform. Although the equations are more com-

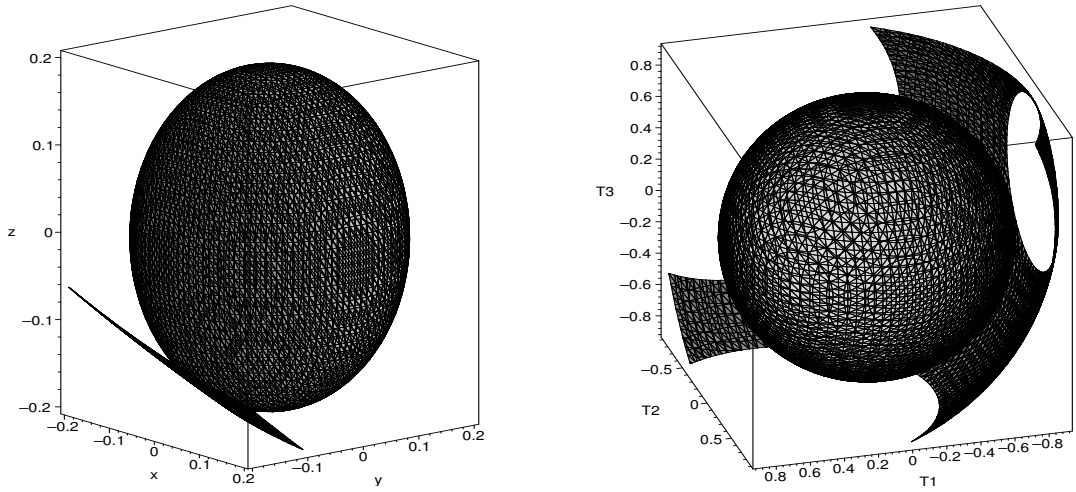

(a) In 3-D position space

(b) In 3-D orientation space

Figure 5.5: Maximal singularity-free 'hyper-sphere' for the simplified singularity equation with $W = 0.9$ (lengths are given in mm).

plex, the principle is the same.

The general mathematical formulation is based on eqs. (5.2) and (5.4) where F, the singularity locus is now given by eq. (2.11).

In order to illustrate graphically each case of the general Gough-Stewart platform, in the following numerical examples, the architectural parameters in Table 3.2 are used.

5.4.1 Case 1: Prescribed ranges of orientation of the general Gough-Stewart platform

According to the notations used in the procedure of the case 1 proposed in section 5.3, referring to eq. (5.4), an extremum of D_1 will be obtained if the partial derivatives of D_1 with respect to $x, y, z, \lambda, \alpha_1, \beta_1$ and μ_1 are equal to zero, i.e., the system of seven nonlinear equations in seven unknowns $x, y, z, \lambda_1, \sin\alpha_1, \sin\beta_1$ and $\sin\mu_1$ is given as follows:

$$\frac{\partial D_1}{\partial x} = 2(x - x_o) + \lambda_1 \frac{\partial F}{\partial x} = 0 \tag{5.38}$$

$$\frac{\partial D_1}{\partial y} = 2(y - y_o) + \lambda_1 \frac{\partial F}{\partial y} = 0 \tag{5.39}$$

$$\frac{\partial D_1}{\partial z} = 2(z - z_o) + \lambda_1 \frac{\partial F}{\partial z} = 0 \tag{5.40}$$

$$\frac{\partial D_1}{\partial \lambda_1} = F(x, y, z, \sin\alpha_1, \sin\beta_1, \sin\mu_1) = 0 \tag{5.41}$$

$$\frac{\partial D_1}{\partial \alpha_1} = \frac{\partial F}{\partial \alpha_1} = A_1 a \cos\alpha_1 = 0 \tag{5.42}$$

$$\frac{\partial D_1}{\partial \beta_1} = \frac{\partial F}{\partial \beta_1} = B_1 a \cos\beta_1 = 0 \tag{5.43}$$

$$\frac{\partial D_1}{\partial \mu_1} = \frac{\partial F}{\partial \mu_1} = C_1 a \cos\mu_1 = 0 \tag{5.44}$$

where A_1, B_1 and C_1 are functions of the six variables, $x, y, z, \sin\alpha_1, \sin\beta_1$ and $\sin\mu_1$, which are written in the following forms:

$$A_1 = h_1(x, y, z, \sin\alpha_1, \sin\beta_1, \sin\mu_1) = 0$$
$$B_1 = h_2(x, y, z, \sin\alpha_1, \sin\beta_1, \sin\mu_1) = 0$$
$$C_1 = h_3(x, y, z, \sin\alpha_1, \sin\beta_1, \sin\mu_1) = 0$$

Example 1: Applying the first procedure of case 1 with the singularity equation of the general Gough-Stewart platform using the seven eqs. (5.38)— (5.44), the maximal singularity-free zones in 3-D position space with Euler angles within the different given ranges are illustrated in Figure 5.6. As shown in the figures, the singularity-free zones are spheres tangent to the singularity manifold in 3-D position space. However, in other spaces, the maximal singularity-free zones are cylinders. In the examples, the spheres are centered in $(0, 0, 0)$ and the cylinders are centered in $(0, 0)$. The plots are shown for the most critical positions.

For ϕ, θ and $\psi \in [-10°, 10°]$, the fourth case solution mentioned in case 1 of section 5.3 is obtained, $\sin\alpha_1 = \sin\beta_1 = \sin\mu_1 = -1$, i.e.,$\phi = \theta = \psi = -10°$, which means the orientation part of the critical point on the singularity manifold is on one of the eight vertices of the given orientation workspace box. As shown in Figure 5.6(a), the singularity-free sphere is tangent to the singularity manifold at point $(x, y, z) = (-0.08572, 0.03932, 0.29065)$ in 3-D (x, y, z) space and the radius square of the singularity-free sphere is equal to $0.09337dm^2$ (lengths are given in dm). As shown in Figures 5.6(b)– 5.6(c), fixing one of the position varaible with the coordinate of the tangent point, the maximal singularity-free zones are cylinders.

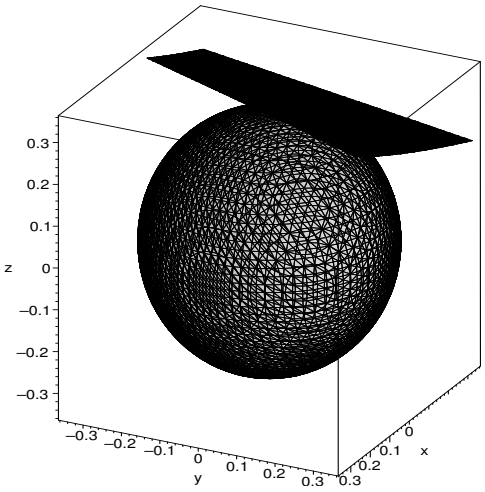

(a) In 3-D position space.

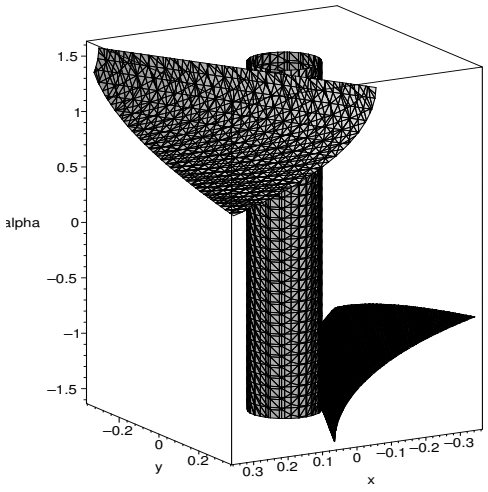

(b) In 3-D (x, y, α) space with $z = 0.29065]$.

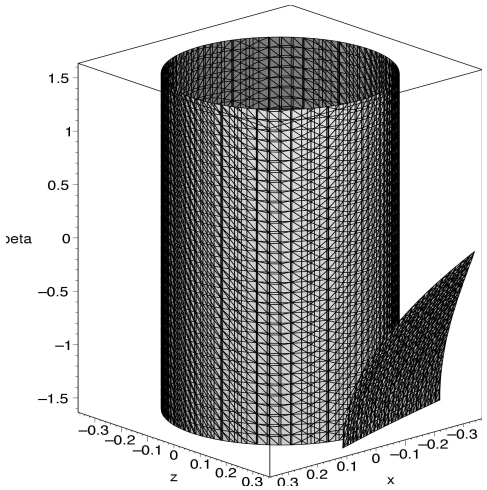

(c) In 3-D (x, z, β) space with $y = 0.03932]$.

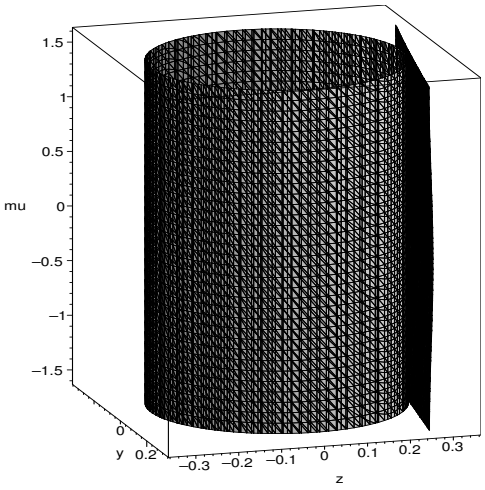

(d) In 3-D (y, z, μ) space with $x = -0.08572]$.

Figure 5.6: Maximal singularity-free zones of the general Gough-Stewart platform with ϕ, θ and $\psi \in [-10°, 10°]$ in different spaces.

For ϕ, θ and $\psi \in [-8°, 8°]$, the fourth case solution mentioned in case 1 of section 5.3 is obtained, $\sin\alpha_1 = \sin\beta_1 = \sin\mu_1 = -1$, i.e, $\phi = \theta = -8°$, which means the orientation part of the critical point on the singularity manifold is on one of the eight vertices of the given orientation workspace box. As shown in Figure 5.7(a), the singularity-free sphere is tangent to the singularity manifold at point

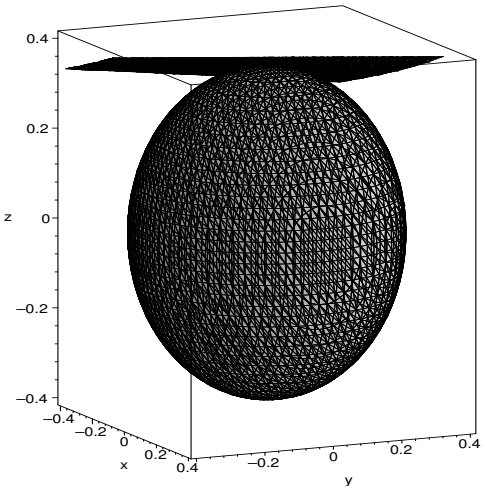

(a) In 3-D position space.

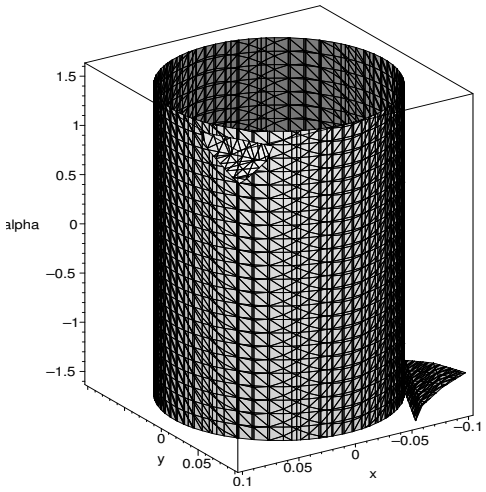

(b) In 3-D (x, y, α) space with $z = 0.35658]$.

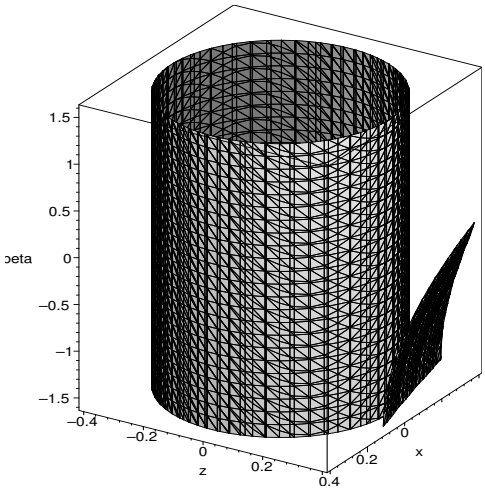

(c) In 3-D (x, z, β) space with $y = 0.03940]$.

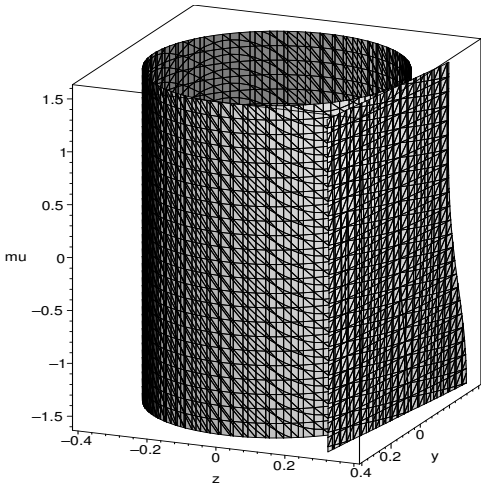

(d) In 3-D (y, z, μ) space with $x = -0.08420]$.

Figure 5.7: Maximal singularity-free zones of the general Gough-Stewart platform with ϕ, θ and $\psi \in [-8°, 8°]$ in different spaces.

$(x, y, z) = (-0.08420, 0.03940, 0.35658)$ in 3-D (x, y, z) space and the radius square of the singularity-free sphere is equal to $0.13579dm^2$ (lengths are given in dm). As shown in Figures 5.7(b)– 5.7(d), fixing one of the position varaible with the coordinate of the tangent point, the maximal singularity-free zones are cylinders.

5.4.2 Case 2: Prescribed ranges of position of the general Gough-Stewart platform

According to the notations used in the procedure of case 2 developed above, referring to eq. (5.4), an extremum of D_2 will be obtained if the partial derivatives of D_2 with respect to $T_1, T_2, T_3, \lambda_2, \alpha_2, \beta_2$ and μ_2 are equal to zero, i.e., the system of seven nonlinear equations in seven unknowns $T_1, T_2, T_3, \lambda_2, \alpha_2, \beta_2$ and μ_2 is given as follows:

$$\frac{\partial D_2}{\partial T_1} = 2(T_1 - T_{1o}) + \lambda_2 \frac{\partial F}{\partial T_1} = 0 \tag{5.45}$$

$$\frac{\partial D_2}{\partial T_2} = 2(T_2 - T_{2o}) + \lambda_2 \frac{\partial F}{\partial T_2} = 0 \tag{5.46}$$

$$\frac{\partial D_2}{\partial T_3} = 2(T_3 - T_{3o}) + \lambda_2 \frac{\partial F}{\partial T_3} = 0 \tag{5.47}$$

$$\frac{\partial D_2}{\partial \lambda_2} = F(T_1, T_2, T_3, \sin\alpha_2, \sin\beta_2, \sin\mu_2) = 0 \tag{5.48}$$

$$\frac{\partial D_2}{\partial \alpha_2} = \frac{\partial F}{\partial \alpha_2} = A_2 a' \cos\alpha_2 = 0 \tag{5.49}$$

$$\frac{\partial D_2}{\partial \beta_2} = \frac{\partial F}{\partial \beta_2} = B_2 b' \cos\beta_2 = 0 \tag{5.50}$$

$$\frac{\partial D_2}{\partial \mu_2} = \frac{\partial F}{\partial \mu_2} = C_2 c' \cos\mu_2 = 0 \tag{5.51}$$

where A_2, B_2 and C_2 are functions of the six variables, $T_1, T_2, T_3, \sin\alpha_2, \sin\beta_2$ and $\sin\mu_2$, which are written in the following forms:

$$A_2 = h_4(T_1, T_2, T_3, \sin\alpha_2, \sin\beta_2, \sin\mu_2) = 0$$

$$B_2 = h_5(T_1, T_2, T_3, \sin\alpha_2, \sin\beta_2, \sin\mu_2) = 0$$

$$C_2 = h_6(T_1, T_2, T_3, \sin\alpha_2, \sin\beta_2, \sin\mu_2) = 0$$

Example 2: Applying the second procedure with the singularity equation of the general Gough-Stewart platform using the seven eqs. (5.45)— (5.51), the maximal singularity-free zones in 3-D orientation space with position variables within the different given ranges are illustrated in Figure 5.7. As shown in the figures, the singularity-free zones are spheres tangent to the singularity manifold. In this example, the spheres are centered at $(0, 0, 0)$. The plots are shown for the most critical position.

For x, y and $z \in [-0.05, 0.05]$, the four case solution mentioned in case 2 of section 5.3 is obtained, where $\sin\alpha_2 = -1$ and $\sin\beta_2 = \sin\mu_2 = 1$, i.e, $x = -0.05$ and

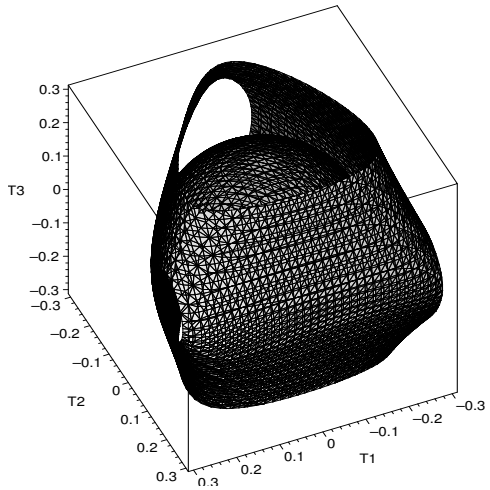

(a) In 3-D orientation space.

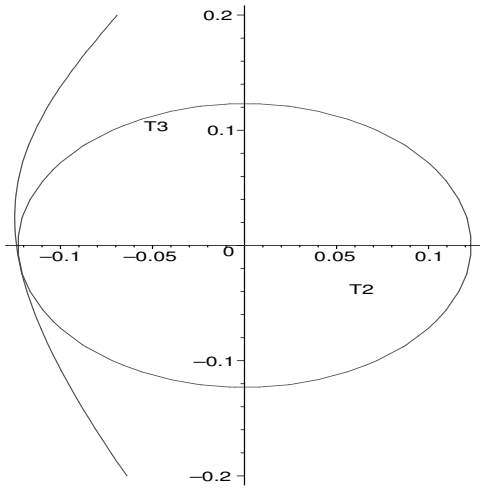

(b) In T_2T_3 plane with $T_1 = -0.19088$.

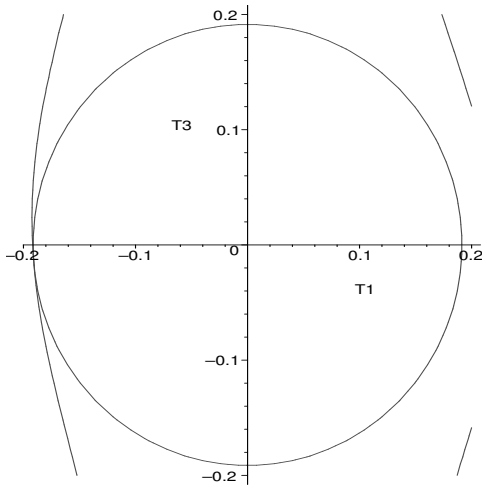

(c) In T_1T_3 plane with $T_2 = -0.12223$.

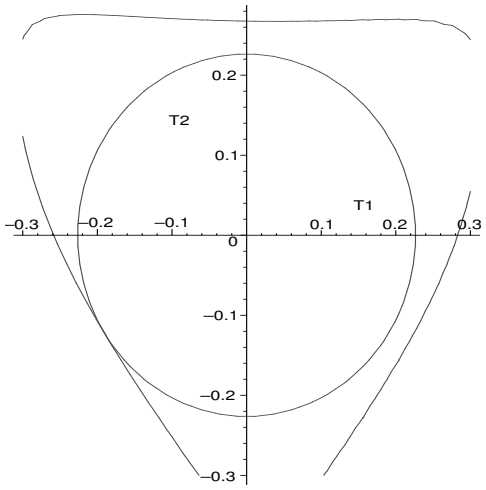

(d) In T_1T_2 plane with $T_3 = -0.01634$.

Figure 5.8: Maximal singularity-free zones of the general Gough-Stewart platform in 3-D orientation space and different planes with x, y and $z \in [-0.05, 0.05]$ (lengths are given in dm).

$y = z = 0.05$ (lengths are given in dm), that means the position part of the critical point on the singularity surface is located on one of the edges of the given position workspace box. As shown in Figure 5.8(a), the singularity-free sphere is tangent to the singularity manifold at point $(T_1, T_2, T_3) = (-0.19088, -0.12223, -0.01634)$ in 3-D (T_1, T_2, T_3) space and the radius square of the singularity-free sphere is equal to 0.05164. The figures of the sections in the planes corresponding to $T_1 = -0.19088$, $T_2 = -0.12223$

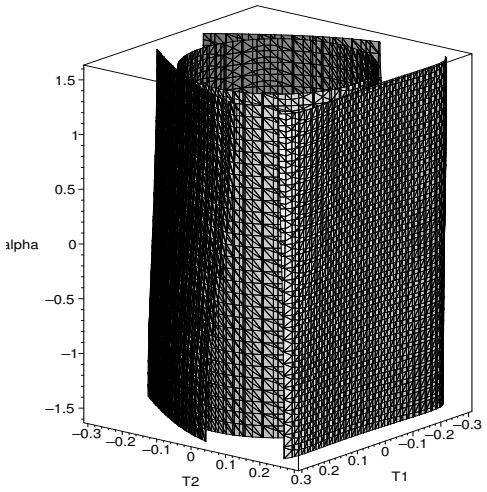

(a) In (T_1, T_2, α) space with $T_3 = -0.01634$.

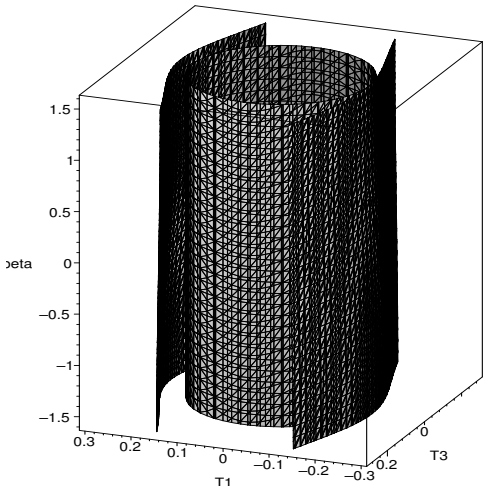

(b) In (T_1, T_3, β) space with $T_2 = -0.12223$.

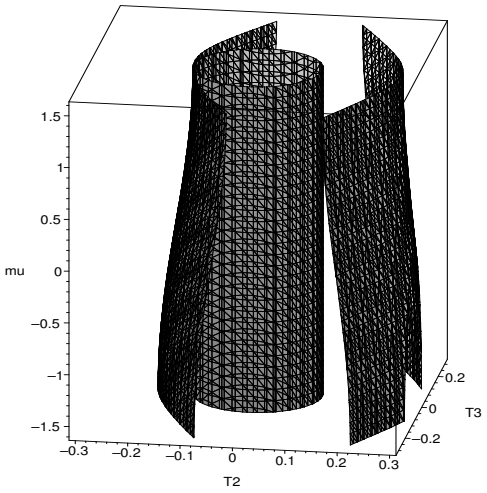

(c) In (T_2, T_3, μ) space with $T_1 = -0.19088$.

Figure 5.9: Maximal singularity-free zones of the general Gough-Stewart platform with x, y and $z \in [-0.05, 0.05]$ in other different spaces (lengths are given in dm).

and $T_3 = -0.01634$ are illustrated in Figures 5.8(b)–5.8(d), respectively.

Fixing any of the three variables of T_3, T_2, T_1 with the coordinate of the tangent point obtained above, the maximal singularity-free zones in other spaces are cylinders, as shown in Figures 5.9(a)–5.9(c), respectively.

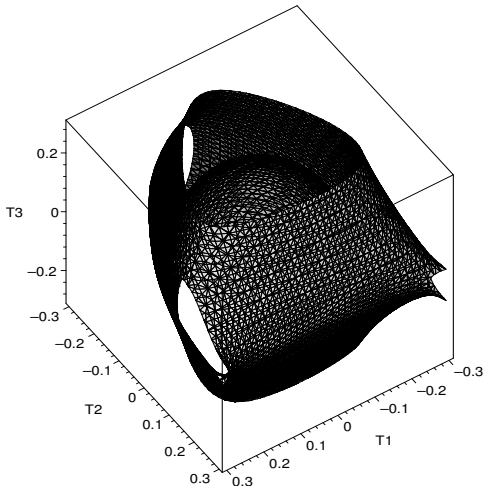

(a) In 3-D orientation space.

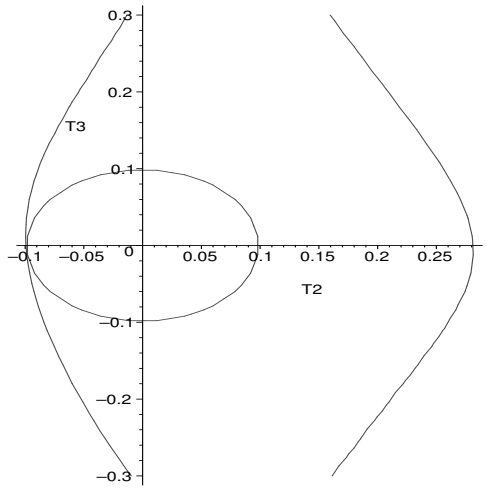

(b) In T_2T_3 plane with $T_1 = -0.16479$.

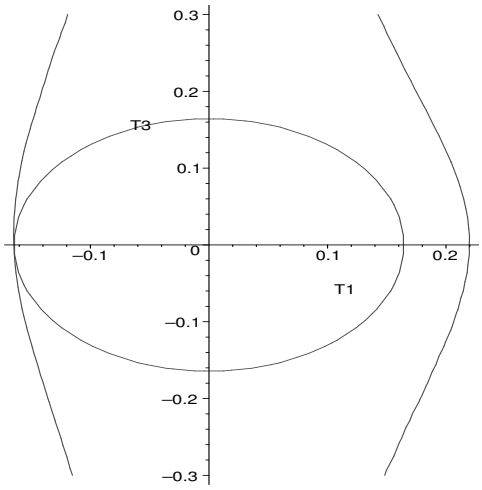

(c) In T_1T_3 plane with $T_2 = -0.09929$.

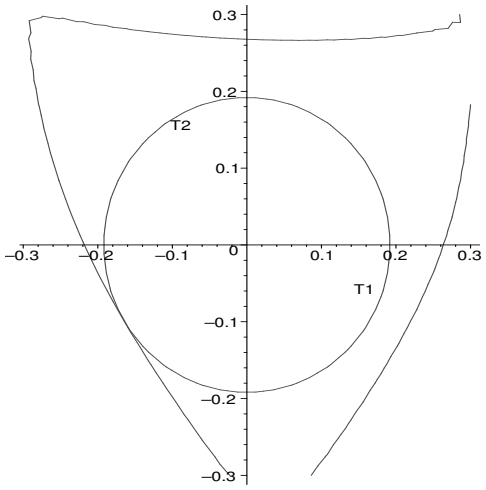

(d) In T_1T_2 plane with $T_3 = -0.00523$.

Figure 5.10: Maximal singularity-free zones of the general Gough-Stewart platform in 3-D orientation space and different planes with x, y and $z \in [-0.1, 0.1]$ (lengths are given in dm).

For x, y and $z \in [-0.1, 0.1]$, the four case solution mentioned in case 2 of section 5.3 is obtained, where $\sin\alpha_2 = -1$ and $\sin\beta_2 = \sin\mu_2 = 1$, i.e, $x = -0.1$ and $y = z = 0.1$ (lengths are given im dm), that means the position part of the critical point on the singularity surface is located on one of the edges of the given position workspace box. As shown in Figure 5.10(a), the singularity-free sphere is tangent to the singularity manifold at point $(T_1, T_2, T_3) = (-0.16479, -0.09929, -0.00523)$ in 3-D (T_1, T_2, T_3) space

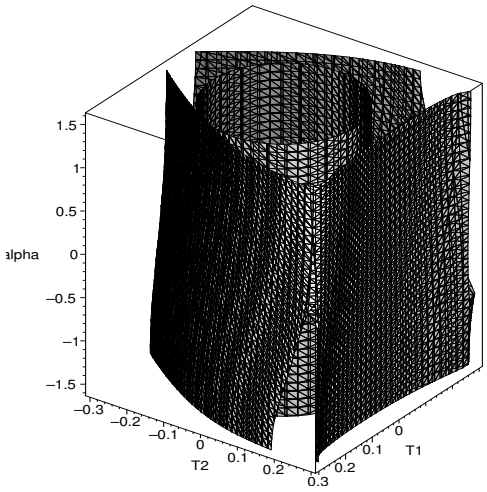

(a) In (T_1, T_2, α) space with $T_3 = -0.00523$.

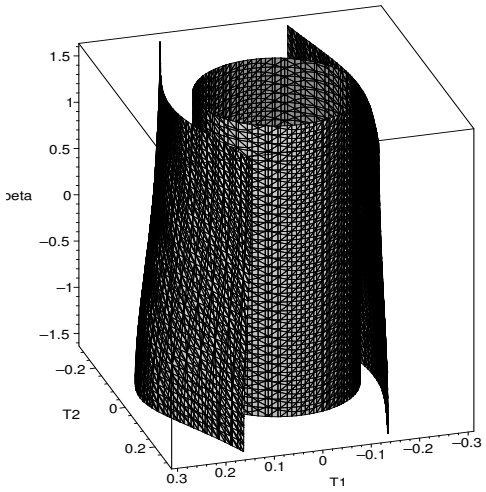

(b) In (T_1, T_3, β) space with $T_2 = -0.09929$.

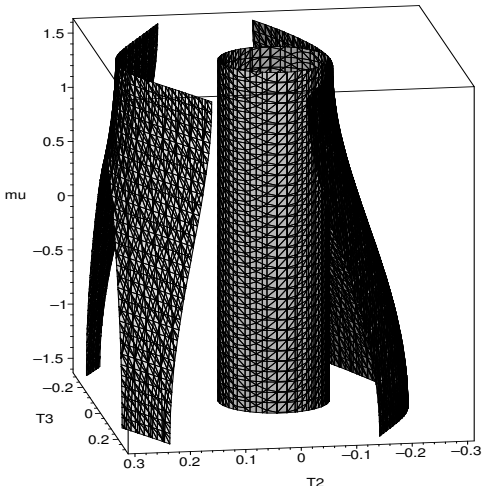

(c) In (T_2, T_3, μ) space with $T_1 = -0.16479$.

Figure 5.11: Maximal singularity-free zones of the general Gough-Stewart platform with x, y and $z \in [-0.1, 0.1]$ in other different spaces (lengths are given in dm).

and the radius square of the singularity-free sphere is equal to 0.03704. The figures of the sections in the planes corresponding to $T_1 = -0.16479$, $T_2 = -0.09929$ and $T_3 = -0.00523$ are illustrated in Figures 5.10(b)–5.10(d), respectively.

Fixing any of the three variables of T_3, T_2, T_1 with the coordinate of the tangent

point obtained above, the maximal singularity-free zones in other spaces are cylinders, as shown in Figures 5.11(a)–5.11(c), respectively.

5.4.3 Case 3: General singularity-free 'hyper-sphere' in the workspace of the general Gough-Stewart platform

Following the notations used in the procedure of case 3 given above, referring to eq. (5.4), an extremum of D will be obtained if the partial derivatives of D with respect to x, y, z, T_1, T_2, T_3 and λ are equal to zero, i.e., the system of sevev nonlinear equations in seven unknowns x, y, z, T_1, T_2, T_3 and λ is given as follows:

$$\frac{\partial D}{\partial x} = 2W(x - x_o) + \lambda \frac{\partial F}{\partial x} = 0 \tag{5.52}$$

$$\frac{\partial D}{\partial y} = 2W(y - y_o) + \lambda \frac{\partial F}{\partial y} = 0 \tag{5.53}$$

$$\frac{\partial D}{\partial x} = 2W(z - z_o) + \lambda \frac{\partial F}{\partial z} = 0 \tag{5.54}$$

$$\frac{\partial D}{\partial \lambda} = F = 0 \tag{5.55}$$

$$\frac{\partial D}{\partial T_1} = 2(1 - W)(T_1 - T_{1o}) + \lambda \frac{\partial F}{\partial T_1} = 0 \tag{5.56}$$

$$\frac{\partial D}{\partial T_2} = 2(1 - W)(T_2 - T_{2o}) + \lambda \frac{\partial F}{\partial T_2} = 0 \tag{5.57}$$

$$\frac{\partial D}{\partial T_3} = 2(1 - W)(T_3 - T_{3o}) + \lambda \frac{\partial F}{\partial T_3} = 0 \tag{5.58}$$

Example 3: Applying the third procedure with the singularity equation of the general Gough-Stewart platform using the seven eqs. (5.52)— (5.58), the maximal singularity-free zones in both 3-D position space and orientation space are illustrated in Figures 5.12— 5.14 with different values of weighting coefficients. As shown in the figures, the singularity-free zones are spheres tangent to the singularity manifold. The center configuration is chosen as $(x_o, y_o, z_o) = (2, 2, 2)$ (lengths are given in dm) and $(T_{1o}, T_{2o}, T_{3o}) = (\tan(\frac{\pi}{12}), \tan(\frac{\pi}{12}), \tan(\frac{\pi}{12}))$. Moreover, the plots are always drawn for the orientation (or position) associated with the point of the manifold closest to the hyper-sphere.

For $W = 0.1$, the critical point on the singularity manifold is $(x, y, z, T_1, T_2, T_3) = (1.81209, 2.11143, 1.83352, 0.32961, 0.31763, 0.28939)$ in 6-D (x, y, z, T_1, T_2, T_3) space and

the radius square of the hyper-sphere is 0.01360. As shown in Figure 5.12, in 3-D (x, y, z) position space, the radius square of the singularity-free sphere is $0.07544dm^2$ and in 3-D (T_1, T_2, T_3) orientation space, the radius square of the singularity-free sphere is equal to 0.00673.

For $W = 0.5$, the critical point on the singularity manifold is $(x, y, z, T_1, T_2, T_3) = (1.95065, 2.02924, 1.96650, 0.38390, 0.37523, 0.30806)$ in 6-D (x, y, z, T_1, T_2, T_3) space and the radius square of the hyper-sphere is 0.01549. As shown in Figure 5.13, in 3-D (x, y, z) position space, the radius square of the singularity-free sphere is $0.00442dm^2$ and in 3-D (T_1, T_2, T_3) orientation space, the radius square of the singularity-free sphere is equal to 0.02656.

For $W = 0.9$, the critical point on the singularity manifold is $(x, y, z, T_1, T_2, T_3) = (1.99339, 2.00392, 1.99588, 0.39896, 0.39333, 0.31300)$ in 6-D (x, y, z, T_1, T_2, T_3) space and the radius square of the hyper-sphere is 0.00356. As shown in Figure 5.14, in 3-D (x, y, z) position space, the radius square of the singularity-free sphere is $0.00008dm^2$ and in 3-D (T_1, T_2, T_3) orientation space, the radius square of the singularity-free sphere is equal to 0.0349.

As shown in Figures 5.12– 5.14, with the increasing of the weighting coefficient, W, the radius square of the maximal singularity-free sphere in 3-D position space increases significantly, while the radius square of the maximal singularity-free sphere in 3-D orientation space decreases. Therefore, by adjusting the weighting coefficent, it is possible to obtain either the desirable position workspace or orientation workspace.

5.5 Conclusions

In this chapter, procedures are introduced to locate maximal singularity-free zones in the 6-D workspace of the general Gough-Stewart platform. With the singularity locus equation of the general Gough-Stewart platform obtained in Chapter 2 and the introduction of a weighting factor, a total of three cases were studied:

1. case 1: with $W = 1$, a procedure is presented to solve the following problem: For a given rotational range of motion $((T_{1min} \leq T_1 \leq T_{1max})$, $(T_{2min} \leq T_2 \leq T_{2max})$

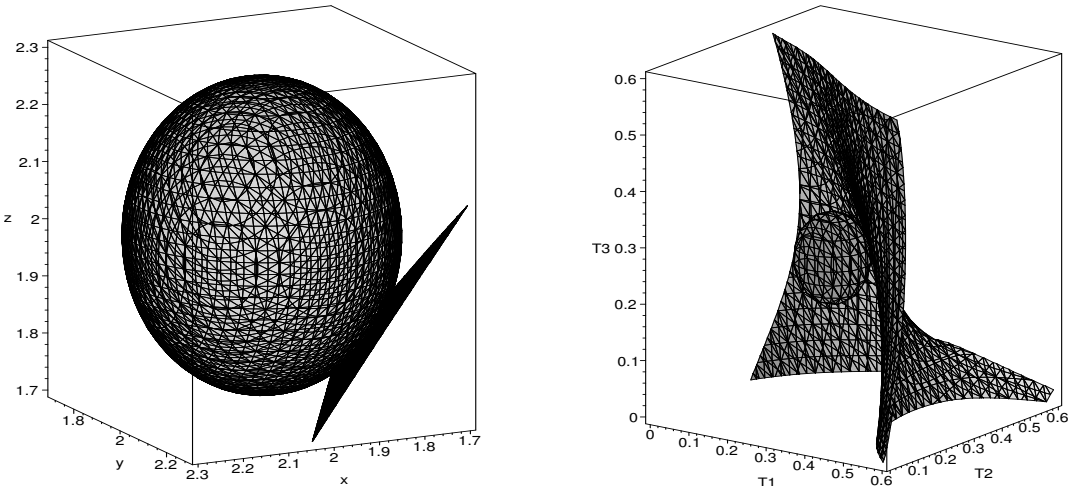

(a) In 3-D position space. (b) In 3-D orientation space.

Figure 5.12: Maximal singularity-free zones of the general Gough-Stewart platform with $W = 0.1$ (lengths are given in dm).

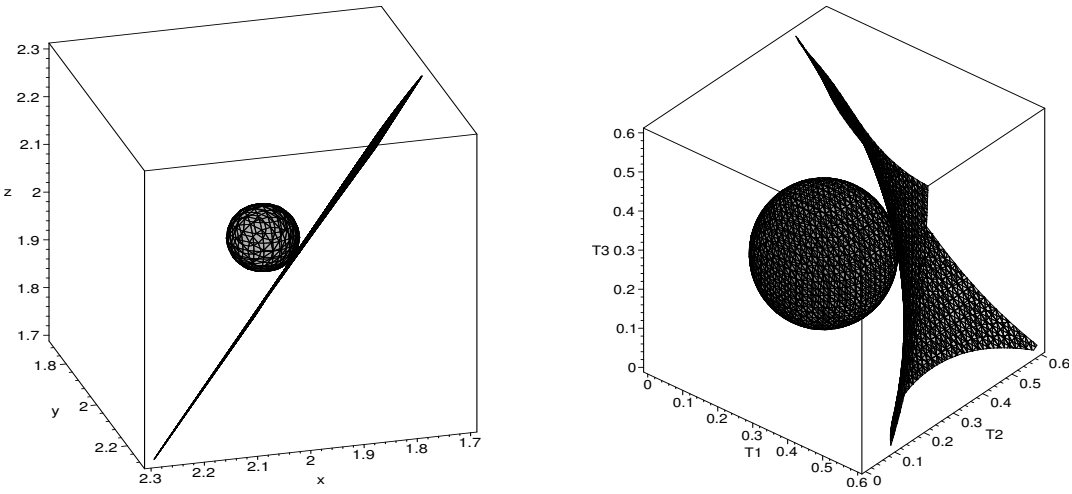

(a) In 3-D position space. (b) In 3-D orientation space.

Figure 5.13: Maximal singularity-free zones of the general Gough-Stewart platform with $W = 0.5$ (lengths are given in dm).

and $(T_{3min} \leq T_3 \leq T_{3max})$) and a given center of position (x_o, y_o, z_o), find the largest singularity-free zone in the 3-D position workspace, which is free from singularities with any orientation in the given ranges.

2. case 2: with $W = 0$, the above procedure is presented to solve the follow-

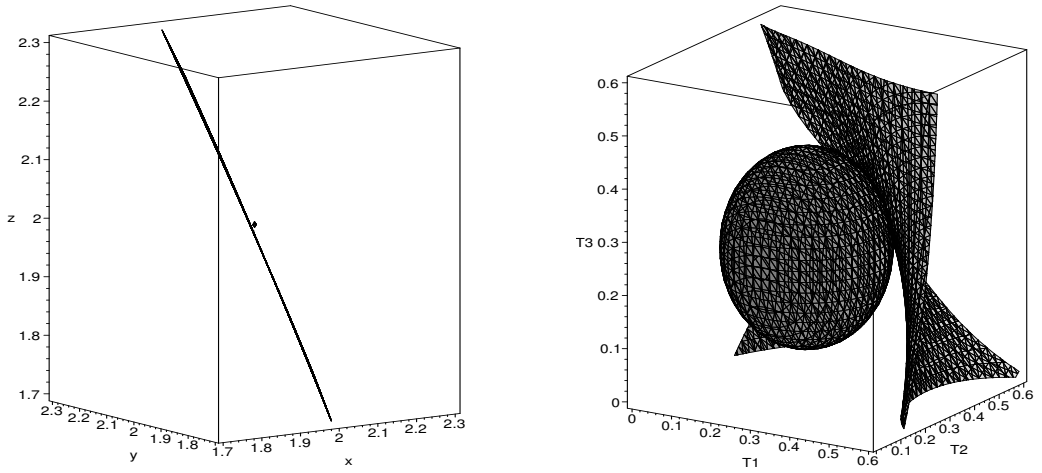

(a) In 3-D position space.

(b) In 3-D orientation space.

Figure 5.14: Maximal singularity-free zones of the general Gough-Stewart platform with $W = 0.9$ (lengths are given in dm).

ing problem: For given positioning ranges of motion ($(x_{min} \leq x \leq x_{max})$, $(y_{min} \leq y \leq y_{max})$ and $(z_{min} \leq z \leq z_{max})$) and a given center of orientation (T_{1o}, T_{2o}, T_{3o}), determine the largest singularity-free zone in the 3-dimensional orientation workspace, which is free of singularities for any position in the given ranges.

3. case 3: with $W \in (0, 1)$ another procedure is introduced to solve the following problem: For a given workspace and a given center of position $(x_o, y_o, z_o, T_{1o}, T_{2o}, T_{3o})$, find the largest singularity-free zone in the 6-dimensional workspace such that this zone will be free from singularities.

Numerical examples are provided to illustrate graphically the three cases.

Conclusion

The analytical singularity locus equation of the general Gough-Stewart platform, which is a function of six variables (three position variables x, y and z, three orientation variables ϕ, θ and ψ) was obtained for the first time in this thesis. This result was obtained by introducing a new procedure to expand the determinant of the Jacobian matrix. It was shown that this procedure is general and can be applied to any Gough-Stewart platform. Then a procedure was developed to determine singularity-free zones in the workspace of 3-DOF planar fully-parallel mechanisms and the general Gough-Stewart platform. For the Gough-Stewart platform, singularity-free zones were obtained in the 3-D workspaces and the 6-D workspaces. The procedures locating the singularity-free zones can be extended to other kinds of parallel mechanisms, provided that their singularity locus equation is known. All these procedures can be used for design or for trajectory planning.

The procedures introduced in Chapter 5 are of special interest since they can be used to determine singularity-free regions in the position space for given ranges of orientations, or vice-versa. This is of great interest in a context of design. The last procedure introduced can also be used to find singulariy-free zones in the 6-D workspace of the Gough-Stewart platform.

The limited and complicated workspace of parallel mechanisms coupled with singularities makes the trajectory planning of the end-effector especially difficult. This

problem has attracted the attention of many researchers. The basic idea of most trajectory planning algorithms is to connect an initial point to a final point through a singularity-free path, which is a fixed path for a special task. With the procedures proposed in this thesis, the end-effector can be moved arbitrarily within a zone, which means that it can have any trajectory, and the trajectories do not have to be further checked for singularities.

The procedures developed in this thesis are all similar in nature. They are based on the known singularity locus equations and obtained via mathematical techniques. The results obtained were not previously available and are easy to understand. For different parallel mechanisms, the procedures allow the determination of singularity-free zones of different shapes, such as, cylinders and spheres. For the Gough-Stewart platform, the singularity-free zones of different cases are thoroughly studied. The maximal singularity-free zones with constant orientation or position are spheres in 3-D space. As shown, the singularity locus equation contains information on both the orientation and the position. Using a weighting coefficient, three other new cases are studied. The singularity-free zones of the three cases are spheres as well, in which the radius of the spheres are different with different coefficients.

In previous work, most of the tools developed for the analysis of parallel mechanisms are based on local properties, e.g., dexterity, manipulability and others. In order to use such tools for the singularity analysis, it is necessary to discretize the workspace of parallel mechanisms, which is tedious, leads to long computation times and, most importantly, cannot provide a definite answer on the presence of singularities.

In [32], a procedure was proposed to determine whether or not singularities are present in a specified workspace. The answer obtained is definite and does not rely on discretization.

In this thesis, one more step was taken towards the development of truly synthetic methods for the design of parallel mechanisms. Indeed, instead of determining whether singularities were present in a prescribed workspace, we have determined the largest possible zones of a given shape without singularities. The user of the procedures proposed here does not have to prescribe a workspace, one only has to specify a center configuration.

The procedures developed here are a first step in this new direction. They could be improved to make them more powerful and practical. For instance, in all the procedures, singularity-free spheres or cylinders are found and the critical point at the surface of the sphere or cylinder is determined. Given this point, it would be possible to modify the shape or center of the sphere or cylinder to repeat the problem and further increase the size of the singularity-free zone. For instance, the use of weighting factors would allow to obtain ellipsoids or cylinders. More complex shapes could also be envisioned, the basic idea being to start from a center configuration and to 'inflate' a singularity-free zone until one point on its surface makes contact with the singularity manifold. Finally, the procedures could also be used with other types of parallel mechanisms.

It is believed that, with the development of algorithms like those proposed in this thesis, the design of parallel mechanisms will become easier and more creative.

Bibliography

[1] Allgower, E.L. and Georg, K., 1990, "Numerical Continuation Methods: A Introduction", *Springer Verlag, New York*.

[2] Bhattacharya, S., Hatwal H., and Ghosh A., 1998, "Coparision of an Exact and an Approximate Method of Singularity Avoidance in Platform Type Parallel Manipulators", *Mechananism and Machine Theory*, 33(7), pp. 965–974.

[3] Bonev, I.A. and Gosselin, C.M., 2002, "Geometric Algorithms for the Computation of the Constant-Orientation Workspace and Singularity Surfaces of a special 6-RUS Parallel Manipulator", *Proceedings of the 2002 ASME Design Engineering Technical Conferences*, Baltimore, MD, USA, DETC00/MECH-14106.

[4] Bonev, I.A. and Gosselin, C.M., 2000, "A Geometric Algorithm for the Computation of the Constant-Orientation Workspace of 6-RUS Parallel Manipulators", *Proceedings of ASME 2002*, Montreal, Canada, DETC2002/MECH-34257.

[5] Bonev, I.A. and Gosselin, C.M., 2001, "Singularity Loci of Planar Parallel Manipulators with Revolute Joints", *2nd Workshop on Computational Kinematics,* , Seoul, Korea, pp. 291–299.

[6] Capek, K., 1923, "Rossum's Universal Robots (R.U.R) (a play)", Doubleday page, New York.

[7] Dash A.K., Chen I.M., Yeo S.H., Yang G., 2003, "Singularity-Free Path Planning of Parallel Panipulators Using Clustering Algorithm and Line Geometry", ICRA-2003.

[8] Dagalakis, N.G., Albus, J.S., Wang, B.L. and Lee, J.D., 1988, "Stiffness Study of a Parallel Link Robot Crane For Shipbuilding Applications", *Proceedings of the Seventh International Conference On Offshore Mechanics and Arctic Engineering*, Huston, TX, pp. 29–37.

[9] Do, W.Q.D. and Yang, D.C.H., 1988, "Inverse Dynamic Analysis and Simulation of a Platform Type of Robot", *Journal of Robotic Systems*, Vol. 5, No. 3, pp. 209–227.

[10] Durfee, W.K., Idris, H.R. and Dubowsky, S., 1991, "Real-Time Control of the Vehicle Emulation System", *Proceedings of the ACC Conference* , Boston, MA, pp. 2057–2058.

[11] Fichter, E.F., 1986, "A Stewart Platform-Based Manipulator: General Theory and Practical Construction", *The International Journal of Robotics Research*, Vol. 5, No. 2, pp. 157–182.

[12] Gosselin, C., 1990, "Determination of the Workspace of 6-DOF Parallel Manipulators", *ASME Journal of Mechanical Design*, Vol. 112, No. 3, pp. 331–336.

[13] Gosselin, C. and Angeles, J., 1988, "The Optimum Kinematic Design of A Planar Three-Degree-of-Freedom Parallel Manipulator", *ASME Journal of Mechanisms, Transmissions and Automations in Design*, Vol. 110, No. 1, pp. 35–41.

[14] Gosselin, C. and Angeles, J., 1990, "Singularity Analysis of Closed-Loop Kinematic Chains", *IEEE Transactions on Robotics and Automation*, Vol. 6, No. 3, pp. 281–290.

[15] Gosselin, C. and Wang, J., 2002, "Singularity Loci of a Special Class of Spherical Three-Degree-of-Freedom Parallel Mechanisms with Revolute Actuators", *The International Journal of Robotics Research*, Vol. 21, No. 7, pp. 649–659.

[16] Gosselin, C., Lavoie, E. and Toutant, P., 1992, "An Efficient Algorithm for the Graphical Representation of the Three-Dimensional Workspce of Parallel manipulators", *22nd Biennial Mechanisms Conf., September 13–16, Scottsdale, AZ.*

[17] Gough, V.E., 1956-1957, "Contribution to Discussion to Papers on Research in Automobile Stability and Control and in Tyre Performance", *Proceedings of the Auto. Div. Instn mech. Engrs, p. 392 by Cornell Staff.*

[18] Gregorio, R.D., 2001, "Analytic Formulation of the 6-3 Fully-Parallel Manipulator's Singularity Determination", *Rotobitica*, Vol. 19, pp. 663–667.

[19] Huang, M.Z., 1991, "On the Kinematics of a Parallel-Chain platform Manipulator", *Proceedings of the Fourth Annual Conference on Recent Advances in Robotics*, Boca Raton, FL, pp. 251–256.

[20] Huang, Z., Chen, L.H. and Li, Y.W., 2003, "The Singularity Principle and Property of Stewart Parallel Manipulator", *Journal of Robotic Systems*, Vol. 20, No. 4, pp. 163–176.

[21] Hunt, K.H., 1978, "Kinematic Geometry of Mechanisms", Oxford University Press,Cambridge.

[22] Hunt, K.H., 1983, "Structural Kinematics of In-Parallel-Actuated Robot Arms", *ASME Journal of Mechanisms, Transmissions and Automation in Design*, Vol. 105, No. 4, pp. 705–712.

[23] Hunt, K.H. and McAree, P.R., 1998, "The Octahedral Manipulator: Geometry and Mobility", *International Journal of Robotics Research*, Vol. 17, No. 8, pp. 868–885.

[24] Hanua, P., Waldron, K.J. and Murthy, V., 1990, "Direct Kinematic Solution of a Stewart Platform", *IEEE Transactions of Robotics and Automation*, Vol. 6, No. 4, pp. 438–443.

[25] Jo, D.Y., and Haug, E.J., 1989, "Workspace Analysis of Closed Loop Mechanisms with Unilateral Constraints", *ASME Design Automation Conf.* , Septermber 17–20, Montréal, Canada

[26] Kim, D. and Chung W.Y., 1999, "Analytic Singularity Equation and Analysis of Six-DOF Parallel Mmanipulators Using Local Structurization Method", *IEEE Transactions on Robotics and Automation*, Vol. 5, No. 4, pp. 612–622.

[27] Lee, J., et al., 1989, "Computer Simulation of a Parallel Link Manipulator", *Journal of Robotics Comp. Integr. Manuf.*, Vol. 5, No. 4, pp. 333–342.

[28] Merlet, J.P., 1989, "Singular Configurations of Parallel Manipulators and Grassmann Geometry", *International Journal of Robotics Research*, Vol. 8, No. 5, pp. 45–56.

[29] Merlet, J-P., 1997b, "Les Robots Parallèl", Paris: Hermès.

[30] Merlet, J-P., 1999, "Detemination of 6D Workspace of Gough-Type Parallel Manipulator and Comparison between Different Geometries", *The International Journal of Robotics Research*, Vol. 18, No. 9, pp. 902–916.

[31] Merlet, J-P., 1994, "Trajectory Verification in the Workspace for Parallel Manipulator, *International Journal of Robotics Research*, 13(4), pp. 326–333.

[32] Merlet, J-P., 1997, "Detemination of the Presence of Singularities in a Workspace Volume of a Parallel Manipulator", *Computational Methods in Mechanisms*, STs. Konstantin and Elena Resort, 16-28 Juin 1997.

[33] Mayer St-Onge, B. and Gosselin, C.M., 1997, "Problème Géométrique Direct et Lieux de Singularité des Maniulateurs Parallèles Plans *à* 3 ddl", *Rapport de Recherche, Université Laval.*

[34] Mayer St-Onge, B. and Gosselin, C.M., 2000, "Singularity Analysis and Representation of the General Gough-Stewart platform", *International Journal of Robotics Research*, Vol. 19, No. 3, pp. 271–288.

[35] Ma,O., and Angeles, J., 1991, "Architecture Singularities of Platform Manipulators", *Proceedings of the 1991 IEEE International Conference on Robotics and Automation, Sacrameno*, pp. 1542–1547.

[36] Masory, O., Wang, J., and Zhuang H., 1993, "On the Accuracy of a Stewart Platform-Part II: Kinemati Calibration and compenstion", *IEEE Int. Conf. on Robotics and Automation,*, May 2–6, Atlanta, GA.

[37] McAree, P.R. and Daniel R.W., 1999, "A Fast, Robust Solution to the Stewart Platform Forward Kinematics", *Journal of Robotic Systems*, Vol.121, No. 1, pp. 45–49.

[38] Ostrowski, A.M., 1966, "Solutions of Equations and Systems of Equations", 2nd ed. (New York: Academic Press).

[39] Pohst, M. and Zassenhaus, H., 1989, "Algorithm Algebraic Number Theory", *Cambridge, England: Cambridge University Press.*

[40] Pernkopf, F., and Husty, M., 2002, "Workspace Analysis of Stewart-Gough Manipulators Using Orientation Plots", *Proceedings of MUSME 2002, the International Symposium on Multibody Systems and Mechatronics*, Mexico City, Septermber 12–14, 2002, Paper n. M33.

[41] Spring, K.W., 1986, "Euler Parameters and the Use of Quaternion Algebra in the Manipulation of Finite Rotations: A Review", *Mechanism and Machine Theory*, Vol. 21, No. 5, pp. 365–373.

[42] Strang, G., 1988, "Linear Algebra and its Applications", Fort Worth, TX: Saunders College.

[43] Spring, D., 1985, "On the Second Derivative Test For Constrained Local Extrema", American Mathiematical Monthly 92: pp. 631–643.

[44] Sefrioui, J. and Gosselin,C., 1993, "Singularity Analysis and Representation of Planar Parallel Manipulators", *Journal of Robotics and Autonomous System* Vol. 10, pp. 209–224.

[45] Sefrioui, J. and Gosselin,C., 1995, "On the Quadratic Nature of the Singularity Curves of Planar Three-degree-of-freedom Parallel Manipulators", *Mechanism and Machine Thoery,* Vol. 30, No. 4, pp. 533–551.

[46] Stewart, D., 1965, "A Platform with Six Degrees of Freedom", *Proceedings of the Institute of Mechanical Engineers* Vol. 180, No. 5, pp. 371–378.

[47] Suginoto, K., 1987, "Kinematics and Dynamics Analysis of Parallel Manipulators by Means of Motor Algebra", *ASME Journal of Mechanisms, Transmissions and Automation in Design*, Vol. 109, pp. 3–7.

[48] Tsai, K.Y. and Kohli, D., 1993, "Trajectory Planning in Task Space for General Manipulators", *Journal of Mechanical Design* Vol.115, pp. 915–921.

[49] Tsai, L.W., 1999, "Robot Analysis: the Mechanics of Serial and Parallel Manipulators", *A Wiley-Interscience Publication.*

[50] Wang, J. and Gosselin, C., 1995, "Singularity Loci of Planar Parallel Manipulators", *Proceedings ofthe Ninth World Congress on the Theory of Machines and Mechanisms*, Milano, Italy, Vol. 2, pp. 1973–1976.

[51] Wang, J. and Gosselin, C., 1997, "Singularity Loci of Planar Parallel Manipulators with Revolute Actuators", *Robotics and Autonomous Systems*, Vol. 21, pp. 377–398.

[52] Wang, J., and Gosselin C.M., 1998, "Kinematic Analysis and Singularity Loci of Spatial Four-Degree-of-Freedom Parallel Manipulators Using a Vector Formulation", *Journal of Mechanical Design*, Vol. 120, pp. 555–558.

[53] Waldron, K.H. and Hunt, K.H. 1987, "Series-Parallel Dualities in Actively Coordinated Mechanisms, in: R.C. Bolles, B. Both (Eds.), ", *Proceedings of the Fourth International Symposium on Robotics Research*, MIT press, Cambridge, MA, pp. 175–180.

[54] Yang, D.C.H. and Lea, T.W., 1984, "Feasibility Study of A Platform Type of Robot Manipulators from a Kinematic Viewpoint", *ASME Journal of Mechanisms, Transmissions and Automation in Design*, Vol. 106, pp. 191–198.

[55] Zlatanov, D., Fenton, R.G. and Behhabid, B., 1994, "Singularity Analysis of Mechanisms and Robots Via a Velocity-Equation Model of the Instantaneous Kinematics", *Proceedings of the IEEE International Conference on Robotics and Automation*, San Diego, CA, USA, pp.986–991.

[56] Zlatanov, D., Bonev, I.A. and Gosselin, C.M., 2002, "Constraint Singularities of Parallel Mechanisms", *Proceedings of the 2002 IEEE International Conference on Robotics and Automation*, Washington, DC, USA, pp. 496–502.

[57] Zhuang, H. and Roth, Z., 1991, "A Method of Kinematic Calibration of Stewart Platform", *Proceedings of ASME Annual Winter Meetings* , Atlanta, GA, pp. 43–48.

Appendix A

Generic Expressions of Some of the Determinants Composing the Singularity Locus Equation For the Gough-Stewart Platform

1. $\det \mathbf{M}_i$, $i = 1, \ldots, 3981$, are determinants of 6×6 matrices constructed by architecture parameters and their combinations, which are in the following form:

$$\begin{aligned}
\det \mathbf{M}_1 &= \det([\mathbf{a}_1, \mathbf{a}_2, \mathbf{a}_3, \mathbf{a}_{41}, \mathbf{a}_{42}, \mathbf{a}_{51}]) \\
\det \mathbf{M}_2 &= \det([\mathbf{a}_1, \mathbf{a}_2, \mathbf{a}_3, \mathbf{a}_{42}, \mathbf{a}_{51}, \mathbf{a}_{62}]) \\
\det \mathbf{M}_3 &= \det([\mathbf{a}_1, \mathbf{a}_2, \mathbf{a}_3, \mathbf{a}_{43}, \mathbf{a}_{51}, \mathbf{a}_{62}]) \\
\det \mathbf{M}_4 &= \det([\mathbf{a}_1, \mathbf{a}_2, \mathbf{a}_3, \mathbf{a}_{51}, \mathbf{a}_{53}, \mathbf{a}_{62}]) \\
\det \mathbf{M}_5 &= \det([\mathbf{a}_1, \mathbf{a}_2, \mathbf{a}_3, \mathbf{a}_{42}, \mathbf{a}_{51}, \mathbf{a}_{63}])
\end{aligned}$$

$$
\begin{aligned}
\det \mathbf{M}_6 &= \det([\mathbf{a}_1, \mathbf{a}_2, \mathbf{a}_3, \mathbf{a}_{43}, \mathbf{a}_{51}, \mathbf{a}_{63}]) \\
\det \mathbf{M}_7 &= \det([\mathbf{a}_1, \mathbf{a}_2, \mathbf{a}_3, \mathbf{a}_{51}, \mathbf{a}_{52}, \mathbf{a}_{63}]) \\
\det \mathbf{M}_8 &= \det([\mathbf{a}_1, \mathbf{a}_2, \mathbf{a}_3, \mathbf{a}_{51}, \mathbf{a}_{53}, \mathbf{a}_{63}]) \\
\det \mathbf{M}_9 &= \det([\mathbf{a}_1, \mathbf{a}_2, \mathbf{a}_3, \mathbf{a}_{41}, \mathbf{a}_{42}, \mathbf{a}_{62}]) \\
\det \mathbf{M}_{10} &= \det([\mathbf{a}_1, \mathbf{a}_2, \mathbf{a}_3, \mathbf{a}_{41}, \mathbf{a}_{43}, \mathbf{a}_{62}]) \\
\det \mathbf{M}_{11} &= \det([\mathbf{a}_1, \mathbf{a}_2, \mathbf{a}_3, \mathbf{a}_{41}, \mathbf{a}_{52}, \mathbf{a}_{62}]) \\
\det \mathbf{M}_{12} &= \det([\mathbf{a}_1, \mathbf{a}_2, \mathbf{a}_3, \mathbf{a}_{41}, \mathbf{a}_{53}, \mathbf{a}_{62}]) \\
&\vdots \\
\det \mathbf{M}_{3975} &= \det([\mathbf{a}_3, \mathbf{d}_2, \mathbf{d}_3, \mathbf{a}_{41}, \mathbf{a}_{63}, \mathbf{u}])) \\
\det \mathbf{M}_{3976} &= \det([\mathbf{d}_2, \mathbf{d}_3, \mathbf{a}_{41}, \mathbf{a}_{42}, \mathbf{a}_{63}, \mathbf{u}]) \\
\det \mathbf{M}_{3977} &= \det([\mathbf{d}_2, \mathbf{d}_3, \mathbf{a}_{41}, \mathbf{a}_{43}, \mathbf{a}_{63}, \mathbf{u}]) \\
\det \mathbf{M}_{3978} &= \det([\mathbf{d}_2, \mathbf{d}_3, \mathbf{a}_{41}, \mathbf{a}_{53}, \mathbf{a}_{63}, \mathbf{u}]) \\
\det \mathbf{M}_{3979} &= \det([\mathbf{a}_3, \mathbf{d}_2, \mathbf{d}_3, \mathbf{a}_{42}, \mathbf{a}_{63}, \mathbf{u}]) \\
\det \mathbf{M}_{3980} &= \det([\mathbf{d}_2, \mathbf{d}_3, \mathbf{a}_{42}, \mathbf{a}_{43}, \mathbf{a}_{63}, \mathbf{u}]) \\
\det \mathbf{M}_{3981} &= \det([\mathbf{d}_2, \mathbf{d}_3, \mathbf{a}_{42}, \mathbf{a}_{53}, \mathbf{a}_{63}, \mathbf{u}])
\end{aligned}
$$

2. K_j, $j = 1, \ldots, 2173$, which are combinations of the above $\det \mathbf{M}_i$.

$$
\begin{aligned}
K_1 = {} & \det \mathbf{M}_1 - \det \mathbf{M}_{13} - \det \mathbf{M}_{30} - \det \mathbf{M}_{69} + \det \mathbf{M}_{141} - \det \mathbf{M}_{179} \\
& - 2 \det \mathbf{M}_{271} + 2 \det \mathbf{M}_{276} + \det \mathbf{M}_{299} - \det \mathbf{M}_{310} + 3 \det \mathbf{M}_{328} \\
& - 3 \det \mathbf{M}_{356} - \det \mathbf{M}_{457} - \det \mathbf{M}_{472} + \det \mathbf{M}_{955} - \det \mathbf{M}_{956} \\
& + \det \mathbf{M}_{1014} + \det \mathbf{M}_{1112} + 2 \det \mathbf{M}_{1129} + \det \mathbf{M}_{1138} - \det \mathbf{M}_{1089} \\
& - \det \mathbf{M}_{1439} + 2 \det \mathbf{M}_{1515} + \det \mathbf{M}_{142} - \det \mathbf{M}_{176} + \det \mathbf{M}_{1746} \\
& + \det \mathbf{M}_{828} + 2 \det \mathbf{M}_{325} + \det \mathbf{M}_{976} + \det \mathbf{M}_{990} - \det \mathbf{M}_{1464} \\
& - \det \mathbf{M}_{1526} + \det \mathbf{M}_{1886} - 2 \det \mathbf{M}_{1893} + 2 \det \mathbf{M}_{1908} + \det \mathbf{M}_{1922} \\
& + \det \mathbf{M}_{1944} + 2 \det \mathbf{M}_{1961} + \det \mathbf{M}_{1969} + \det \mathbf{M}_{2043} - \det \mathbf{M}_{2066} \\
& - \det \mathbf{M}_{2080} + \det \mathbf{M}_{2334} + \det \mathbf{M}_{2338} + \det \mathbf{M}_{2438} + \det \mathbf{M}_{2445} \\
& - 2 \det \mathbf{M}_{2417} - 3 \det \mathbf{M}_{2422} - \det \mathbf{M}_{2607} + \det \mathbf{M}_{1617} + \det \mathbf{M}_{2658} \\
& - 2 \det \mathbf{M}_{2643} - \det \mathbf{M}_{2675} - \det \mathbf{M}_{2672} - \det \mathbf{M}_{2887} + \det \mathbf{M}_{3006} \\
& - \det \mathbf{M}_{3057} - \det \mathbf{M}_{3063} + \det \mathbf{M}_{3093} + \det \mathbf{M}_{3144} + \det \mathbf{M}_{3314} \\
& + \det \mathbf{M}_{869} - 2 \det \mathbf{M}_{1074} + 2 \det \mathbf{M}_{2649} - \det \mathbf{M}_{2964} - \det \mathbf{M}_{3269} \\
& + \det \mathbf{M}_{828} + \det \mathbf{M}_{1014} - \det \mathbf{M}_{364} - 2 \det \mathbf{M}_{1940} - \det \mathbf{M}_{1078}
\end{aligned}
$$

$$
\begin{aligned}
& - \det \mathbf{M}_{1001} - \det \mathbf{M}_{1753} + 2 \det \mathbf{M}_{1470} + \det \mathbf{M}_{2076} + 3 \det \mathbf{M}_{2447} \\
& + 3 \det \mathbf{M}_{2447} + \det \mathbf{M}_{2661} + \det \mathbf{M}_{3007} + \det \mathbf{M}_{3334} + \det \mathbf{M}_{3357} \\
K_2 \;=\; & \det \mathbf{M}_2 - \mathbf{M}_6 - \mathbf{M}_{11} + \mathbf{M}_{16} + \mathbf{M}_{35} + \mathbf{M}_{53} - \mathbf{M}_{62} - \mathbf{M}_{83} \\
& - \det \mathbf{M}_{147} + \det \mathbf{M}_{161} + \det \mathbf{M}_{172} - \det \mathbf{M}_{185} + 2 \det \mathbf{M}_{262} \\
& - 2 \det \mathbf{M}_{306} - 2 \det \mathbf{M}_{313} - 2 \det \mathbf{M}_{361} + \det \mathbf{M}_{428} + \det \mathbf{M}_{429} \\
& - \det \mathbf{M}_{479} - \det \mathbf{M}_{485} + 2 \det \mathbf{M}_{841} - 2 \det \mathbf{M}_{871} + 2 \det \mathbf{M}_{866} \\
& + \det \mathbf{M}_{946} - \det \mathbf{M}_{959} + \det \mathbf{M}_{988} - \det \mathbf{M}_{1006} - \det \mathbf{M}_{1010} \\
& - \det \mathbf{M}_{1086} + 2 \det \mathbf{M}_{1061} - \det \mathbf{M}_{1121} + \det \mathbf{M}_{1430} + \det \mathbf{M}_{1444} \\
& + 2 \det \mathbf{M}_{1451} - \det \mathbf{M}_{1503} + 2 \det \mathbf{M}_{837} + 2 \det \mathbf{M}_{1913} + 2 \det \mathbf{M}_{1963} \\
& - \det \mathbf{M}_{2088} - \det \mathbf{M}_{2095} + \det \mathbf{M}_{2307} + \det \mathbf{M}_{2342} + \det \mathbf{M}_{2342} \\
& + \det \mathbf{M}_{2346} - \det \mathbf{M}_{2468} - 2 \det \mathbf{M}_{1878} - \det \mathbf{M}_{2430} - \det \mathbf{M}_{2620} \\
& - \det \mathbf{M}_{2684} - \det \mathbf{M}_{2603} + 2 \det \mathbf{M}_{1929} - \det \mathbf{M}_{2316} - \det \mathbf{M}_{2317} \\
& + \det \mathbf{M}_{2670} - 2 \det \mathbf{M}_{2906} - 2 \det \mathbf{M}_{2902} - \det \mathbf{M}_{3013} + \det \mathbf{M}_{3037} \\
& - \det \mathbf{M}_{3075} - \det \mathbf{M}_{3099} + \det \mathbf{M}_{3164} - \det \mathbf{M}_{3284} + \det \mathbf{M}_{3290} \\
& + 2 \det \mathbf{M}_{1133} - 2 \det \mathbf{M}_{1255} + \det \mathbf{M}_{995} + \det \mathbf{M}_{1478} + \det \mathbf{M}_{2059} \\
& + \det \mathbf{M}_{2073} - \det \mathbf{M}_{2289} + 2 \det \mathbf{M}_{2403} + 2 \det \mathbf{M}_{2479} + 2 \det \mathbf{M}_{2629} \\
& - 2 \det \mathbf{M}_{2700} + 2 \det \mathbf{M}_{2959} + 2 \det \mathbf{M}_{2970} + \det \mathbf{M}_{3049} - \det \mathbf{M}_{3122} \\
& + \det \mathbf{M}_{3129} + \det \mathbf{M}_{3350} - \det \mathbf{M}_{3366} \\
\vdots & \\
K_{2163} \;=\; & 3 \det \mathbf{M}_{661} - 3 \det \mathbf{M}_{694} - 3 \det \mathbf{M}_{689} - 3 \det \mathbf{M}_{670} \\
K_{2164} \;=\; & 3 \det \mathbf{M}_{665} - 3 \det \mathbf{M}_{695} + 3 \det \mathbf{M}_{688} + 3 \det \mathbf{M}_{669} \\
K_{2165} \;=\; & \det \mathbf{M}_{672} - \det \mathbf{M}_{682} + \det \mathbf{M}_{662} - \det \mathbf{M}_{691} + \det \mathbf{M}_{1289} + \det \mathbf{M}_{1292} \\
K_{2166} \;=\; & \det \mathbf{M}_{681} + \det \mathbf{M}_{658} + \det \mathbf{M}_{685} + \det \mathbf{M}_{666} + \det \mathbf{M}_{1288} + \det \mathbf{M}_{1295} \\
K_{2167} \;=\; & - \det \mathbf{M}_{753} + \det \mathbf{M}_{663} - \det \mathbf{M}_{687} - \det \mathbf{M}_{692} - \det \mathbf{M}_{1301} - \det \mathbf{M}_{1294} \\
K_{2168} \;=\; & \det \mathbf{M}_{754} - \det \mathbf{M}_{686} - \det \mathbf{M}_{1285} - \det \mathbf{M}_{1287} \\
K_{2169} \;=\; & - \det \mathbf{M}_{681} - \det \mathbf{M}_{1357} - \det \mathbf{M}_{685} + \det \mathbf{M}_{1288} \\
K_{2170} \;=\; & \det \mathbf{M}_{686} + \det \mathbf{M}_{660} - \det \mathbf{M}_{667} - \det \mathbf{M}_{693} \\
K_{2171} \;=\; & \det \mathbf{M}_{687} + \det \mathbf{M}_{692} + \det \mathbf{M}_{668} - \det \mathbf{M}_{663} \\
K_{2172} \;=\; & - \det \mathbf{M}_{524} - \det \mathbf{M}_{520} + \det \mathbf{M}_{550} - \det \mathbf{M}_{543} \\
K_{2173} \;=\; & - \det \mathbf{M}_{525} - \det \mathbf{M}_{544} + \det \mathbf{M}_{516} - \det \mathbf{M}_{549}
\end{aligned}
$$